

**MASTER**

**Optofluidic control of photonic crystal cavities**

Speijcken, N.W.L.

*Award date:*  
2012

[Link to publication](#)

**Disclaimer**

This document contains a student thesis (bachelor's or master's), as authored by a student at Eindhoven University of Technology. Student theses are made available in the TU/e repository upon obtaining the required degree. The grade received is not published on the document as presented in the repository. The required complexity or quality of research of student theses may vary by program, and the required minimum study period may vary in duration.

**General rights**

Copyright and moral rights for the publications made accessible in the public portal are retained by the authors and/or other copyright owners and it is a condition of accessing publications that users recognise and abide by the legal requirements associated with these rights.

- Users may download and print one copy of any publication from the public portal for the purpose of private study or research.
- You may not further distribute the material or use it for any profit-making activity or commercial gain

# Optofluidic control of photonic crystal cavities

---

Research group: Photonics and Semiconductor Nanophysics (PSN)  
Eindhoven University of Technology (TU/e)  
Supervisor: Dr. R.W. van der Heijden  
Dr. M. Dündar  
Professor: Prof. Dr. A. Fiore

## Abstract

During the last decade, the combination of the fields of optics and micro-fluidics has been investigated for their mutual benefits, which resulted in the emerging field of optofluidics. In this project the possibilities and applications of integrating fluids in photonic crystal (PhC) structures are explored.

A PhC is an artificial material with a periodic variation in refractive index, fabricated by etching holes into a suspended dielectric slab. PhCs are used to control the propagation of light, for example by trapping or guiding it. The optical properties of PhC structures are sensitive to small changes in refractive index and can easily be adjusted by shifting the holes or by changing their size. These methods can only be used during fabrication and do not provide tuning capabilities afterwards. In the present work, new and versatile ways of locally changing the refractive index of the PhC structure were investigated by selectively filling holes with fluids in carefully chosen patterns.

A range of novel and unique phenomena has been demonstrated. The wavelength scale refractive index changes were not only used to tune the resonances of fabricated cavities, but also to induce cavities in uniformly fabricated PhC structures. Focussed laser light was used to selectively remove liquid from the holes, which makes the local changes in refractive index reconfigurable. Different modes in the same cavity can be tuned independently, both towards higher and lower wavelengths. The liquid induced cavities can be positioned and moved to different parts of the structure at will. Finally it is presented how light can be used to selectively re-infiltrate the holes with liquid which shows that light can also be used to gain control over the transport of fluids.

# Contents

<b>Abstract</b> .....	<b>1</b>
<b>Contents</b> .....	<b>2</b>
<b>1. Introduction</b> .....	<b>4</b>
1.1 Goal .....	6
1.2 Outline.....	6
<b>2. Theory</b> .....	<b>7</b>
2.1 Photonic crystal slab .....	7
2.2 From Maxwell's equations to the master equation.....	7
2.3 Periodic structures .....	9
2.4 Photonic crystal band gap.....	9
2.5 Perturbations in periodicity .....	12
2.5.1 <i>Liquid induced changes of refractive index</i> .....	13
<b>3. Fabrication methods and characterization</b> .....	<b>14</b>
3.1 Fabrication methods .....	14
3.2 Finite-difference time-domain simulations .....	15
3.3 Nano-scale fluid manipulation stage .....	17
3.4 Characterization.....	18
<b>4. In-situ reconfigurable opto-fluidic double hetero structure cavities</b> .....	<b>22</b>
4.1 Introduction .....	22
4.2 Double hetero structures induced by selective infiltration .....	23
4.2.1 <i>Description of the experiment</i> .....	23
4.2.2 <i>Waveguide dispersion calculations</i> .....	24
4.2.3 <i>Experimental results</i> .....	25
4.2.4 <i>Multiple infiltrations and reconfigurable infiltration</i> .....	28
4.2.5 <i>Fabrication problems and a new photonic crystal cavity design</i> .....	31
4.2.6 <i>Conclusion</i> .....	33
4.3 Double hetero structures induced by micro-droplets .....	34
4.3.1 <i>Description of the experiment</i> .....	34
4.3.2 <i>Waveguide dispersion calculations</i> .....	34
4.3.3 <i>Results</i> .....	35
4.3.4 <i>Conclusion</i> .....	41

<b>5. Selective cavity mode tuning by controlled local liquid infiltration.....</b>	<b>42</b>
5.1 Introduction .....	42
5.2 Breaking degeneracy by selective infiltration.....	43
5.2.1 <i>Description of the experiment</i> .....	43
5.2.2 <i>Mode identification and calculation results</i> .....	43
5.2.3 <i>Mode splitting by selective removal of liquid</i> .....	45
5.2.4 <i>Mode splitting by selective infiltration of liquid</i> .....	51
5.2.5 <i>Mode splitting in a L3 cavity</i> .....	54
5.3 Breaking degeneracy by micro-droplet positioning.....	57
5.3.1 <i>Description of the experiment</i> .....	57
5.3.2 <i>Results</i> .....	58
5.3.3 <i>Conclusion</i> .....	61
<b>6. Optical fluid-manipulation.....</b>	<b>62</b>
6.1 Introduction .....	62
6.2 Description of the experiment.....	63
6.3 Results.....	65
6.3.1 <i>Laser power required for evaporation</i> .....	65
6.3.2 <i>Exposure time required for evaporation</i> .....	69
6.3.3 <i>Optical re-infiltration of the PhC membrane</i> .....	70
6.3.4 <i>Summary and overview of the experiment</i> .....	73
6.4 Conclusion .....	74
<b>7. Summary.....</b>	<b>75</b>
<b>Acknowledgments.....</b>	<b>76</b>
<b>Bibliography.....</b>	<b>77</b>

## 1. Introduction

The field of optics started to work together with the field of micro-fluidics to form the emerging field of optofluidics that provided capabilities that neither of the fields could have achieved alone. In this chapter the fundamental advantages and interesting new applications emerging from the field of optofluidics are discussed.

The term optofluidics was first used in the name of a research center in 2003 that tried to integrate microfluidics into their research to develop optical devices that profit from the smooth, changeable and reconfigurable properties of liquids. There is large range of advantages that can be obtained from implementing microfluidics into optics. Immiscible fluids can be used to form optically smooth interfaces. A property already used in 1982 to create mirrors for telescopes and gaining new interest on a much smaller scale in optofluidic lensing projects. An example is a fluidic planar lens of which the curvature can be tuned using electro-wetting [1][2], providing real-time focussing possibilities. The smooth interfaces of flowing liquids were used to guide light. Soft lithography is used to etch microchannels in layers of an organic polymer (PDMS) grown on top of optical structures. The controlled flow of fluids with different refractive indices in these channels can be used to produce tunable optical waveguides [3] and due to their dynamic nature, their optical properties can be controlled in a continuous way. Small irregularities in the walls of the micro-channel are smoothed out before reaching the fluid waveguide, greatly reducing optical losses. This type of fluidic waveguides was later used, among other applications, to create movable and tunable liquid lenses [4]. Due the ease of transport of fluids, the properties of an optical device can be made adaptive by changing the properties of the liquid. This way optical properties like refractive index, absorption and scattering can be made changeable. The liquids in the structure can easily be renewed which can for example increase the life-time of dye lasers, of which the dye bleaches during use. The flow of liquids can be mixed in a controlled way using diffusion. This can be used to create and control smooth gradients in optical properties [5], something that would never be possible in solid state optics alone.

All these examples still imply the use of liquids to create novel optical devices. Nowadays the research field of micro-fluidics also fully utilizes the advantages of optics and the term optofluidics has become more balanced. The research field is still rapidly expanding and gains a lot of interest [6,7,8,9]. There is for example a large range of optical devices for sensing. The detail in chemical and biological characterization strongly depends on the fast and highly sensitive responses of optical sensing methods. The field of biology has benefitted from the increasing resolution of microscopy and the possibility to probe optical properties using evanescent fields. Knowledge on the sub-micro scale is required to gain a deeper understanding of the meso-scale. Before, this research would require light with short wavelengths like X-rays to image structures on the sub-micron scale. High frequency radiation is difficult to focus and is hazardous to health.

Light can also be used to move fluids or objects in fluids. Optical tweezers [10], originally called single-beam gradient force map, use a highly focussed laser beam to assert an attractive or repulsive force on dielectric objects. This force can be used to hold or move microscopic objects. The technique knows many applications, like optical-force based cell-sorting techniques [11]. The optical force was later enhanced by using the evanescent waves of dielectric waveguides, called near-field micromanipulation [12], to trap the dielectric particles at the surface of the device. Another way of using light to move liquid is by controlled evaporation and condensation, which will be discussed

later in this report. An optofluidic maskless lithography system was designed that can “dynamically synthesize free-floating polymeric microstructures inside microfluidic channels by selectively polymerizing photocurable resin with high-speed two-dimensional spatial light modulators”[13]. A more in-depth discussion on the emerging field of optofluidics and the large range of application can be found in the recently published book “Optofluidics” [14].

Photonics is defined as interaction of light with matter [15]. Photonics is the part of optics in which the propagation of light is being controlled by the design of dielectric materials. Its name is copied from electronics in which compositions of materials are designed to control the propagation of electrons. A photonic crystal (PhC) is such a material, designed to gain control on the flow of light. A PhC is a structure with a periodic variation in refractive index for the light that propagates through it. Light with a wavelength in the range of this periodicity is strongly affected. Depending on the design of the PhC this can result in prohibiting the propagation of the light for a range of wavelengths, called a photonic band gap. Other effects are the reduction of the speed of light due to its dispersion in the material, or the strong localization in micro-scale defects. PhCs were called to “mold the flow of light”[16] and were first discovered in 1987 [17,18]. A three dimensional PhC with photonic band gap in the GHz range was first presented in 1991 [19], but was not suitable for light in the telecommunication range. This would require a size reduction beyond the practical possibilities of fabrication. A planar two-dimensional PhC design was presented in 1996 [20] where the light was confined in the vertical direction by total internal reflection. This type of structure can more easily be obtained by fabricating a stack of three layers, where the middle layer has a larger refractive index than its surroundings. Later the confinement in the vertical direction was improved by fabricating a PhC membrane suspended in air, where the interface between the dielectric slab and the air is used for containing the light with total internal reflection. Subsequently the 2D PhC is fabricated by vertically drilling holes into the slab or layer stack, to induce the in-plane periodic potential.

An important property of PhCs is the ability to trap light in micro-cavities by removing a single hole [21] or guide in waveguides by removing a line of holes [22] from the otherwise periodic structure. There is a range of optical components that require the high quality factor of the cavity combined with its small modal volume. This means to strongly confine the light to the cavity and trap it for long periods of time. Examples of applications for important on-chip components are narrow optical filters [23], optical switches [24], low-threshold lasers [25,26], negative refraction lenses [27,28], and structures based on the stopping of light propagation [29].

Most optical properties of a PhC are sensitive to small changes in refractive index. This is an important property that can be used dynamically to control the diverse properties of the PhCs and is required for many practical applications [30]. The resonances of the different PhC structures can be manipulated by local changes in the size of the holes or by slightly shifting the holes from their original position. These tuning possibilities are implemented into the PhC during fabrication and cannot be changed afterwards. Thermal and electro-optical tuning can change the refractive index of the dielectric material after fabrication, but the tuning range of these methods is small compared to changes during fabrication. The contrast in refractive index between the air in the holes and the dielectric material of the slab can easily be changed by filling the holes with a material with a different refractive index. The large variety of fluids and other materials that can be used for the infiltration opened up a whole world of tuning possibilities and applications. The infiltration with

liquid crystals makes it possible to increase the range of thermal tuning [31] to modify cavity resonances after fabrication. Not only liquid crystal but also infiltration by (organic-) liquids, polymers, nanoparticle-based composites, colloidal quantum dots and fluorescent organic dyes have been used to control the optical properties of PhCs. The uniform infiltration of the PhC holes opened up a range of new possibilities in optofluidics and was greatly expanded with the proposition to selectively infiltrate the holes with single hole precision [32]. Waveguides, Y-junctions, bends, waveguide intersections and beam splitter among others could be 'written' in a PhC pattern by infiltration with liquid and would not require the defects to be fabricated in the structure. This would not only increase the possibilities in tunability but also make the structures reconfigurable. Experimentally, several groups have demonstrated the local selective infiltration of PhC holes with liquid [33,34,35,36,37].

## 1.1 Goal

The combination of microfluidics and photonic crystals results in tunable and reconfigurable structures that are important for future integration on chips. On the same time the increased light-liquid interaction as a result of the close integration of the liquid into the optical structures results in improved sensing features, important for the chemical and biological sensing applications.

The research presented in this report was performed with the goal to gain more knowledge on the selective integration of fluids into photonic crystal structures. The fluids can induce local refractive index changes on a length scale below the wavelength of the light itself. Fluids were used to not only control the propagation or excitation of light in optical cavities, but also to induce the cavities themselves. The latter has the great advantage that the cavity, together with all its functions, can be induced and removed from the original structure with little effort and with arbitrary positioning. At the same time light was used to gain control over the liquid in the same devices. Not only can the light be used to remove liquid from parts of the structure, it can also be used to selectively put the liquid back into the structure. The combination gives a new level of freedom in the post-fabrication reconfigurable control of light in these optical structures.

## 1.2 Outline

First a theoretical background of photonic crystals and the different type of cavities that can be made by them will be described. Next the fabrication of the samples and the different setups for the characterization will be discussed. Here also the stage designed for the selective infiltration of the PhC patterns will be described.

The first investigation describes the use of liquids to induce a double hetero structure cavity and provides calculations of how these structures could be further improved. The next chapter focuses on the selective mode tuning in single hole defects, using liquid to change the refractive index of the holes or the background directly surrounding the defect. In the last part of the investigation the possibility of using light to manipulate the patterns of infiltration by moving the liquid is explored.



## 2. Theory

A Photonic crystal (PhCs) is a material that can control the flow of light. The periodic variation in the refractive index of the structure strongly affects light with wavelengths in the range of the periodicity. For some PhC designs this can result in a photonic band-gap (PBG) for which frequencies cannot propagate through the PhC. Defects in the PhC periodicity can push local modes into the PBG resulting in resonant cavities or waveguides.

### 2.1 Photonic crystal slab

The PhCs used in this report consist of a suspended InGaAsP slab in which a triangular pattern of holes is etched. In the direction perpendicular to the slab (the z-direction), the light is confined by total internal reflection (TIR). For light propagating in the slab at an angle smaller than the critical angle of the interface, there is no transmission and all the light will be reflected. The angles are defined as the angle between the incident wavevector and the interface surface. The critical angle depends on the contrast in refractive index between the slab and the material surrounding it by

$$\bar{\theta}_c = \cos^{-1} \left( \frac{n_{\text{surrounding}}}{n_{\text{slab}}} \right). \quad (1)$$

In this report the slab is made of InGaAsP and is surrounded by air. The amount of modes that can be guided in the slab depends on the wavelength, thickness of the slab and the difference in refractive index between the slab and the air. By decreasing the thickness of the slab, the waveguide is made single mode for the wavelength  $\lambda_0$  by the following condition:

$$\frac{2d}{\lambda_0} \sqrt{n_1^2 - n_2^2} < 1. \quad (2)$$

### 2.2 From Maxwell's equations to the master equation

The propagation of the light through the PhC materials can be described by Maxwell's equations, as can be found in [38]:

$$\nabla \cdot \mathbf{B} = 0, \quad (3)$$

$$\nabla \cdot \mathbf{D} = \rho, \quad (4)$$

$$\nabla \times \mathbf{E} + \frac{\partial \mathbf{B}}{\partial t} = 0, \quad (5)$$

$$\nabla \times \mathbf{H} - \frac{\partial \mathbf{D}}{\partial t} = \mathbf{J}. \quad (6)$$

$\mathbf{B}$  is the magnetic induction,  $\mathbf{D}$  is the electric displacement,  $\mathbf{E}$  is the electric and  $\mathbf{H}$  the magnetic field.  $\rho$  and  $\mathbf{J}$  are the free charge and the current density respectively.

For the optical properties of the periodic PhC structures, several simplifications can be made to solve the equations. It is assumed that the field strength is small enough to consider the relation between  $\mathbf{D}$  and  $\mathbf{E}$  and between  $\mathbf{B}$  and  $\mathbf{H}$  to be linear. Since the dielectric material has low losses, the permittivity is considered to be real and the dependence on frequency is ignored. The relations between  $\mathbf{D}$  and  $\mathbf{E}$  and between  $\mathbf{B}$  and  $\mathbf{H}$  can in that case be described by

$$\mathbf{D}(\mathbf{r}) = \varepsilon_0 \varepsilon(\mathbf{r}) \mathbf{E}(\mathbf{r}) \quad \text{and} \quad \mathbf{B}(\mathbf{r}) = \mu_0 \mu(\mathbf{r}) \mathbf{H}(\mathbf{r}). \quad (7)$$

The materials are nonmagnetic which means that the magnetic permeability is close to unity. Finally it is assumed that there are no free charges or currents. These assumptions and substitutions result in the modified Maxwell's equations

$$\nabla \cdot \mathbf{H}(\mathbf{r}, t) = 0, \quad (8)$$

$$\nabla \cdot [\varepsilon(\mathbf{r}) \mathbf{E}(\mathbf{r}, t)] = 0, \quad (9)$$

$$\nabla \times \mathbf{E}(\mathbf{r}, t) + \mu_0 \frac{\partial \mathbf{H}(\mathbf{r}, t)}{\partial t} = 0 \quad \text{and} \quad (10)$$

$$\nabla \times \mathbf{H}(\mathbf{r}, t) - \varepsilon_0 \varepsilon(\mathbf{r}) \frac{\partial \mathbf{E}(\mathbf{r}, t)}{\partial t} = 0. \quad (11)$$

The macroscopic magnetic and electric field are functions of space and time and can be expanded into the set of harmonic oscillations

$$\mathbf{H}(\mathbf{r}, t) = \mathbf{H}(\mathbf{r}) e^{-i\omega t} \quad \text{and} \quad \mathbf{E}(\mathbf{r}, t) = \mathbf{E}(\mathbf{r}) e^{-i\omega t}. \quad (12)$$

This way the temporal and spatial part of the fields are separated. By substituting equations (12) into (10) and (11) the following set of equations can be derived:

$$\nabla \times \mathbf{E}(\mathbf{r}) - i\omega \mu_0 \mathbf{H}(\mathbf{r}) = 0 \quad \text{and} \quad (13)$$

$$\nabla \times \mathbf{H}(\mathbf{r}) + i\omega \varepsilon_0 \varepsilon(\mathbf{r}) \mathbf{E}(\mathbf{r}) = 0. \quad (14)$$

By taking the curl of equation (14) and substituting the curl of the electric field by equation (13) the master equation for the magnetic field is derived:

$$\nabla \times \left( \frac{1}{\varepsilon(\mathbf{r})} \nabla \times \mathbf{H}(\mathbf{r}) \right) = \left( \frac{\omega}{c} \right)^2 \mathbf{H}(\mathbf{r}) \quad (15)$$

The corresponding electric field can be calculated by

$$\mathbf{E}(\mathbf{r}) = \left( \frac{i}{\omega \varepsilon_0 \varepsilon(\mathbf{r})} \right) \nabla \times \mathbf{H}(\mathbf{r}) \quad (16)$$

The master equation can be written as

$$\Theta \mathbf{H}(\mathbf{r}) = \left( \frac{\omega}{c} \right)^2 \mathbf{H}(\mathbf{r}), \quad (17)$$

where  $\Theta$  is the linear Hermitian operator

$$\Theta = \nabla \times \left( \frac{1}{\varepsilon(\mathbf{r})} \nabla \times \right) \quad (18)$$

with real eigenvalues  $(\omega^2/c^2)$ . The operator does not have a constant with the dimension of length and is therefore scale invariant. This means that the frequency of the resonances of the structure decrease with the increase of the length scale of the structure. Therefore a reduced frequency  $a/\lambda$ ,

which is independent on the length scale of the structure, is used. The characteristic length  $a$  is the lattice constant of the PhC structure.

### 2.3 Periodic structures

The master equation can be simplified to a periodic eigenvalue problem by introducing the periodic modulation of the refractive index

$$\varepsilon(\mathbf{r}) = \varepsilon(\mathbf{r} + \mathbf{R}), \quad (19)$$

with  $\mathbf{R}$  any lattice vector of the PhC. By using Bloch's theorem, the solutions of equation (15,17) can now be represented as

$$\mathbf{H}_k(\mathbf{r}) = \mathbf{u}_{n,k}(\mathbf{r}) \cdot e^{i\mathbf{k}\cdot\mathbf{r}}, \quad (20)$$

with  $\mathbf{u}_{n,k}(\mathbf{r}) = \mathbf{u}_{n,k}(\mathbf{r} + \mathbf{R})$  a periodic function of position and  $\mathbf{k}$  the wavevector. Every  $\mathbf{k}$  has a set of eigensolutions with eigenvalues  $\omega_n(\mathbf{k})$ , with  $n$  the bandnumber of the mode.

Bloch's theorem implies that  $\mathbf{k}$  is a conserved quantity in a periodic system and solutions can be equally well characterized by  $\mathbf{k} + \mathbf{G}$ , with  $\mathbf{G}$  any reciprocal lattice vector defined by  $\mathbf{G} \cdot \mathbf{R} = N2\pi$  for integer  $N$ . This means that the set of solutions with wavevectors  $-\mathbf{G}/2 < \mathbf{k} \leq \mathbf{G}/2$ , called the Brillouin zone, is unique and all allowed mode frequencies  $\omega_n(\mathbf{k})$  can be calculated in this range. The zone can further be reduced due to symmetries in the reciprocal lattice to what is called the irreducible Brillouin zone. The triangular lattice and (irreducible) Brillouin zone of the PhC structures used in this report are shown in Figure 1.

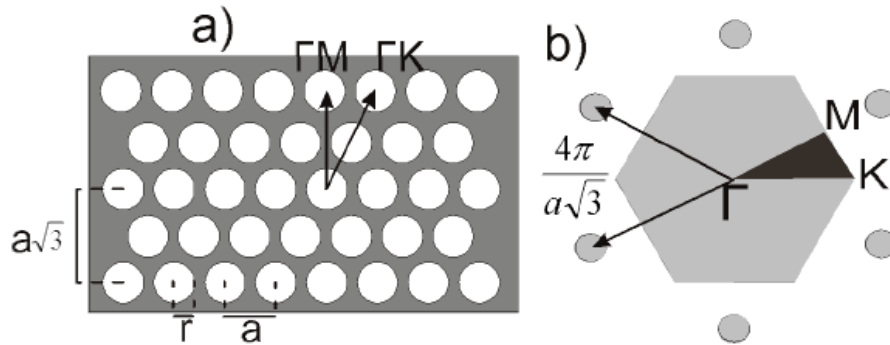


Figure 1: Schematic illustration of a) the triangular lattice in real space b) the Brillouin zone. The dark area in b) is the irreducible Brillouin zone. The image is taken from the thesis of M. Dundar [39].

The high symmetry points of the PhC are labelled  $\Gamma$ ,  $K$  and  $M$  as depicted in Figure 1. When presenting the band structure of a PhC, the frequencies for every  $\mathbf{k}$  in the high symmetry directions ( $\Gamma M$ ,  $\Gamma K$  and  $MK$ ) are calculated. The gradual change in  $\omega_n(\mathbf{k})$  corresponding to the dispersion relations of the modes in a PhC.

### 2.4 Photonic crystal band gap

In a homogeneous dielectric material the speed of light is reduced by the refractive index. The modes lie on the light line given by

$$\omega(\mathbf{k}) = \frac{c\mathbf{k}}{\sqrt{\epsilon}} \quad (21)$$

The band structure of such a homogeneous dielectric is shown in Figure 2 on the left.

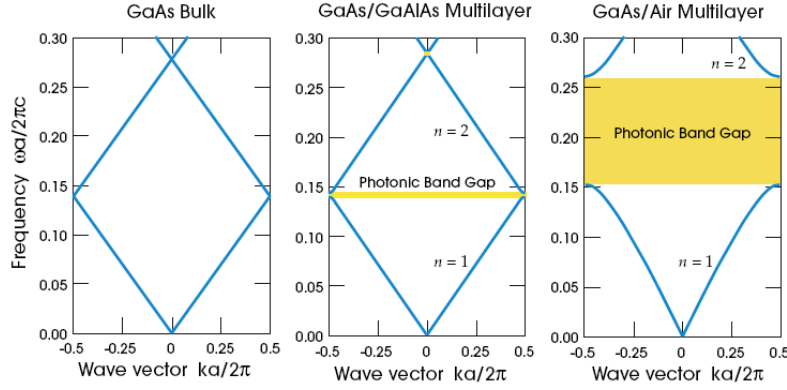


Figure 2: Photonic band structures for a multilayer structure. Left: homogeneous medium with artificial periodicity. Center: layers alternate between  $\epsilon$  of 13 and 12. Right: layers alternate between  $\epsilon$  of 13 and 1. The image is taken from [16].

By assigning an artificial periodic constant, the dispersion relation can be folded back inside the Brillouin zone as in Figure 2 on the left. The center band structure in Figure 2 presents the dispersion of a low- $\epsilon$  contrast one-dimensional modulation of the dielectric constant as is shown in Figure 3. Close to the Brillouin zone edge, the dispersion function bends away from the linear function seen for the homogeneous dielectric material. This results in a small photonic band gap for which no modes are allowed. At the Brillouin zone edge, the wavelength of the mode is exactly twice the lattice constant of the PhC structure. This leads to standing waves due to the constructively interfering Bragg reflections from all interfaces. For that case there are two ways in which the mode can be localized with respect to the dielectric modulation, as is shown in the left image of Figure 3.

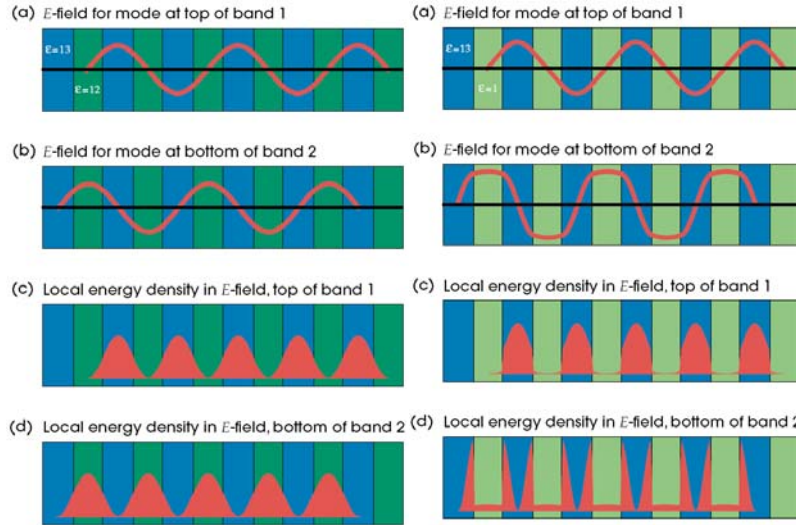


Figure 3: The Electric field (a,b) and the energy density of the E-field (c,d) in a one dimensional periodic modulation of the dielectric constant. In (a,c) the field is concentrated in the high- $\epsilon$  region and in (b,c) in the low- $\epsilon$  region. The left image shows a small contrast in  $\epsilon$  and corresponds to the center band diagram of Figure 2. The right image shows a high contrast in  $\epsilon$  and corresponds to the right band diagram in Figure 2. The images are taken from [16].

The nodes of the mode can be centered in the low- $\epsilon$  layer as is shown in (a) and (c), or in the high- $\epsilon$  layer as is shown in (b) and (d). Any other position would violate the symmetry of the unit cell about its center. The mode with the larger portion of its energy in the high- $\epsilon$  layer has a decreased frequency, while the frequency of the mode in the low- $\epsilon$  is increased. Since the PhCs used in this project are design by etching holes in a dielectric slab, the lower frequency band is called the dielectric-band, while the higher frequency band is called the air-band.

The band diagram and mode profile for the structure with a large contrast in dielectric constant are shown on the right in Figure 2 and Figure 3 respectively. In this case the mode of both bands is primarily concentrated in the high- $\epsilon$  layer. Still the mode of the dielectric-band is more concentrated in the high- $\epsilon$  than the mode of the air-band. The gap again arises from this difference in field energy location.

The magnetic field profiles and band structure of a PhC membrane with a triangular holes pattern can be calculated and are shown in Figure 4.

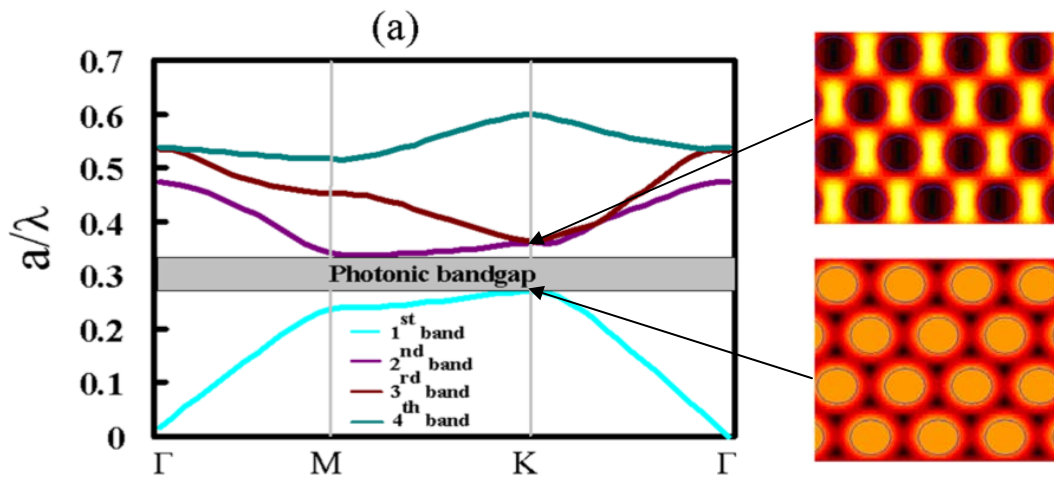


Figure 4: The band structure of a PhC structure. The diagram presents the first four bands, with the band gap between the first (dielectric) and the second (air) band. Right: magnetic field distribution of the mode at K of the dielectric (bottom) and the air (top) band. The images are taken from [39].

The diagram presents the first four bands of the PhC, with a band gap between the first (dielectric) and the second (air) band. The light is TE polarized, which means that both electric-field components are aligned perpendicular to the hole axis. The images on the right in Figure 4 depict the  $H_z$ -field profile of the modes. Equation (16) describes the curl relation between the electric and the magnetic field. This means that the nodes of the magnetic field in the mode profiles represent an anti-node in the electric field in the slab and vice versa. The presented mode profiles show magnetic field localization in the air holes for the dielectric-band and in the dielectric material for the air-band.

The width and position of the PBG depends on several structural parameters. The ratio of the radius of the holes and the lattice constant (or the air-filling factor); the refractive index ratio between the dielectric material and its surroundings; and the thickness of the slab are all important for the width and position of the PBG.

## 2.5 Perturbations in periodicity

Local changes of the dielectric constant can break the periodicity of the PhC structure and can induce single localized modes with a frequency within the band gap. This can be done by removing an air hole or by increasing or decreasing its radius. Also shifting holes can result in perturbations in the periodicity of the dielectric constant. A localized mode inside the band gap cannot couple to other modes and will be trapped. The mode can only exist in the perturbed area of the PhC and will be evanescent in the surrounding PhC.

An example is a uniform PhC where a single hole remains un-etched, called a H1 cavity. The locally increased dielectric constant pulls down higher order bands into the PBG. These newly induced modes do not exist in the surrounding PhC and the light from the cavity is trapped. The quality factor (Q) of a mode in such a perturbation is defined as its energy build up inside the defect with respect to the energy lost per cycle in the cavity.

In the same way as the H1 cavity a line of holes can be left un-etched forming a line defect called a W1 waveguide. The 1 in W1 indicates the width of the waveguide. The modes in one position of the defect can now couple to the modes in neighbouring positions and form new propagating modes inside the waveguide. Still the modes are evanescent in the bordering PhCs, where there are no modes in the PBG and the light intensity decreases exponentially. Light propagating in the waveguide is therefore reflected from the PhC and confined to the line defect.

A more specific example that is used in this project is the double hetero structure (DHS). This is a second order perturbation of a W1 line defect. For a short part of the waveguide, the lattice constant of the surrounding PhC is increased in the direction of the waveguide. A schematic illustration of the structure is shown in Figure 5.

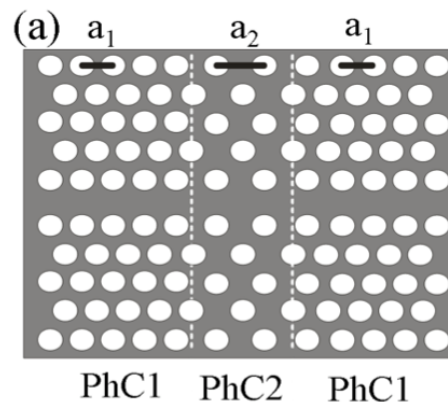


Figure 5: Schematic illustration of a double hetero structure. The image is taken from [39].

The result is an increase in the effective refractive index, locally pushing down the bands. The modes that already existed in the PBG forming the waveguide are also shifted down in the area of the increased lattice constant. The waveguide modes in the affected area can now not couple to the other parts of the waveguide and are reflected at the interface. This so called DHS cavity exhibits modes with a high quality factor and is therefore interesting for many optical applications.

### 2.5.1 Liquid induced changes of refractive index

The infiltration of a PhC hole using liquids is another way to locally increase the refractive index and induce a perturbation in the periodicity of the PhC. In the same way as described above, this can be used to locally create modes in the PBG and form cavities or waveguides. Also liquid on top of, or below the PhC membrane result in local changes of the effective refractive index and can be used to create cavities. Infiltrating liquid in fabricated PhC defect structures shifts the bands even further down in the PBG and can be used to tune the modes of the cavities.

### 3. Fabrication methods and characterization

This chapter describes the different steps in the fabrication process of the 220nm thick InGaAsP photonic crystal membrane. Also the experimental characterization methods used to measure the spectral response of the structures are presented. Furthermore the method to infiltrate the PhC with liquid will be explained. Finally, the calculation methods used to confirm the experimental data and to calculate the parameter needed for the PhC design are described.

#### 3.1 Fabrication methods

Metal organic vapour phase epitaxy (MOVPE) is used to grow a 1 $\mu$ m thick sacrificial buffer layer of InP on top of the InP substrate. Subsequently 220 nm of InGaAsP is grown on top of the InP layer to form the PhC slab. InGaAsP is a semiconductor suitable for generation of light in the telecommunication wavelength range near 1.5  $\mu$ m. In fiber-optics the range of wavelengths around 1.5  $\mu$ m show a minimum in optical absorption. Halfway during the growth of the InGaAsP layer, a layer of InAs quantum dots (QDs), with a density of  $3 \times 10^{10} \text{ cm}^{-2}$ , is grown to provide the PhC with an internal light source. The QDs are grown by a strain relieve method, called the Stranski-Krastanov [40] mode. There is a lattice mismatch between the InGaAsP and the InAs that is grown on top of it. When the strained InAs layer reaches a thickness of 1.6 monolayers, the layer snaps into small islands of InAs [41]. The size of the QDs can be controlled during the growth and determines their emission wavelength. On top of the InGaAsP a 20 nm InP capping layer is grown to protect the slab during the etching of the silicon nitride described below. A schematic side-view of the sample after the MOVPE growth is depicted in Figure 6 (a).

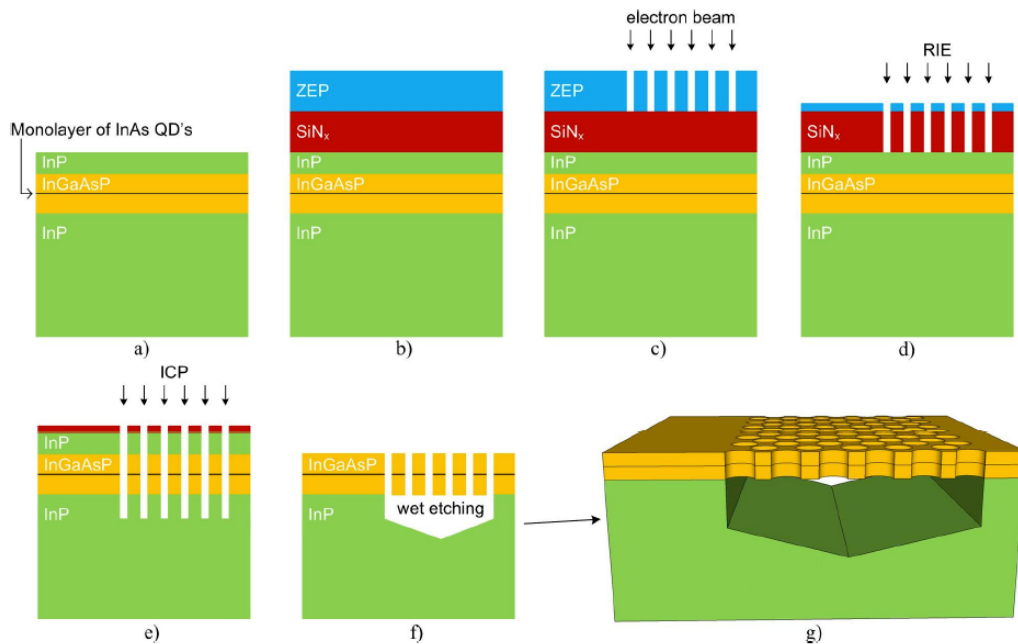


Figure 6: Schematic representation of the different steps required for sample fabrication. A side-view of the different layers of the sample is shown. a) The sample after MOVPE growth of InP/InGaAsP/InP layers with InAs QD's. b) SiNx and electron resist are deposited on the sample by PECVD and spin coating respectively. c) EBL is used to transfer the pattern to the electron resist, which is then developed and rinsed. d) RIE is used to transfer the pattern from the resist to the SiNx mask. e) The pattern is etched into the InP/InGaAsP/InP layers by ICP-RIE after which f-g) the InP is removed by wet chemical etching. This image is taken from the report of J. Voorbraak [42].



To transfer the PhC hole pattern to the sample several deposition and etch steps are required. First plasma enhanced chemical vapour deposition (Oxford Plasma-PECVD) is used to deposit silane and ammonia on the sample forming a 400 nm silicon nitride ( $\text{SiN}_x$ ) mask. Subsequently a 400nm thick layer of electron resist (ZEP 520-A) is spin-coated on top of the  $\text{SiN}_x$  mask and the sample is baked for 2 min at 200°C. The schematic side-view of the sample after this stage is shown in Figure 6 **(b)**.

Electron beam lithography (Raith-150 EBL) is used to expose the electron resist with nano-scale precision. A focussed beam of electrons is scanned over the sample to transfer a predefined pattern to the electron resist layer. The resist is developed using n-amyl acetate for 60 s and is subsequently rinsed using a solution of methyl isobutyl ketone in isopropyl alcohol for 45 s. The top view of the sample now shows the triangular pattern of holes that are etched in the resist layer. A side-view of the sample is shown in Figure 6 **(c)**.

The next step is to transfer the pattern from the electron resist to the  $\text{SiN}_x$  mask. This is done by reactive ion etching (RIE) using tri-fluor-methane (RIE-Oxford Instruments Plasma Lab). The side-view after this step is shown in Figure 6 **(d)**. The remaining electron resist that is still the sample is removed using an oxygen plasma.

The pattern can now be transferred to the InP/InGaAsP/InP layer stack. This is done using inductively coupled plasma (ICP) RIE using chlorine, argon and hydrogen (ICP-Oxford Instruments Plasma Lab). The holes now reach beyond the InGaAsP slab and into the InP layer underneath (see Figure 6 **(e)**). The etching rate of the InP and InGaAsP is faster than that of the  $\text{SiN}_x$  mask, but there might still be part of the mask left. This residue of the mask is removed by rinsing the sample with a solution of hydrogenfluoride (HF) in water.

The extra step of using a  $\text{SiN}_x$  mask seems redundant, for the pattern could be transferred to the InP/InGaAsP/InP layer stack directly from the electron resist. Not only does the resist deform at higher temperatures, but also its etch-rate is a lot higher than the etch rate of the InP and InGaAsP. The resist would be gone before the pattern is successfully transferred to the InP layer.

In the final step the InP is removed by wet chemical etching using a solution of hydrogen chloride and water for 10 minutes at 2°C. This process etches both the InP on top of the InGaAsP slab and the area underneath. The result is a PhC membrane suspended in air as shown in Figure 6 **(f-g)**.

### 3.2 Finite-difference time-domain simulations

The dispersion relations and mode profiles of the structures are calculated using finite-difference time-domain (FDTD) calculation methods. The propagation of the light in the dielectric materials is completely governed by the Maxwell equations. Since the solutions of these equations cannot be found analytically for a non-uniform PhC, numerical methods were developed to calculate the propagation of light. The FDTD method is a successful way to calculate time-depend magnetic and electric fields by discretizing both time and space [43]. A cubic cell, called a Yee cell (see Figure 7), is defined and for each point in the grid the electric and magnetic field components are calculated based on the components at the four closest points surrounding it. This is done by approximating the spatial and temporal derivatives in the Maxwell's equations by finite differences. The calculations are repeated with discrete time steps.

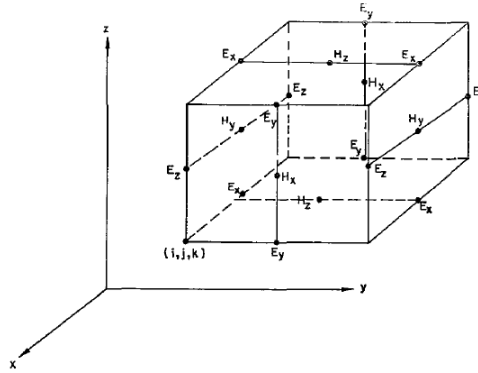


Figure 7: The cubic cell used for the FDTD calculations called a Yee-cell [43].

In the simulations presented in this report the free software from Massachusetts Institute of Technology called MIT Electromagnetic Equation Propagation (MEEP) [44] is used. A recipe is used to define the structure, boundary conditions, sources, detectors, resolution and so on. The simulation first generates the grid, with the different dielectric constants for each point in the grid, and then initiates the electric and magnetic field components defined by the source. The source in this case consists of a point dipole source generating a sinusoidal pulse with a Gaussian frequency distribution.

For the calculations of the dispersion diagram of PhC waveguide structure a unit-cell was defined and the simulation was run with periodic boundary conditions to mimic an infinitely long structure. An accompanying program called Harminv was then used to find the resonance of the structure. This program was used to calculate the frequency, decay constant, amplitude and the phase of these resonances for every wave vector defined in the recipe.

MEEP was also used to calculate the mode-profiles of the resonances of the different structures. For this the whole structure needed to be simulated and required a lot more memory and calculation time. Reflections of the light are suppressed using absorbing layers at the boundaries of the structure, called perfectly matched layers. All the fields were polarized in the plane (TE) and therefore the  $H_z$ -field of the signal in the center of the slab was used to present the mode-profiles.

The calculations were performed on computation nodes in a cluster. The intention was to run the software in parallel on 16 nodes, each containing two E5620 2.4 Ghz processors and 12 GB of memory. The batch-mode of the cluster did not work for MEEP and the nodes were used separately.

### 3.3 Nano-scale fluid manipulation stage

To infiltrate the holes with liquids a tapered optical fiber is used to pull the liquid over the sample surface. The tapered fiber is made using a step-index optical fiber. First the plastic jacket of the fiber was burned off leaving a 125  $\mu\text{m}$  diameter glass wire (see Figure 8).

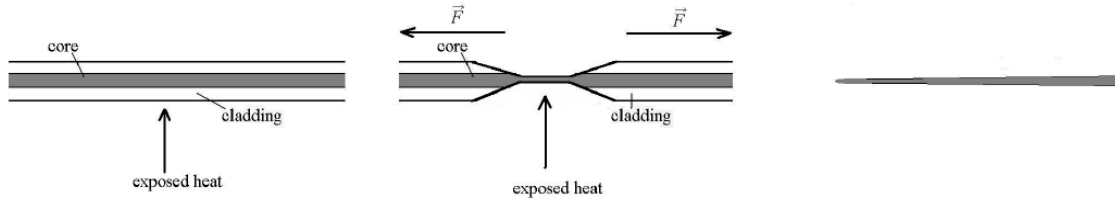


Figure 8: Illustration of the steps required to make a tapered fiber. This image is taken from the report of T. Siahhan [45].

While exerting force on both ends of the fiber, it was heated by the flame of a hydrogen micro-torch. The heated part starts to melt and elongates due to the exerted force. The fiber rapidly decreases in thickness until it splits up in two parts. Both parts now have a long and sharp tip that can be used for selective infiltration. The tip diameter after pulling is less than 1  $\mu\text{m}$ .

The fiber is fixed in a nano-manipulator stage where it can be moved in all three spatial directions with micro-scale precision using piezo-transducers. A schematic illustration of the stage is presented in Figure 9.

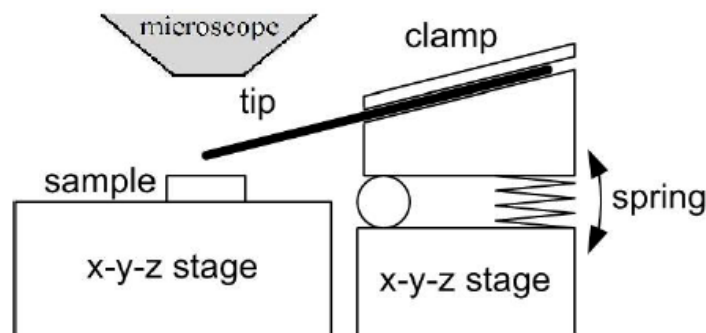


Figure 9: Schematic illustration of the stage used for selective infiltration of the PhC holes. The image is taken from the report of T. Siahhan [45].

The sample is positioned on another nano-manipulator stage underneath the tapered fiber tip. Before the sample is positioned on the stage, a droplet of liquid is placed on the sample close to the PhC structures using the needle of a syringe. Once the sample is on the stage, the fiber is used to pull small parts of the liquid from the relatively big droplet and drag it towards the PhC structure that will be infiltrated (see the microscope image on the left in Figure 10). This technique to manipulate liquid on a submicron scale was used by [35].

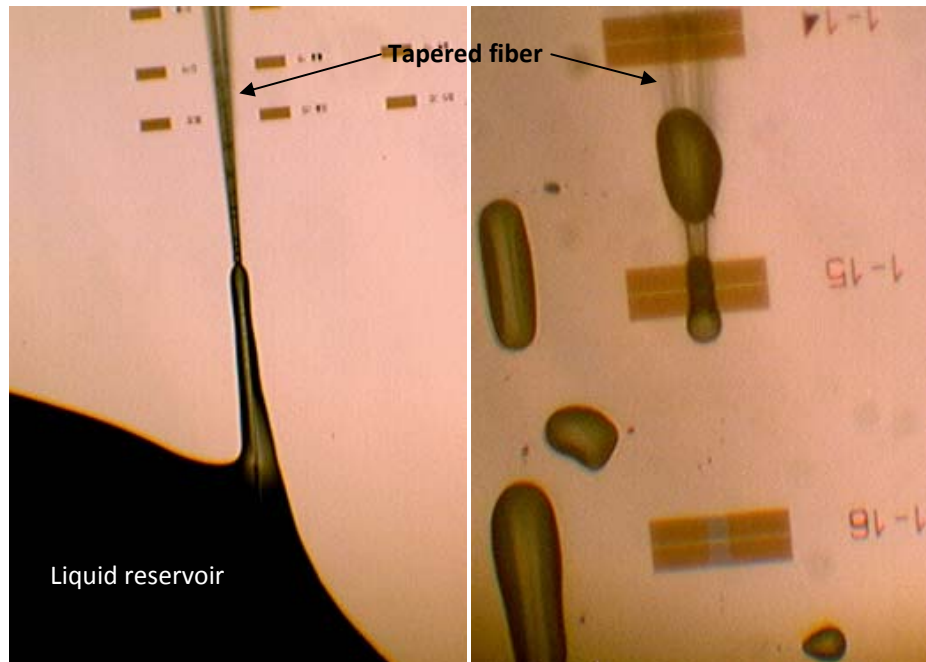


Figure 10: Optical microscope images used to illustrate the infiltration process. The scale can be inferred from the etched structures: one square is  $35 \times 13 \mu\text{m}$ .

There the tip of the fiber is used to pull small amounts of liquid over the PhC pattern, infiltrating the holes in its path (see the microscope image on the right in Figure 10). The fiber can also be used to produce small droplets that can be positioned on top of the PhC pattern as will later be explained in the experimental results. The photoluminescence setup that will be described in the next section can be moved over this stage. The microscope is used to view the sample while moving the liquid (Figure 10) and can at the same time be used to collect the far-field emission of the cavities.

### 3.4 Characterization

For the characterization of the structure, a customized scanning near-field optical microscope (SNOM) setup was used (Nanonics Multiview 4000). This is a photoluminescence (PL) setup that can be used to collect the emission from the structures in both the far- and the near-field. In the same setup the transmission spectrum can be measured using the end-fire method. Also the topography of the structures can be measured using Atomic Force Microscopy. For the experiments in this report only the PL part of the setup was used. A schematic of the setup is shown in Figure 11.

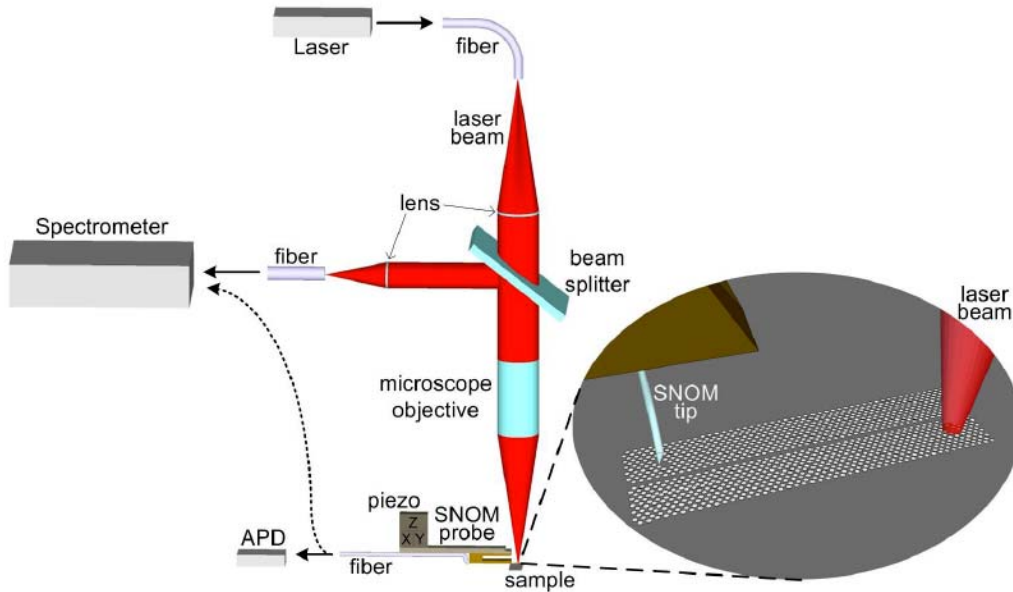


Figure 11: Schematic overview of the photoluminescence setup. This image is taken from the report of J. Voorbraak [42].

The setup is built on a vibration control table (WS-4 Compact Vibration Isolation Table). The sample is positioned on a nano-manipulator stage that can be moved in all spatial directions using piezoelectric controllers. The sample cannot be cooled and all experiments were performed in room temperature. A continuous wave red laser ( $\lambda=660$  nm) is focused on the sample by a high numerical aperture microscope objective (50x or 100x, N.A.=0.5) to excite the QDs in the center of the slab. The focused laser spot has a diameter of approximately  $3 \mu\text{m}$ , in which area the QDs are excited. The nano-manipulator stage on which the sample is positioned can be used to focus the laser spot on the desired position of the PhC pattern. Due to the size distribution of the QDs the emitted light is inhomogeneously broadened with a maximum in emission around  $1.5 \mu\text{m}$ . For the wavelengths of the light that match with one of the modes of the structure, the light can be trapped or guided.

The light that scatters from the structures is collected in the far-field using the same microscope objective as was used for the excitation. The objective sends the collected light through a beam splitter, after which it is focused on an optical fiber by a second lens. The fiber guides the light through a low pass filter after which it is focused into the spectrometer (Princeton Instruments Acton 2500i). The filter for light with wavelengths below  $1350$  nm is installed to block visible light and residual IR emission from the laser. Also for wavelengths above  $1575$  nm the collection of light is limited due to a decreased efficiency of the detector system. In the spectrometer the light is dispersed by either a  $300$  g/mm or a  $600$  g/mm grating after which it is detected by liquid nitrogen cooled InGaAs array. For the range of wavelengths around  $1.5 \mu\text{m}$  the gratings, in combination with the pixels of the photodiode array, have a spectral resolution of  $0.7$  nm and  $0.4$  nm for the two gratings respectively. The quality factors of the measured resonances are therefore limited by the spectrometer resolution to  $3500$  and  $2200$  respectively.

The emission of the structures can also be collected in the near-field, using the evanescent waves of the structure. The light of the modes that resonate in the structure is confined to the plane by total internal reflection. The interface between the dielectric slab and the air allows the light to penetrate

the air surrounding the slab, where its intensity decays exponentially with the distance from the slab (see Figure 12).

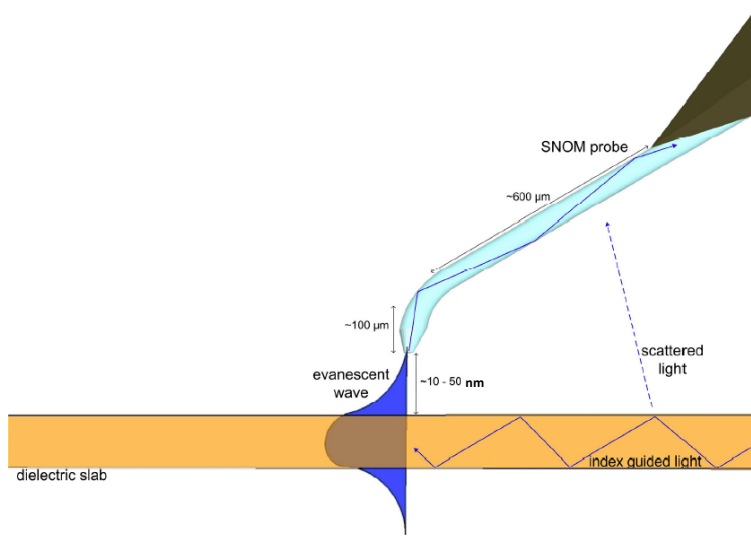


Figure 12: Schematic overview near-field probing method. This image is taken from the report of J. Voorbraak [42].

This evanescent light can be coupled to a tapered optical fiber tip, after which it is guided to the spectrometer.

For the fiber to be able to collect the evanescent light, the tip has to be brought very close to the sample surface. To achieve this, the tapping-mode feedback technique is used. A schematic representation of this part of the setup is shown in Figure 13. The fiber is mounted on another nano-manipulator stage with a tuning fork in between. A dithering piezo-element is used to oscillate the fiber at its resonance frequency, perpendicular to the sample surface. The tuning fork can also be used to measure slight changes in the amplitude of the optical fiber. When the fiber tip interacts with the samples surface, by for example dipole-dipole interactions or Van der Waals or electrostatic forces, the change in the amplitude is registered by the tuning fork and the fiber is retracted by the piezoelectric element. This way the tip is kept at a constant, close, distant to the sample surface where it can couple to the evanescent light of the structure.

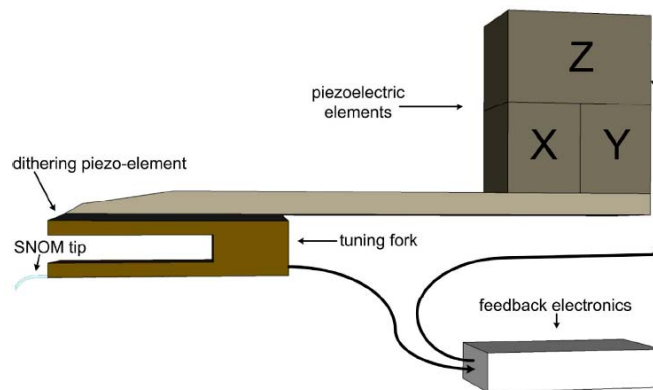


Figure 13: Schematic overview of the tapping-mode feedback system. This image is taken from the report of J. Voorbraak [42].

The SNOM tips that are used in this setup have a different shape than conventional SNOM tips. Due to the two bends in the fiber (see Figure 12) it is easier to use it in tapping mode, since the shape of the fiber acts like a cantilever. Another advantage of the shape is the fact that with this design it is possible to measure the PL simultaneously in the far field at the position of the excitation.

Collecting the emission of the structure using SNOM does not require that the excitation is at the position as the collection. The laser can be focussed on one part of the cavity while the SNOM can collect the emission at another spot. This is an important feature for measuring the Fabry-Perot modes in different positions in the DHS cavities described later in this report.

The microscope can be rotated on the vibration controlled table and be moved over the infiltration setup, as was mentioned before. This way the far-field PL can be measured directly after infiltrating the PhC holes with liquid. This is not possible for the SNOM setup and the sample has to be moved from the infiltration stage to the SNOM stage to measure the near-field PL.

## 4. In-situ reconfigurable opto-fluidic double hetero structure cavities

### 4.1 Introduction

It was the group of Song et al. [46] who first designed a hetero-interface in a PhC waveguide by changing the overall lattice constant of one side of the PhC waveguide. The shift in the band-gap resulted in high reflectivity of the interface for certain wavelengths of light propagating on one side of the interface.

The same group reported the first double-hetero structure (DHS) [47], where for a small part of the waveguide the lattice constant was increased in the direction of the waveguide. Due to the local shift of the band-gap and the waveguide modes, the light becomes trapped in the adjusted part of the waveguide, resulting in a high quality factor cavity.

Different ways of fabricating a cavity in a PhC waveguide were proposed. The group of Kuramochi et al. [48] showed that locally shifting the holes close to the line defect (perpendicular to the waveguide) resulted in high-Q cavities. Asano et al. [49] and Tomljenovic-Hanic et al. [50] proved that a more Gaussian profile of light confinement results in higher quality factors. Asano et al. proved that the Q is then ultimately limited by fabrication errors. Tomljenovic-Hanic et al. suggested that the Gaussian profile can be reached by selective exposure of photosensitive materials on top of the PhC pattern. The exposure results in a permanent refractive index change of the material.

The group of Mock et al. [51] investigated the different modes in a PhC DHS and demonstrated the possibility to suppress certain modes in the cavity. They also showed that the Q-factor increases when the mode is less tightly bound.

Tomljenovic-Hanic et al. [52] proved theoretically that DHS cavities can be made by local air-holes infiltration. This can be done any time after the fabrication process. They suggested that the smooth surfaces and interfaces together with a more gradual confinement of the light should result in higher quality factors. This was first confirmed by Smith et al. [35], where they used a micropipette to infiltrate the holes with liquid. They also showed how the quality factor of the cavity depends on the width of the infiltration [36]. They demonstrated the possibility to remove the fluid by rinsing the structure with toluene. This makes the cavity reconfigurable, in the sense that it can be made and re-established, but only after a chemical processing step.

Bedoya et al. [53] investigated the infiltration and evaporation of liquid induced DHSs. They presented the possibility of liquid crystal infiltration, by using a 50nm spatial resolution micromanipulator and subsequently investigated the spectra of the cavity while the liquid evaporated. They showed that the cut-off frequency of the DHS cavity is a measure of the total volume of liquid in the holes and possibly on top of them. The cavity length (together with the dispersion function) determines the spacing between the Fabry-Perot (FP) resonances.

In the present investigation the experiments of Smith et al. and Bedoya et al. are reproduced for verification. As a next step the goal was to examine the control of the cavity size by selective infiltration of liquid in the PhC pattern. Furthermore the possibility of manipulating the cavity by relocating the liquid using laser light driven motion would be investigated. The future goal is to



control the local evaporation of the liquid and therefore show the controlled in-situ reconfigurability of the DHS nanocavity.

The existence of the DHS cavity is in all cases based on an increase in effective refractive index in a small part of the PhC line defect. The local index change results in a mode-gap which locally traps the light, leading to resonances in the cavity. Tomljenovic-Hanic et al. [54] show that it indeed suffices to change the refractive index of the background material. They consider different background-fillings of the PhC pattern: single layer on top of the PhC pattern, a layer on top of- and below the PhC pattern, only filling the holes of the PhC pattern and filling the holes with a layer on top of the PhC pattern.

In the second part of this experiment the possibility of inducing a DHS cavity by positioning nano-droplets on top of the fully infiltrated PhC pattern is investigated. The dispersion for a corresponding type of structure is presented in the work of Tomljenovic-Hanic et al. [54]. Although their calculations show a small mode-gap, they describe a working DHS cavity for a similarly small mode-gap. This indicates that it should also be possible for a droplet on top of the fully infiltrated PhC pattern. The droplet induced DHS should result in an increase in effective refractive index and give a more smooth confining potential for the light. This should result in a high quality factor DHS nanocavity. Also the droplet can be easily positioned on and removed from the PhC pattern surface, making it an easily reconfigurable process.

## 4.2 Double hetero structures induced by selective infiltration

### 4.2.1 Description of the experiment

The measurements presented in this chapter were performed on a so-called L60 cavity. This type of cavity is the same as a normal PhC waveguide, except for the fact that in this case the waveguide is closed by PhC holes on both sides that reflect the propagating light. The length of this waveguide part was in this case 60 periods long. The reflections result in higher order standing waves called Fabry-Perot resonances. The use of a finite length, closed waveguide section, is not a limitation for the infiltration experiments. On the sample several L60s were fabricated with three different lattice constants  $a$ : 445nm, 435nm and 425nm, in all cases with an  $r/a$  of 0.3. The increase in lattice constant results in bigger cavity lengths and therefore red-shifts the modes in the pattern. In this experiment only the 425nm lattice spacing was used. The L60 cavity width was  $a \cdot \sqrt{3}$ , the same as a W1. This cavity was chosen for having the even and the uneven waveguide mode in the range of the monochromator in both the empty and the fully infiltrated configuration. The liquid that was used is a very low vapour pressure oil to minimize the evaporation under normal operating conditions. Evaporation severely affects the experiments due to the small amount of liquids involved [53]. The oil is a polyphenyl ether, with trade name Santovac 5, used in oil diffusion pumps. Its refractive index is 1.63.

The sample is positioned on the infiltration stage described before and infiltrated with DPO using the tapered optical fiber. A small stripe of holes, perpendicular to the waveguide direction is infiltrated to induce a DHS cavity. The infiltrated configuration can be observed from the contrast in the microscope image and is confirmed by measuring the spectrum. The microscope is used for both the excitation of the quantum dots and the collection of the far-field emission of the cavity. This means that only slow-light modes can be collected with this method. When the dispersion-function reaches

the Brillouin-zone borders, it is almost flat. This results in a group-velocity of these modes that is almost zero. These modes are called slow-light modes and most parts of their light scatters at the same spot as where they were excited. Since the collection is done by the same objective and thus on the same spot as the excitation, far-field PL can only be used to measure the slow-light modes. To measure the FP-modes of the liquid-induced DHS the SNOM setup is used to collect the near-field emission.

#### 4.2.2 Waveguide dispersion calculations

First the structure was simulated using MEEP. The dispersion diagram of the waveguide was calculated for the empty and the fully infiltrated case. From such calculations, the existence of a DHS cavity and approximate resonance positions can be deduced. A unit cell was defined with periodic boundary conditions, mimicking an infinite long waveguide. The cavity was excited with a Gaussian light pulse and after 500 time steps of FDTD the resonances were calculated in the  $\Gamma$ -K direction. The simulation results were combined and shown in the graph in Figure 14.

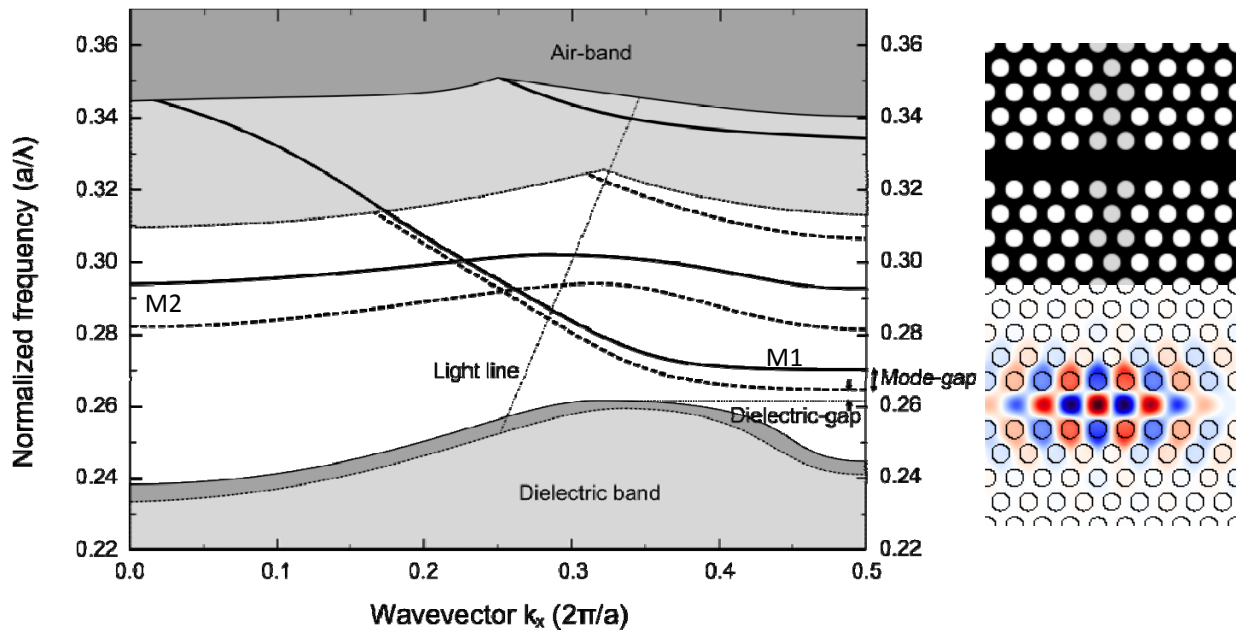


Figure 14: Left: dispersion diagram of a W1 when the holes are empty (solid black lines) and when the holes are filled with DPO (dashed black lines). Right-top: the configuration used for simulation, a W1 waveguide with three columns of infiltrated holes. Right-bottom: the simulated  $H_z$ -field of the even mode in the DHS infiltration.

The solid black lines show the waveguide modes, dielectric- and air band of the empty PhC pattern, and the dashed black lines those of the fully infiltrated PhC holes (the undercut and top layer are empty). The slow-light even-mode (at  $k_x=0.5$ ) is called M1 and the slow-light uneven-mode (at  $k_x=0$ ) is called M2. The infiltration results in an increased effective refractive index, red-shifting the modes and the photonic bands. When a small part of the PhC is infiltrated in the configuration shown on the top-right in Figure 14, the light with frequencies in the mode-gap cannot escape the infiltrated area as described before. As can be seen from the dispersion, light in the M1 mode in the infiltrated section (dashed black line) cannot couple to either the M1 mode or the dielectric band in the adjacent un-infiltrated areas. The light will reflect from the interfaces and form standing waves. These Fabry-Perot modes will exist only in the mode-gap. At the high-frequency side they are cut-off because the radiation leaks into the un-infiltrated part of the waveguide, causing excessive losses. At

the low-frequency side, they are cut-off by the cut-off of the infiltrated waveguide dispersion relation edge. The liquid infiltrated DHS cavity was simulated and the  $H_z$ -field of the first order M1 mode is shown in the bottom-right in Figure 14.

### 4.2.3 Experimental results

Before the infiltration the L60 cavity is measured with far-field PL, as shown in Figure 15. The spectrum is very similar to that of an infinitely long waveguide.

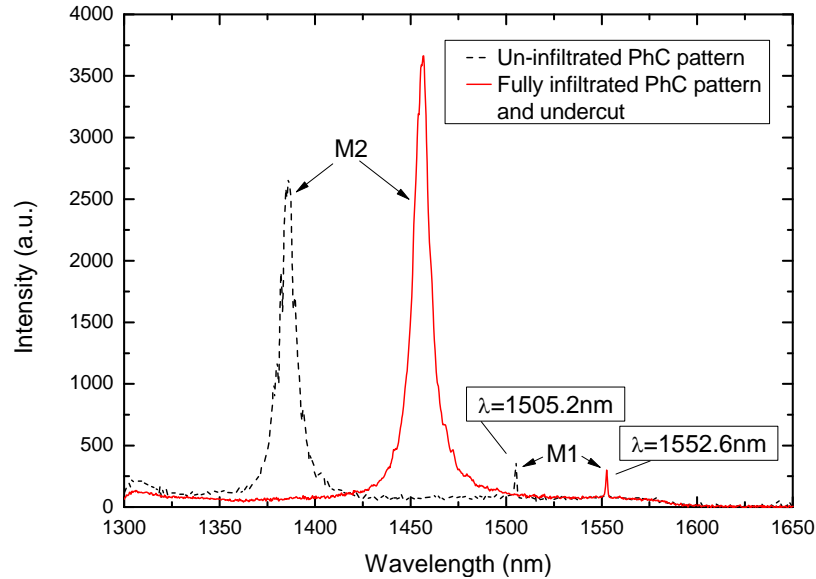


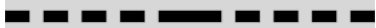


Figure 15: Spectrum of the empty (dashed black line) and the fully infiltrated (solid red line) L60 cavity.

At the end of this experiment the PhC pattern is fully infiltrated and the far-field PL spectrum is also shown in Figure 15 as a reference for the rest of the experiments in this chapter. The spectra show the broad M2 mode and the sharper M1 mode at higher wavelength. The M1 mode is the most interesting one, because it has a high quality factor, and will be investigated throughout this experiment. The low intensity of the even mode is due to the good in-plane confinement of this mode. After infiltration the M2-peak is red-shifted by 70nm, the M1-peak is red-shifted by 47nm. The calculated red-shifts from Figure 14 are 32nm for the M1-peak and 62nm for the M2 peak. These calculations were performed for a PhC pattern where only the holes are infiltrated with DPO. The infiltrated spectrum shown in Figure 15 was taken from a fully infiltrated structure. The measured red-shift is larger than the red-shift calculated from Figure 14, which means that there is probably also liquid in the undercut. The calculations were repeated for the same PhC pattern. First with a DPO filled undercut and second with a filled undercut and a layer of DPO on top of the PhC pattern. The results are shown in Table 1.

Table 1: Red-shift of the M1 and the M2 mode between the empty PhC pattern and three different types of infiltration.

Pattern used for simulation	Red-shift in M1 (nm)	Red-shift in M2 (nm)
	32	62
Experiment Figure 15	47	70
	56	90
	77	116

From these calculations it can be seen that there is indeed more liquid above or below the PhC pattern in the spectrum in Figure 15. The calculations also show that the M1 mode is more sensitive to a change in refractive index above or below the PhC pattern than for a change in the refractive index of the holes. This is reasonable for a mode that is strongly confined to the waveguide and does not penetrate into the PhC very deep.

The emission of the empty L60 is also collected in the near-field using SNOM and shown in Figure 16

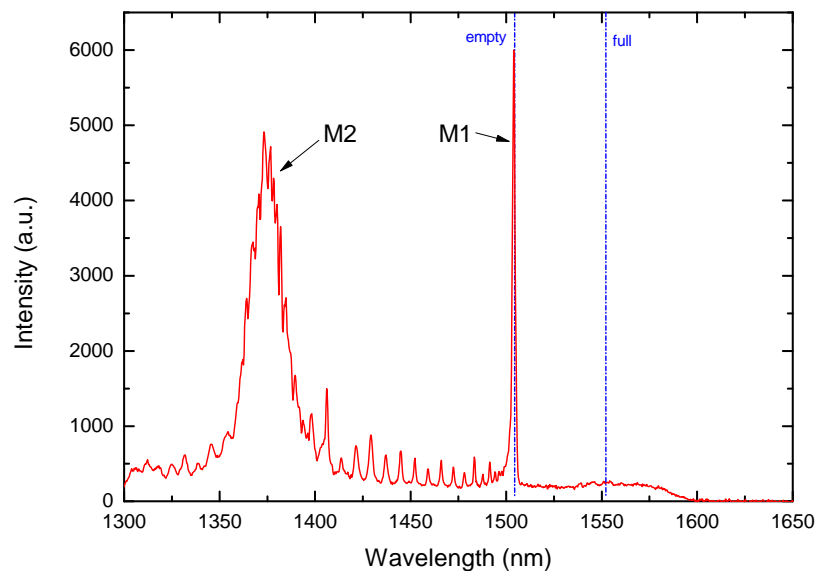


Figure 16: spectrum of the empty L60 cavity collected in the near-field using SNOM. The reference far-field spectra of the empty and fully infiltrated PhC pattern are shown with dashed blue lines.

The spectrum shows a sharp and intense M1 mode and FP-resonances above the cut-off frequency. The SNOM tip extracts light from the evanescent field and therefore is more sensitive for light that weakly scatters. In this spectrum the asymmetry of the M1 mode is clearly shown. The collection starts abruptly at the cut-off frequency of the dispersion, but decreases more gradually towards higher frequencies. The spectrum reflects the density of states (DOS) of the M1 mode, which is inversely related to the slope of the dispersion relation. At the cut-off frequency of the M1 mode the

slope is almost zero resulting in a high DOS. The dispersion slowly increases its slope with increasing frequency, resulting in a more gradual decrease in intensity seen in the spectrum.

### *Selective, partial infiltration*

In the next step the L60 is partly infiltrated forming a DHS and subsequently measured with far-field PL at several positions in the waveguide. The spectra and microscope image are shown in Figure 17.

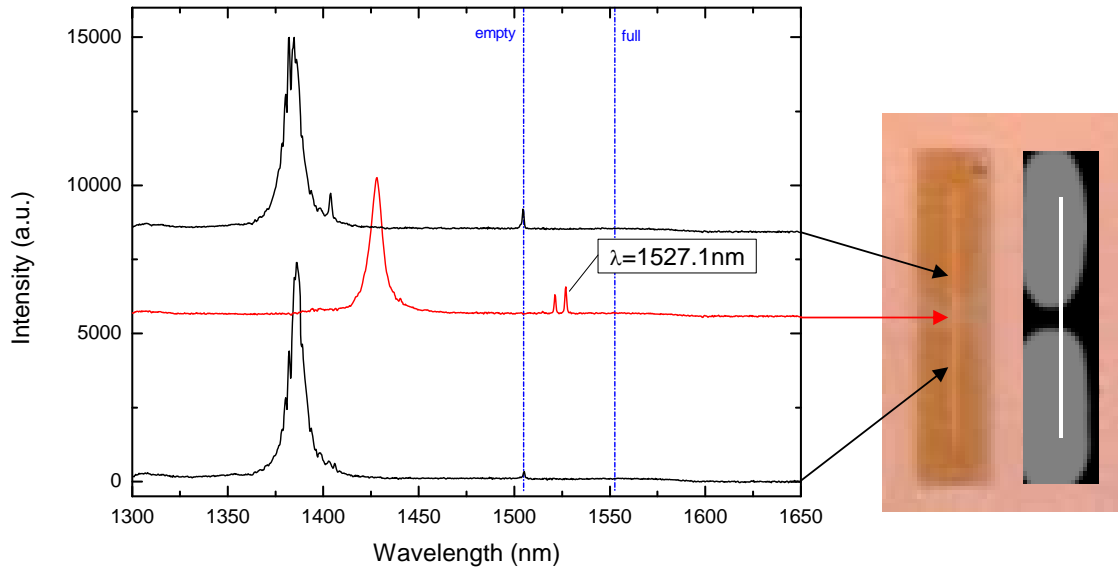


**Figure 17:** Far-field PL spectra of the DHS infiltrated L60. With two spectra taken right next to the infiltration (solid black lines) and one spectrum taken from the infiltrated area (solid red line). The positions of the respective waveguide cut-off frequencies of the empty and fully infiltrated PhC pattern are shown with dashed blue lines. To the right a microscope image of the infiltration is shown together with a schematic to indicate the areas filled with liquid (black). The total PhC pattern is 34.4 $\mu$ m long.

The spectrum taken in the un-infiltrated area still shows the empty-spectrum seen in Figure 15. In the part of the L60 that is infiltrated with liquid, the cut-off cavity mode is 22nm red-shifted from the empty PhC pattern M1 mode. This means that the mode is already close to the calculated 32nm red-shift for a PhC pattern with only the holes infiltrated (see Table 1). The fact that the cavity mode is at a smaller shift, could be a result of shallow infiltration in the holes and thus an overall smaller amount of liquid than for the calculated case, or it could be due to the small size of the DHS cavity. More calculations on this will be presented later. Also second resonance can be seen, tentatively attributed to a higher order FP-resonance of the infiltrated waveguide section. As described before, when higher-order standing waves in the DHS-cavity reach the cut-off frequency of the M1 mode in the empty waveguide, they can couple and propagate in the rest of the waveguide. More assignment is difficult if only two modes are present.

To confirm the DHS infiltration the spectrum of the L60 is measured using SNOM again. The result is shown in Figure 18.

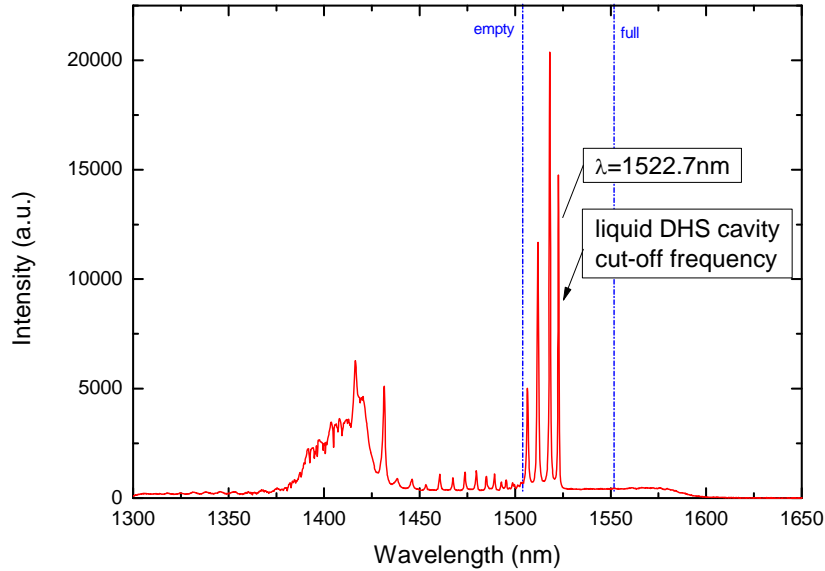


Figure 18: SNOM spectrum taken with both the laser spot and the SNOM-fiber in the infiltrated area. The reference spectra of the empty and fully infiltrated PhC pattern are shown with dashed blue lines.

The spectrum shows very sharp DHS cavity modes and also the expected cut-off when reaching the wavelength of the un-infiltrated waveguide M1 mode. A Lorentz-fit of the cut-off frequency mode gives a Q of  $\sim 2800$ . The FWHM of the modes in the spectrum are limited by the resolution of the spectrometer. This means that it is not possible to give an indication of the quality factor of the modes other than that they are above  $\sim 2000$ . It is difficult to discuss the free spectral range (FSR) of the FP-resonances for the liquid induced DHS cavity. The small cavity-size should result in a larger FSR than the L60 cavity but is decreased due to the small slope of the dispersion relation. In Figure 16 it can be seen that the FP-resonances close to the M1 are indistinguishable due to the resolution of the spectrometer.

#### 4.2.4 Multiple infiltrations and reconfigurable infiltration

The intention of the experiment was to show the dependency of the DHS modes on the width of the infiltration. The optical fiber would be used to show controlled infiltration of several different widths. Furthermore it was planned to use the laser to locally remove liquid from the PhC pattern to show the reversibility of the liquid infiltration.

The sample with the L60 was not suitable for multiple infiltrations due to the alignment of the undercut. This can be explained with the cross-sectional SEM images shown in Figure 19.

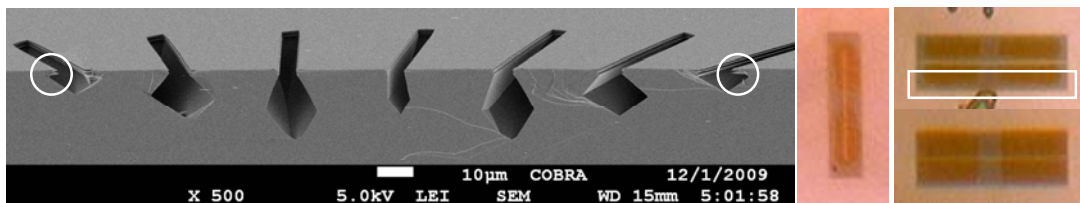
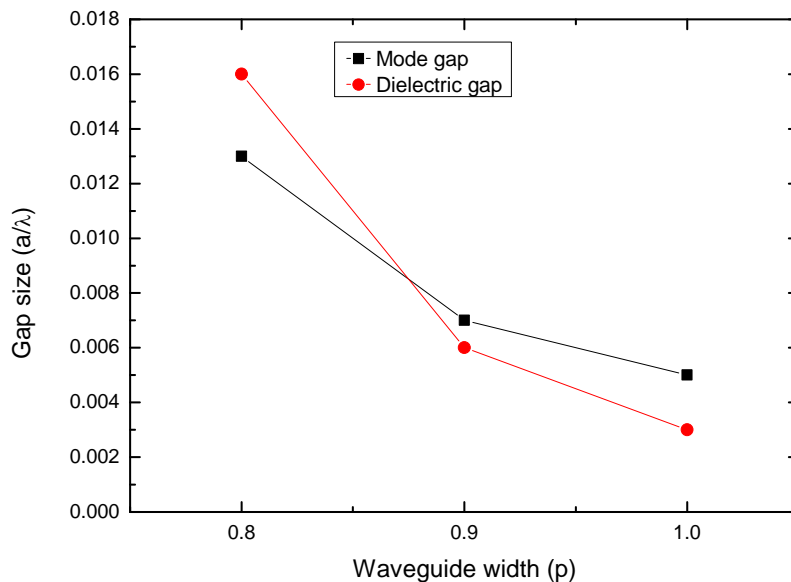


Figure 19: Left: cross-sectional SEM of wet-chemically etched structures under different angles with respect to the substrate orientation. The fabrication and SEM imaging are done by Leonardo Midolo. Middle: microscope image after the second DPO infiltration in the L60 cavity used in the experiments before. Right: microscope images of W1 waveguides after single line DPO infiltration. The structures are aligned perpendicular to each other on the sample.

From these SEM images it can be seen that the form of the sidewalls of the undercut depends on the orientation of the structure on the substrate. This is due to etching-stop planes, where certain InP crystallographic planes of the substrate prevent etching. When the sidewalls are close to the membrane, like the outer most left and right structure in the SEM image, capillary forces infiltrate the holes at the border of the PhC pattern. An example is shown in the left microscope image in Figure 19. This is the result of a second infiltration in the L60 cavity used in these experiments and shows liquid in the holes at the boundary of the PhC pattern.

A new sample was fabricated (with waveguide structures) where the structures were duplicated and positioned perpendicular to each other on the substrate. This was done to make sure at least one set of structures was useful for the experiment. The importance of the undercut can clearly be seen from the microscope images on the right in Figure 19. Two exact copies of PhC waveguide structures are infiltrated. They are positioned perpendicular to each other on the substrate. The top image shows liquid infiltration around the boundary of the structure, while the bottom PhC pattern shows a clean line-infiltration.

A more fundamental improvement of the new sample was a waveguide design with different waveguide widths to increase the distance between the infiltrated M1 mode and the band-edge of the empty PhC pattern. The dispersion diagram was simulated for W0.9 and W0.8, where the width of a  $Wp$  waveguide is  $p \cdot a\sqrt{3}$ . The mode gap and the dielectric gap are shown for three waveguide widths in Figure 20. It is thought to be important to separate the infiltrated waveguide dispersion from the dielectric edge [52].



**Figure 20: Mode gap between the even mode of the empty and fully infiltrated PhC pattern (black squares). Dielectric gap: distance between the fully infiltrated PhC pattern even mode and the band-edge of the empty PhC pattern.**

A definition of the gaps is given in Figure 14. The mode gap is the frequency difference between the even mode of the empty and the fully infiltrated PhC waveguide. The dielectric gap is the frequency difference between the M1 mode of the fully infiltrated PhC pattern and the band-edge of the empty PhC pattern. From the graph in Figure 20 it can be seen that the dielectric gap increases when the width of the waveguide is decreased. The reason is that the effective waveguide index decreases

when it becomes narrower, which moves its dispersion up. Also the holes become more important so that the effect of filling them is more significant. The gap increase will result in smaller losses from light scattering into the dielectric material. For the same reason the mode-gap increases when the waveguide becomes narrower, resulting in stronger confinement of the DHS cavity modes.

For the W1 waveguide several widths of infiltration were simulated (analogous to Figure 14 on the right) to obtain the cavity resonances and Q factors. The results, together with the empty and fully infiltrated even mode waveguide edges, are shown in Figure 21.

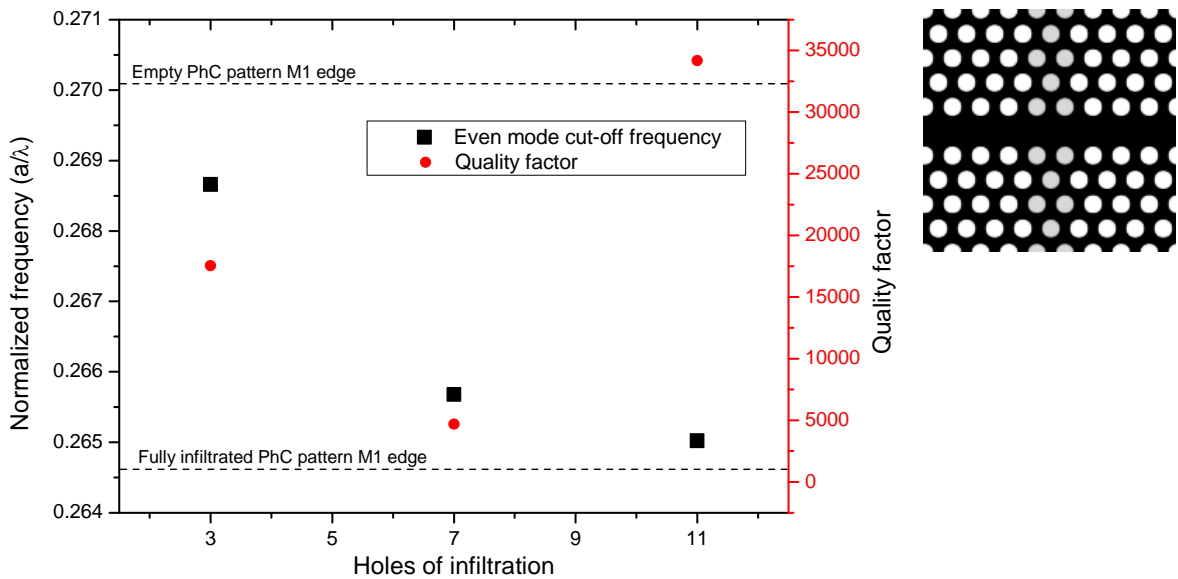


Figure 21: Left: simulations of the liquid DHS cavity resonances with 3, 7 and 11 columns of holes infiltrated with DPO. For reference, the M1 mode of the empty PhC pattern and the fully infiltrated PhC pattern are shown (dashed black lines). Right: the configuration used for simulation, a W1 waveguide with three columns of infiltrated holes.

It can be seen that the liquid DHS cavity cut-off frequencies are positioned nicely between the M1 mode of the empty and the fully infiltrated PhC waveguide. As described in [53], the cut-off frequency of the cavity is a measure of the amount of liquid infiltrated in the PhC pattern. It is also shown that high quality factor cavities can be made by infiltration and that stronger confinement (fewer columns of liquid) results in a decrease in quality factor (as shown in [51]).

The microscope image in Figure 17 shows a cavity of 7 to 8 columns of infiltration. The calculations in Figure 21 show that the cut-off frequency of the DHS cavity modes should indeed be close to the fully infiltrated M1 mode. The calculated red-shift for 7 columns of infiltration is 26nm, which means that indeed the holes are not fully infiltrated in the results in Figure 17, where a red-shift of 22nm was observed.

For seven columns of infiltrated holes, the cavity resonances are simulated for W1, W0.9 and W0.8 PhC waveguides and shown in the graph in Figure 22.



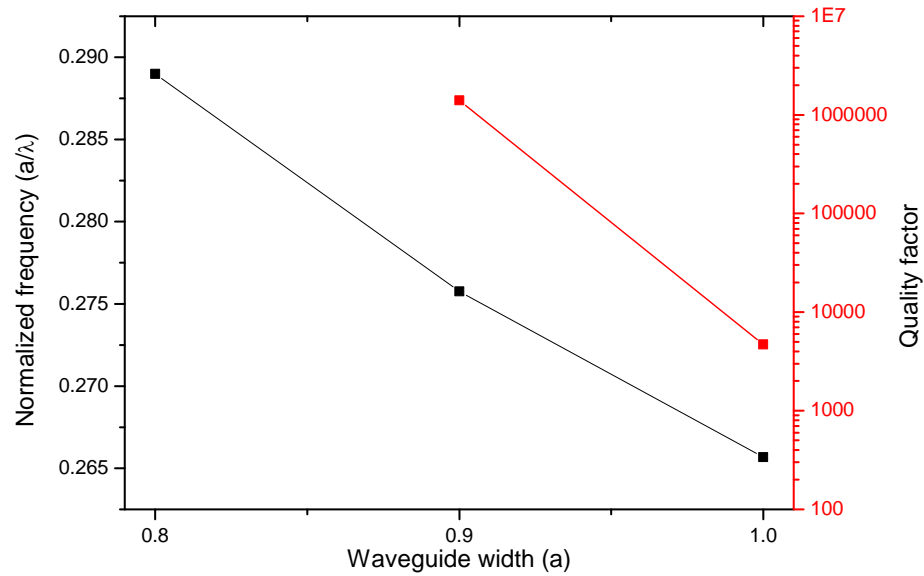


Figure 22: Simulation of the cavity resonances of liquid DHS infiltration of seven columns as a function of the waveguide width.

It can be seen that a decrease in waveguide width results in a strong increase in quality factor, which was already predicted from the increase in dielectric gap shown in Figure 20. The software used for the simulation could not cope with the W0.8 M1 mode. It managed to simulate the mode profile but could not calculate the quality factor of the mode. Note that the Q-factors in Figure 22 tend to be extremely large, which makes it extremely demanding to reliably calculate them. While the absolute quality factor of the calculations might not be reliable, the large relative change from W1 to W0.9 is a good motivation to fabricate the structure for experiments and measure Q-factors experimentally.

#### 4.2.5 Fabrication problems and a new photonic crystal cavity design

The sample that was fabricated to experimentally confirm the simulation results above did not show the expected results. The expected DHS cavity resonances were not found and several structures showed resonances at positions within the dielectric gap. To check the fabrication, the sample was cleaved and the cross-sectional SEM images are shown in Figure 23.

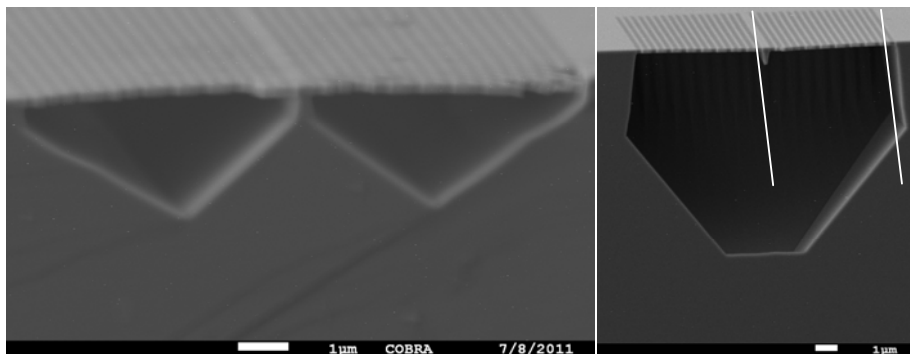


Figure 23: cross-sectional SEM images of the sample. The PhC patterns shown are fabricated on the same substrate and positioned perpendicular to each other.

In the left SEM image it can be seen that the membrane is not free from the undercut. The light in the waveguide cannot be confined by TIR and can scatter into the substrate. The effect of infiltrating

the boundary of the sample described before can be explained with this image. The liquid infiltrated in the holes on the boundary of the PhC pattern is pulled to the sides of the structure by capillary forces. Along the way, the holes are filled with liquid. In the top-right microscope image in Figure 19 it can be seen that also the holes right next to the line-defect are infiltrated with liquid, which can now be understood from the undercut in the left SEM image.

In the right SEM image we can see that the line-defect is not completely under-etched, which can be explained from the stop-planes in the chemical etching process. The side facet of the ridge underneath the waveguide is parallel to the side-walls of the undercut (as shown with the parallel white lines in the SEM image). This confirms that the side facets of the ridge are indeed stop-planes. The under-etching of the membrane starts from the holes and etches in the direction parallel to the waveguide. The line-defect does not have holes on the ends of the structure, which is probably why the ridge underneath the slab is not etched. It is known that selective under-etching of InP, is a delicate process because of etch stop planes. Here a standard process was used that is routinely used for PhCs with only slightly different geometries.

To be able to continue with the measurements described before, a new sample was designed. Images of the EBL design patterns are shown in Figure 24.

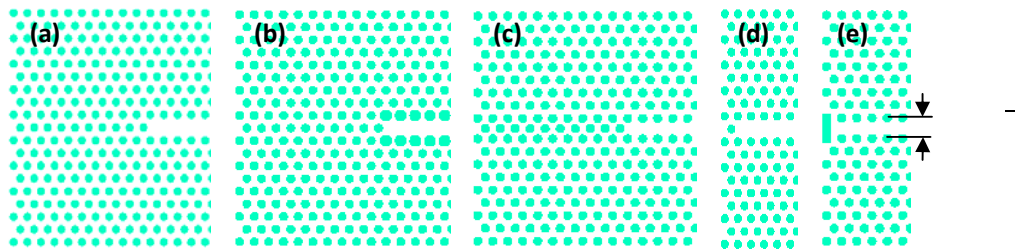


Figure 24: Pattern design for a new sample. Only a small part of the left side of the pattern design is shown to indicate important features of the design. (a) Normal L60. (b) L60 with the holes around the line-defect slightly increased in size. (c) L60 with a width of the line-defect of  $0.8 \mu\text{m}$ . (d) W1 waveguide with a single hole at both ends of the line-defect. (e) W1 waveguide with a trench at both ends of the line-defect.

All structures were again designed with waveguide width of 0.8, 0.9 and  $1 \mu\text{m}$  and varying lattice constants. To prevent the previously mentioned undercut problems, several different solutions were implemented. (a) shows the normal L60 cavity, used in the experiments in this chapter but this time the structures are aligned with the substrate to obtain undercut sidewalls as shown in the right SEM image in Figure 23. The increase in dielectric-gap can also be reached by increasing the radius of the holes surrounding the line-defect as shown in (b). Again several steps of hole radius increase are designed to investigate the result on the confinement. A 0.8-L60 (with a line-defect width of  $0.8 \mu\text{m}$ ) was proposed where the PhC patterns on both sides of the L60 cavity are moved closer towards each other to induce an effect similar to a W0.8 (c). The same was done for a 0.9-L60 cavity. Normal waveguide structures were designed with a single hole (d) or trench (e) at both ends of the line-defect. This should initiate the under-etching of line-defect from the sides of the structure.

Due to fabrication problems the designed patterns were not fabricated in time for this thesis.

#### 4.2.6 Conclusion

In the first part of the investigation the work of Smith et al. was repeated and high-quality liquid infiltration DHS cavity modes were observed with both far- and near-field photoluminescence. In the previous experiments, the cavity modes were observed using a strongly bend, tapered fiber coupled to the waveguide [53],[36]. This fiber taper interacts with the waveguide and could distort the modes. The far-field PL detection method does not disturb the modes, but gives poor signal. The SNOM tip used for the PL detection, due to its small size, has little influence on the modes, but yields a strong signal. Therefore it is well suited to couple to DHS cavities. The continuation of the work was to investigate the possibility of selective tuning of the cavity modes by controlling the width of the infiltration. Due to fabrication problems with the undercut of the membrane structures, the PhC patterns on the fabricated sample could not be used for the proposed experiments.

The DHS cavity modes and quality factor dependence on the width of the line-defect and amount of infiltrated columns of holes was simulated and the results were presented. Huge improvements in Q-factor are predicted for narrower waveguides. PhC pattern designs to solve the fabrication problems of the undercut of the structure were proposed. A new sample was designed, but not fabricated in time for this thesis due to delay in processing capabilities in the cleanroom.

## 4.3 Double hetero structures induced by micro-droplets

### 4.3.1 Description of the experiment

In this chapter a liquid DHS cavity similar to the one in the previous chapter is investigated using a droplet to induce a local increase in refractive index. The investigation continues with the fully infiltrated L60 cavity used in the previous chapter. The idea is that a droplet on an infiltrated structure is very mobile on the surface and can be easily displaced. This creates a mobile cavity in an optical circuit. The L60 cavity has a lattice constant of 425nm and an  $r/a$  of 0.3. The PhC pattern was fully infiltrated using the fiber stage. With fully is meant that a large droplet is repeatedly moved over the PhC pattern using the tapered fiber. As a result the pattern and undercut are saturated with liquid. The same DPO oil as described in the previous chapter is used for infiltration and for making the droplets.

The sample is positioned on the infiltration stage and the tapered optical fiber is used to position DPO droplets of various sizes on top of the fully infiltrated PhC pattern. The cavity is excited by the laser using the microscope objective. The emission is collected in the far-field using the same microscope objective. It is not possible to measure the near-field response of the cavity. The SNOM fiber would stick to the surface due to capillary forces once it would touch the liquid surface of the droplet.

### 4.3.2 Waveguide dispersion calculations

The proposed structure was simulated using MEEP. Again a unit cell was defined with periodic boundary conditions to mimic an infinitely long waveguide. The cavity was excited with a Gaussian light pulse at the beginning of the simulation. The FDTD simulation was continued for 500 time steps before calculating the resonances in the  $\Gamma$ -K direction. The combined results, together with the configurations used for simulation are shown in Figure 25.

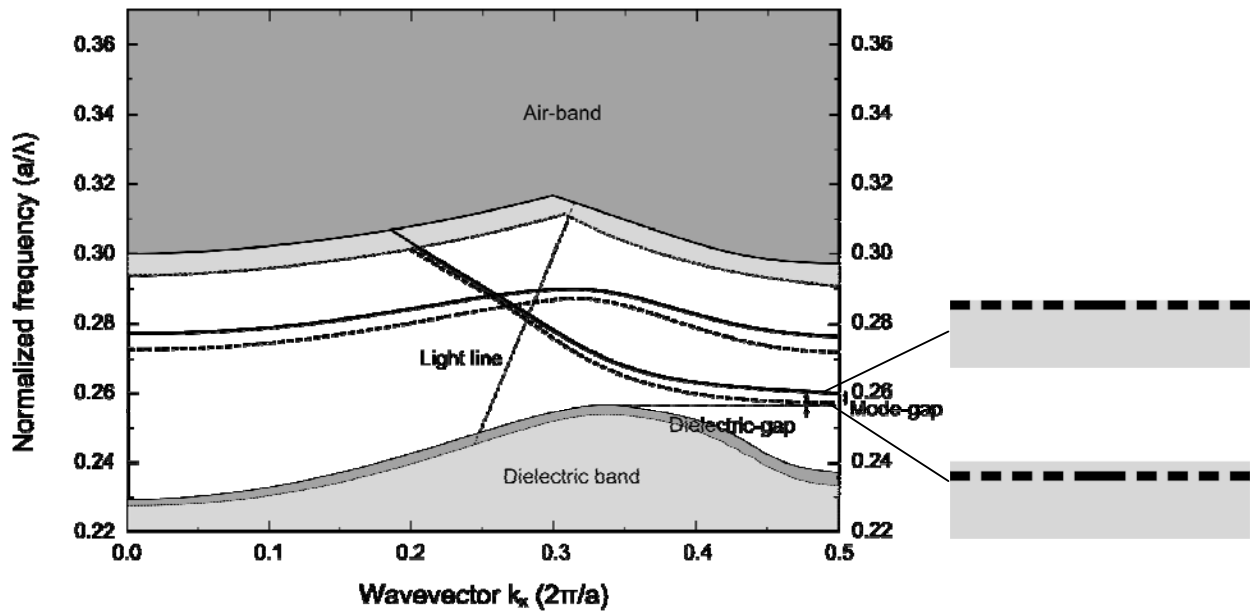


Figure 25: Left: dispersion diagram of a W1 when the holes of the PhC pattern and the undercut of the structure are infiltrated (solid black line) and with an additional layer of liquid on top of the PhC pattern (dashed black line). Right: side-views of configurations used for the simulations.

The solid black lines show the waveguide modes, dielectric- and air band of the configuration with infiltrated PhC holes and fully infiltrated undercut (shown in the top image on the right in Figure 25). This represents the fully infiltrated structure. The dashed black lines show the result for a configuration with filled PhC holes, undercut and a layer on top of the PhC pattern (shown in the bottom image on the right in Figure 25). This represents the part of the waveguide with a droplet on top of the PhC pattern. Again the slow-light even-mode (at  $k_x=0.5$ ) is called M1 and the slow-light uneven-mode (at  $k_x=0$ ) is called M2. The liquid on top of the waveguide results in an increased effective refractive index with respect to the fully infiltrated structure. This again results in a red-shift of the modes and the photonic bands.

When a droplet is put on top of the PhC pattern a DHS cavity, similar to the liquid infiltration DHS cavity is formed. As can be seen from the dispersion diagram in Figure 25, the light of the M1 mode with liquid on top of the PhC pattern cannot couple to the M1 mode in the part of the waveguide without liquid on top nor can it couple to the dielectric band. Modes excited in the droplet DHS cavity will reflect on the interface with the adjacent waveguide parts and form FP-resonances. These will again only exist in the mode-gap as shown in the dispersion diagram in Figure 25. At the low-frequency end they will be cut-off by the dispersion relation edge of the structure with a layer of liquid on top. On the high-frequency end they will be cut-off by coupling to M1 mode in the part of the waveguide without liquid on top. The mode-gap for the droplet DHS case is 21nm, which is narrower than the 32nm mode-gap for the liquid infiltration DHS case shown in Figure 14.

A droplet DHS cavity was simulated using MEEP. The configuration used for simulation, together with the results, are shown in Figure 26.

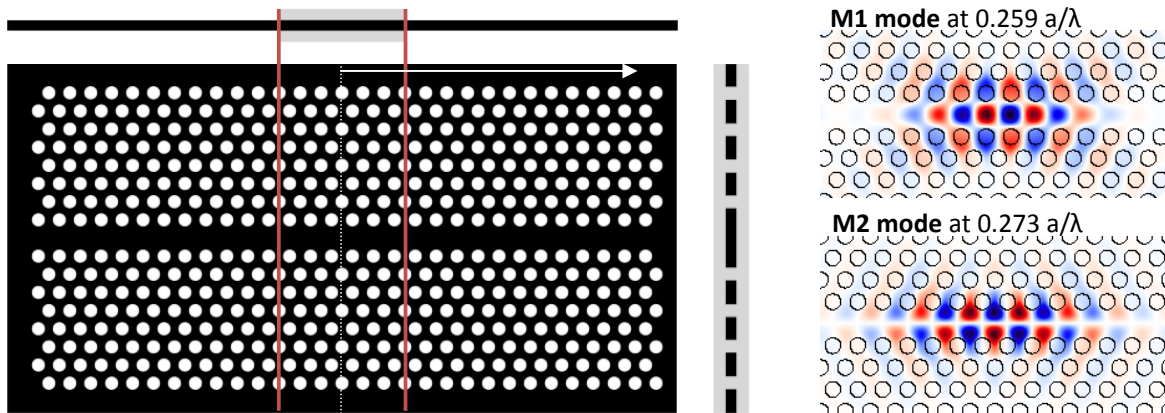


Figure 26: Simulation results of a droplet DHS cavity. On the left: the top and side views of the configuration used for the simulation. On the right: the simulated  $H_z$ -field of the M1 and M2 modes.

As can be seen in the top-left side view of the configuration in Figure 26, the undercut is not infiltrated. The simulation could not handle the large configuration without using symmetry in the z-direction. The structure of a droplet on top of the fully infiltrated PhC pattern is approximated by an extra liquid layer (~220nm) above and below the membrane. Still the simulations indicate that a droplet DHS cavity with the small mode-gap should be possible.

### 4.3.3 Results

A reference spectrum for these measurements is shown in the graph in Figure 27 and will be shown as dashed blue lines in the following spectra in this chapter.

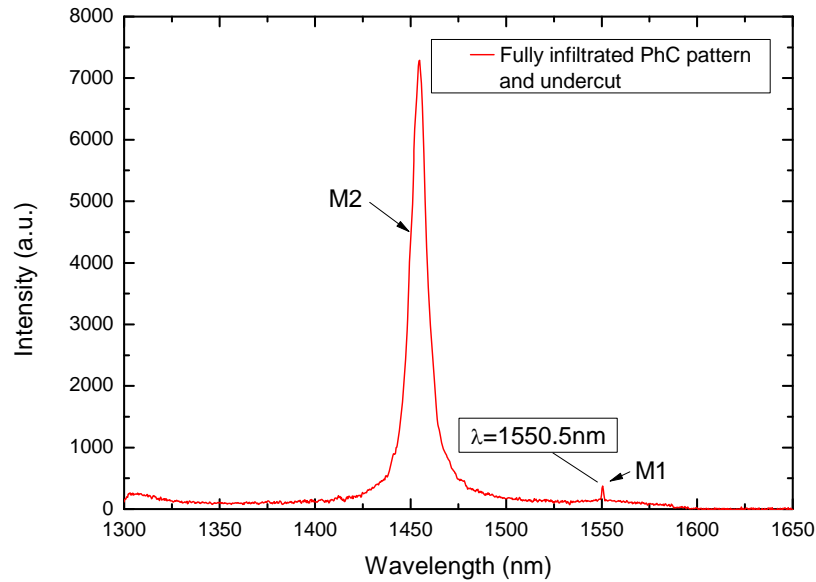


Figure 27: Spectrum of the fully infiltrated PhC pattern L60 cavity with a liquid filled undercut. This is a new measurement of the spectrum shown in Figure 15.

A droplet is positioned on top of the PhC pattern using the tapered fiber, as is shown in the microscope image in Figure 28. The far-field emission is collected and shown in the graph on the left in Figure 28.

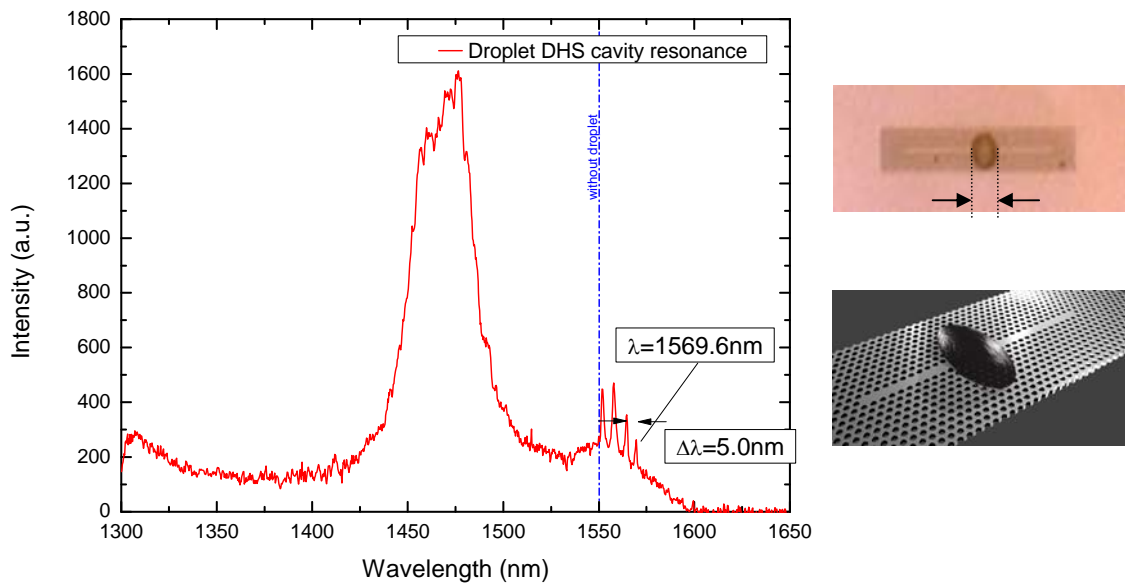


Figure 28: Left: Far-field spectrum of the droplet DHS cavity. Right: microscope image of the L60 with a droplet on top together with a schematic image for clarification.

In the graph a red-shift of 19nm can be seen, which is only a little smaller than the calculated 21nm mode-gap. The spectrum shows FP-resonances from the droplet DHS cavity, which are now visible even in the far-field collection. The in-plane confinement of the modes is probably decreased due to the decreased refractive index contrast. The interface between the droplet boundary and the rest of the waveguide results in a change in refractive index on top of the PhC pattern, which might cause

extra out of plane losses. Furthermore, from the calculation results in Figure 25 it can be seen that the dielectric-gap is very small, which might result in leaking of the droplet DHS modes to the substrate. This also results in a decrease in quality factor of the modes. The quality factor of the cut-off frequency mode, measured from the spectrum in Figure 28, is  $\sim 1300$ . In the previous chapter the importance of the dielectric gap for the quality factor was suggested from Figure 20 and Figure 22. The increase in out of plane scattering at the droplet interface explains why it is possible to measure the FP-resonance with the microscope objective. The FP-resonances are cut-off at higher frequency due to leakage to the M1 mode of the adjacent waveguide parts as expected. The droplet was measured to be 11 lattice constants long. As described before, it is difficult to discuss the absolute FSR of the FP-resonances. The FSR increases with decreasing cavity width but at the same time heavily depends on the slope of the dispersion curve (as explained in the previous chapter). The FSR is measured between the cut-off mode and the next higher order mode. For the droplet DHS cavity in this experiment the FSR was 5.0nm. The results in this spectrum show that it is indeed possible to induce a DHS cavity using a droplet positioned on top of a fully infiltrated PhC pattern.

The experiment is repeated for several sizes of droplets. For all the droplets the cut-off wavelengths and FSRs are measured and plotted as a function of the droplet size, as shown in Figure 29.

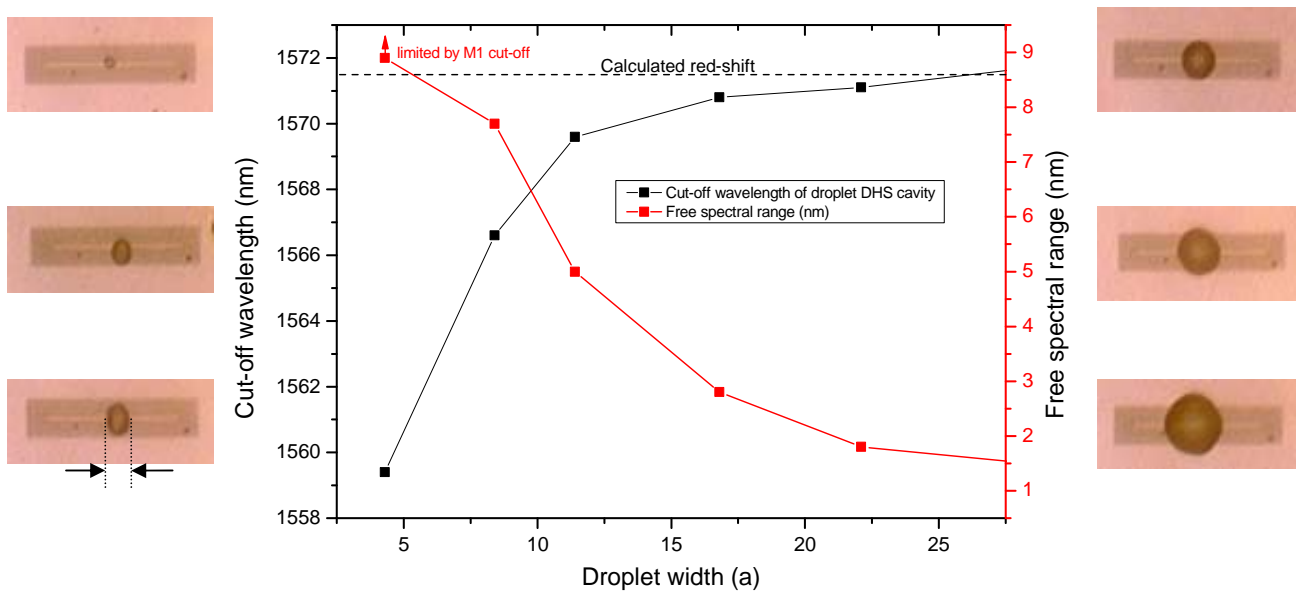


Figure 29: Center: DHS cavity cut-off wavelength and free spectral range as a function of the droplet diameter. Border: microscope images of the droplets.

The cut-off wavelength of the droplet DHS cavity as a function of the droplet diameter looks the same as the calculated infiltrated DHS cut-off frequency as a function of columns with infiltrated holes shown in Figure 21. In this case the cut-off wavelength depends on the total amount of liquid on top of the PhC pattern, as was expected for the modes in a DHS cavity. The FSR depends on the size of the cavity as is clearly shown in the graph. The smallest droplet, with a diameter of four lattice constants shows only a single mode below the M1 cut-off frequency of the adjacent waveguide parts. This means that the FSR is larger than the total red-shift of the mode.

The results presented above demonstrate a method to induce a DHS cavity on top of a waveguide, that can be positioned where desired. The cavity size can be changed by changing the droplet size

and can be removed from the PhC pattern without difficulty. The signal strength and quality factors shown in these results are rather small as a result of the small dielectric gap. They can be enhanced by using narrower waveguides. These narrower waveguides have been described and designed in the previous chapter. They could not be realized for practical reasons.

### *Mechanically tuneable DHS cavity*

The droplet DHS type of cavities can also be made with the tapered infiltration fiber in contact with the PhC pattern. The fiber by itself could not be used to induce a cavity, which is probably due to the poor optical contact with the waveguide. Also was it difficult to move the fiber into the laser-spot while in contact with the surface. Due to high friction the fiber would stick to the sample and slowly start to bend when moved further, until at one point the force surpasses the friction and fiber makes a jump to another position. By putting the fiber in a small droplet of DPO these problems are solved. The fiber is pulled to the sample surface by capillary forces once it touches the droplet. The fiber can then be retracted a small amount to decrease the friction with the sample. That way the oil functions as a lubricant for the sliding fiber. At the same time the liquid provides improved optical contact with the waveguide. The laser is focussed on the waveguide and optimized for maximum intensity. The fiber together with the small droplet is moved over the waveguide by piëzo-motors. When the droplet moves into the laser focus a DHS cavity is induced. Due to the transparency of the tapered fiber and the fact that the laser spot is larger than the fiber diameter the laser can still excite the quantum dots inside the PhC slab and the emission of the induced cavity can be collected by the microscope objective. A typical spectrum is shown in Figure 30.

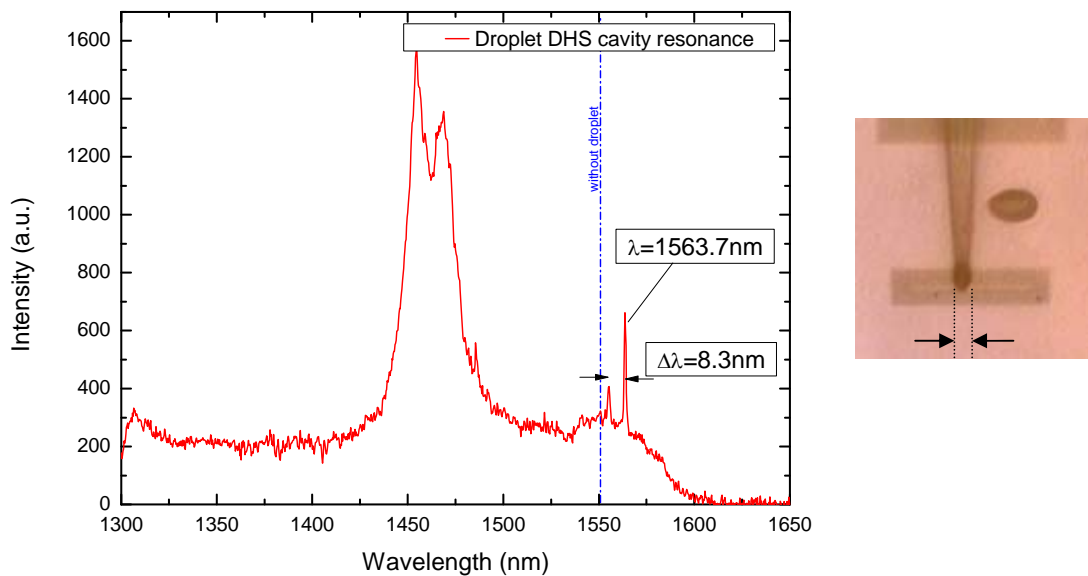


**Figure 30:** Left: Far-field spectrum of the droplet DHS cavity, with the tapered fiber inside the droplet. Right: microscope image of the L60 with the tapered fiber inside a droplet on top of the PhC pattern.

The cavity shows a spectrum similar to the droplet DHS cavity spectrum shown in Figure 28. The cavity can only be observed when the droplet is aligned with the laser spot, but can be moved to any position on the waveguide. The cut-off wavelength of the cavity is 1563.7nm and the FSR is 8.3nm. The width of the droplet on top of the line-defect is measured from the image to be  $\sim 7.6$  lattice constants wide. From the previous measurements in Figure 29 it can be seen that this cavity width fits perfectly with the measured FSR. The measured red-shift is smaller than what would be



expected from the graph in Figure 29. The cavity is not entirely made of the DPO but partly of the tapered optical fiber. The fiber has a refractive index of 1.47 [55], which is smaller than the refractive index of 1.63 of the DPO. This means that the effective refractive index of the cavity is smaller than that of a normal droplet which should indeed result in a smaller red-shift. Despite the small dielectric-gap the modes still show a quality factor of approximately 1500.

In the microscope image on the right in Figure 30, the tapered fiber can be seen coming from the top. The tip is inside the droplet that is on top of the line-defect. The cavity size can be controlled by moving the fiber perpendicular to the waveguide or by retracting/landing the fiber. This way several cavity sizes were formed with the FSR ranging from 5.9 to 8.3 nm. This means that cavity size with a single droplet was varied from 8 to 10 lattice constants (from Figure 29). The red-shift could be tuned between 1563.7 and 1568.0 nm.

### Smooth interface transition

As mentioned in the introduction, the droplet DHS cavity was expected to have an improved quality factor due to a smoother interface. Mock et al. [51] show that the Q-factor increases when the mode is less tightly bound and Tomljenovic-Hanic et al. [50] prove that a more Gaussian profile of light confinement results in higher quality factors. A droplet should provide a more gradual interface, where the refractive index changes gradually due to the curvature of the droplet surface. A high quality factor was not found in the experiments, which is probably a result of the small dielectric-gap. The difference in interface between the liquid infiltration and droplet DHS cavity was still observed in the experiments by watching the M2 mode when crossing the interface. From the liquid infiltration DHS cavity of the previous chapter a step-by-step profile has been made. The spectra are shown in Figure 31.

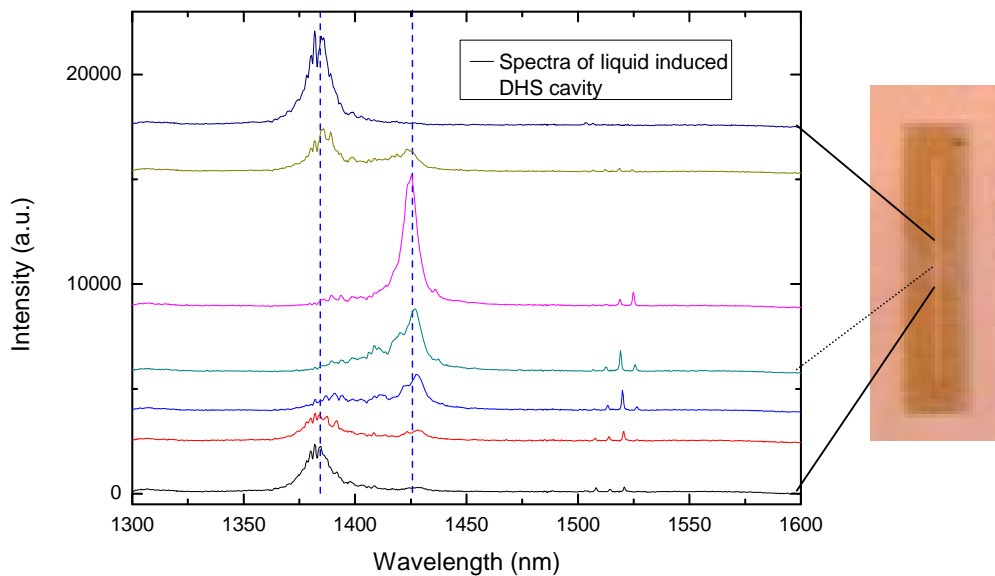


Figure 31: Left: spectra of the liquid infiltrated DHS cavity. The spectra form a step-by-step profile of the infiltration. Right: microscope image of the infiltrated PhC pattern.

The first (lowest) spectrum is taken below the infiltration and the last one above the infiltration, with several collections in between to form a profile of the infiltration. The first and the last spectrum show the broad M2 mode of the empty PhC pattern. The spectra inside the infiltrated area show the

red-shifted M2 mode. On the interface between the empty PhC pattern and the infiltration, both modes show up. Due to the size of the laser spot and the area of collection, both modes can be excited and are collected by the objective. There is no clear mode that exists between these two modes, caused by an averaged effective refractive index on the interface of the infiltration.

The same profile was measured for a droplet DHS cavity and is shown in Figure 32.

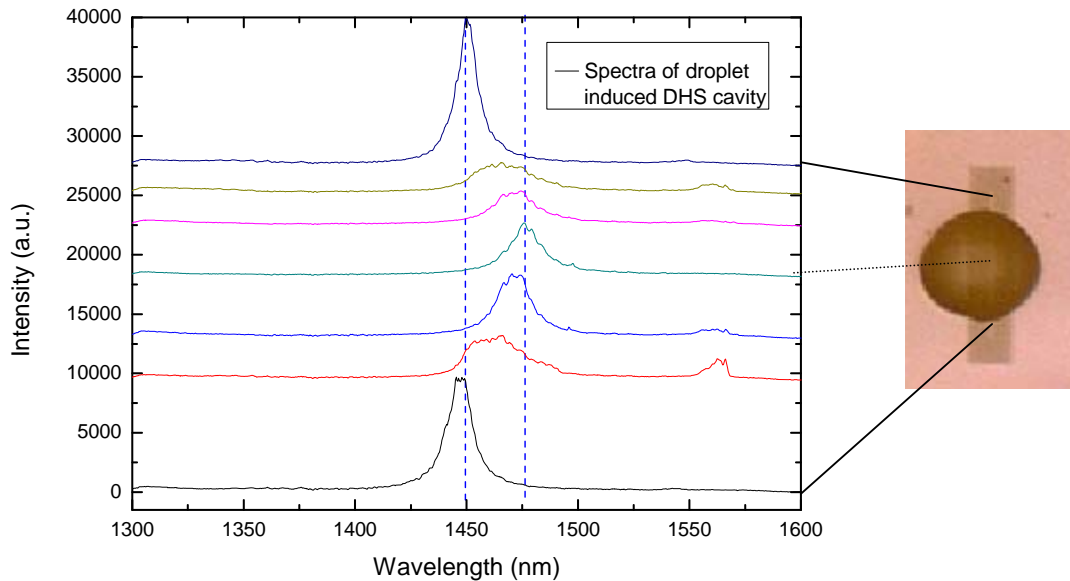


Figure 32: Left: spectra of the droplet DHS cavity. The spectra form a step-by-step profile of the droplet. Right: microscope image of the PhC pattern with a large droplet on top.

On both sides next to the droplet the M2 mode of the fully infiltrated PhC pattern can be seen. The spectrum in the centre of the droplet shows the red-shifted mode. When going from the area next to the droplet to the boundary of the droplet, the M2 mode broadens. A schematic to help explain this effect is shown in Figure 33.

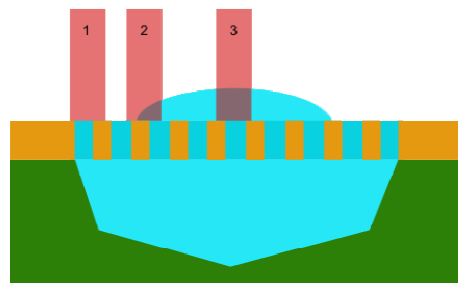


Figure 33: Schematic side view of the fully infiltrated PhC pattern and undercut, with a droplet on top of the PhC pattern.

Due to the curvature of the droplet, the amount of liquid on top of the PhC pattern slowly increases (depicted as laser spot 2 in Figure 33). This results in a gradually changing refractive index. The wave vector of the M2 mode is pointed perpendicular to the waveguide direction. The mode is similar to a FP-resonance reflecting on the PhCs on both sides of the waveguide. The M2 mode therefore strongly depends on local changes in refractive index. The spectrum shows the collection of a range of modes, each from a slightly changed refractive index. The mode continues to become broader

until the droplet surface slope decreases. The variation in refractive index decreases and the emission of the structure becomes narrower. When the droplet surface is flat (depicted as laser spot 3 in Figure 33) the emission looks like a single mode again. When leaving the droplet on the other side, the process repeats in reversed order. This indicates that the droplet indeed forms an interface with a gradual change in refractive index. This should result in a more smooth confinement for the light and this for an increased quality factor of the modes. To confirm these expectations, the infiltration has to be repeated on a structure with a higher dielectric-gap. A structure like that is already proposed in the previous chapter.

#### 4.3.4 Conclusion

The first part of the experiment shows that a DHS cavity can be made by locally changing the background refractive index as proposed by Tomljenovic-Hanic et al. [54]. A droplet of oil is positioned on a fully infiltrated PhC pattern to locally change the effective refractive index of the waveguide. Several different sizes of droplets are presented and the dependency of the free spectral range of the Fabry-Perot resonances and the red-shift of the cut-off modes on the droplet diameter are reported. This shows the possibility to induce a DHS cavity where-ever it is desired in a waveguide structure. Furthermore the position of the modes can be tuned by changing the droplet in size. The droplet can be removed from the PhC pattern by using the tapered fiber, making it a easily reconfigurable structure.

The possibility of mechanical tuning of the cavity was shown. The tapered fiber was positioned inside a small droplet and moved into the focused laser-spot to induce a DHS cavity. It was shown that the size of the droplet, and thus the spacing of the FP-modes, could be modified by moving the fiber perpendicular to the waveguide or by moving it up or down. The mobility of the cavity was demonstrated by moving the droplet along a PhC waveguide with a tapered fiber tip.

As a last step, the gradual change of the effective refractive index was demonstrated by making a step-by-step profile of the droplet cavity. The M2 mode broadens when the laser spot crosses the boundary of the droplet. The increase in liquid volume on top of the PhC pattern results in an increase in effective refractive index of the waveguide. The microscope therefore collects the M2 modes of effectively a distribution of waveguide refractive indexes, resulting in the broadened spectrum. When reaching the flat top surface of the droplet, the mode regains its original size. This shows the smoothness of the interface and might result in a more Gaussian confinement for the light than the liquid infiltration DHS cavity. The expected increase in quality factor was not observed due to a small dielectric gap.

## 5. Selective cavity mode tuning by controlled local liquid infiltration

### 5.1 Introduction

In this experiment the local infiltration of photonic crystals is explored. As a sensitive probe for the control of infiltration, the splitting of two modes that are degenerate in the ideally fabricated and un-infiltrated case is studied. Due to the difference in mode profiles, the modes experience a different effective refractive index and shift with respect to each other. It is shown that selective infiltration is useful for establishing the spatial distribution of the modes and therefore for their identification. Apart from providing a detailed demonstration of selective infiltration, there are also applications that require the tunability of nearly degenerate modes, either to remove the degeneracy or to exactly establish degeneracy.

One application is in the research of quantum communication networks and quantum information processing algorithms, where the development of deterministic sources of entangled photons is important. The sources that are used for generating the photon pairs combine narrow spectral bandwidths with high generation rates, but suffer from Poissonian statistics. This decreases the fidelity of the entanglement. A H1 cavity, a PhC pattern with a single hole defect, might be a suitable structure to restore the entanglement of the photons emitted by a quantum dot. It is therefore proposed as a replacement source by Larque et al. [56]. The small mode volume, but more importantly, the polarization degeneracy of the cavity is an important requirement for the photon source. Due to technological imperfections, the H1 cavities are in practice not degenerate, making them unsuitable for the generation of strongly entangled photon pairs. A method to tune the degenerate modes of a H1 cavity separately is therefore of high importance to the success of cavity quantum electrodynamics (cQED).

Faraon et al. [57] present precise temperature tuning of both the emitting quantum dot and the resonances of the PhC cavity. They are unable to tune the degenerate modes separately by only using temperature differences. Marki et al. [58] and Gac et al. [59] show theoretical and experimental results of tuning the cavity modes by inserting a silicon AFM tip inside the PhC holes. They did not use a H1 cavity and did not present the specific tuning of degenerate modes. This technique should in principle be suitable to split the degenerate modes, but requires a second level of sample manufacturing to implement the mechanical tuning feature.

An important feature of the H1 cavity is the difference in mode profiles of the degenerate modes. This makes the cavity sensitive to asymmetric changes in refractive index of the structure. This was first shown theoretically by Wang et al. [60] and Dundar et al. [61]. They present experimental results of the possibility to use the different states of liquid crystal (LC) to separately tune the nearly degenerate modes of the cavity. The degenerate modes react differently to the relative contribution of the ordinary and extra-ordinary refractive indices of the LC. The contribution of the two types of refractive index of the LC can be controlled by varying the temperature near the phase transition temperature. This makes it possible to separately tune the degenerate modes of the H1 cavity.

Selective liquid infiltration should make it possible to shift the modes over a larger range than the temperature tuning of the LC. The LC has a tuning range that is limited by the refractive index

change as function of temperature of the different states of the liquid. Also can the LC only be used up until its critical temperature.

Beside the larger tuning range, the DPO infiltration can easily be removed from the PhC pattern by using a focussed laser spot. Due to this reconfigurability, the same cavity can be used for several different purposes. Later in this report also the in-situ re-infiltration of the holes is presented.

Hennessy et al. [62] describe atomic force microscope nano-oxidation of the PhC pattern surface. They present the relative tuning of the cavity modes to restore the degeneracy by careful choice of oxide pattern. This is also based on the difference in mode profile of the degenerate modes. Although they show relative tuning, their process is irreversible. Being able to also break the degeneracy is needed for the specific polarization state case in cQED as explained by Larque et al. [56].

## 5.2 Breaking degeneracy by selective infiltration

### 5.2.1 Description of the experiment

For this experiment a H1 cavity is used. This is a PhC pattern with single hole defect. The PhC was fabricated with a lattice spacing of 480 nm and a  $r/a$  of 0.3. The six holes surrounding the defect are reduced in size by 38 nm and radially shifted outwards by 15 nm to increase the quality factor of the cavity modes. Several more cavities with varying lattice constant were fabricated on the same sample while maintaining the  $r/a$ . A larger cavity size, caused by the increase in lattice constant, results in a red-shift of the cavity modes. The 480 nm lattice constant was selected to match the position of the modes with the range of the monochromator. For infiltration the same diffusion pump oil (DPO) as before was used. The oil is called Santovac 5 and has a refractive index of 1.63.

The sample was positioned on the infiltration stage that was described before. The sample was selectively infiltrated with the DPO using the tapered optical fiber tip. The PhC pattern is infiltrated in the area around the defect in carefully chosen patterns. The infiltration is checked from the colour contrast in the microscope images. The selective local changes in refractive index result in mode-dependent changes in the emission spectrum.

A laser is used to excite the quantum dots inside the PhC membrane. The far-field PL is collected with the microscope objective and is then guided to the monochromator. The same laser is used to locally heat the sample and evaporate part of the oil from the PhC holes. More details on the local evaporation and the possibility of re-infiltration are presented in the following chapter. The evaporation is used to free part of the holes directly surrounding the defect. The microscope images and the spectral response are used to examine the effect of the specific infiltration patterns.

### 5.2.2 Mode identification and calculation results

The mode identification used in this chapter is based on the work of Shirane et al. [63]. A typical spectrum of a H1 cavity is presented in Figure 34.

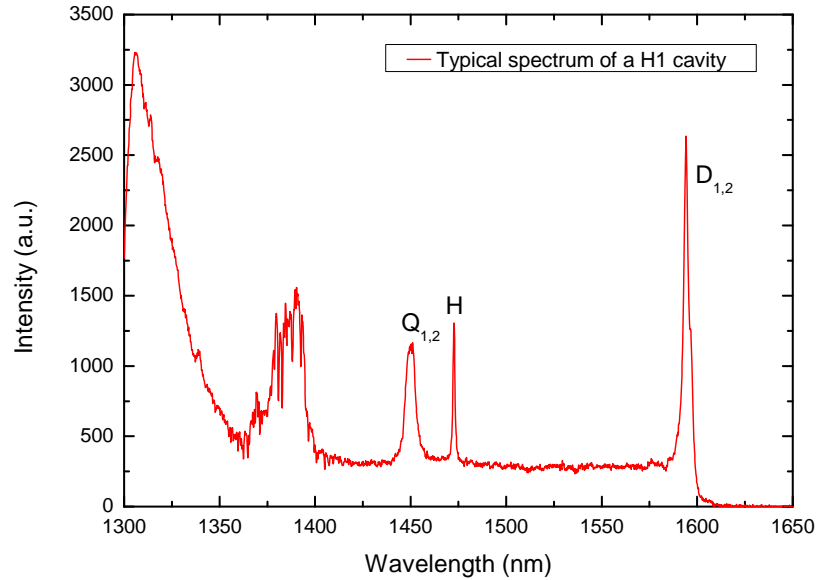


Figure 34 Spectral response of a typical H1 pattern. The  $H_z$ -field profiles of the modes are shown in Figure 35.

The modes in the spectrum are represented from left to right by a Q for the quadrupole modes, an H for the hexapole mode and a D for the dipole modes. The mode profiles were calculated and are shown in Figure 35.

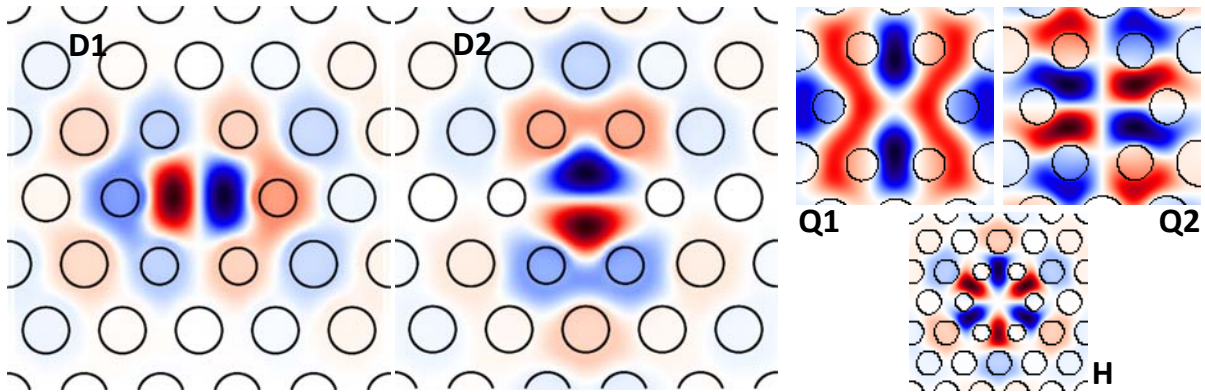


Figure 35: The  $H_z$ -field profiles in the centre of the PhC slab of the modes in a H1 cavity calculated with Meep. The calculations were done by Bowen Wang. The modes are labelled with D for the dipoles, Q for the quadrupoles and H for the hexapole.

Both the dipole- and the quadrupole-modes are degenerate. For both the dipole-modes and the quadrupole-modes, the subscript 1 is for the mode with the  $H_z$ -field aligned in the  $\Gamma$ -K direction and the subscript 2 for the mode with the  $H_z$ -field mostly aligned in the  $\Gamma$ -M direction. For the  $D_2$ -mode the holes in the  $\Gamma$ -K direction have no  $H_z$ -field, while the  $D_1$ -mode the field also penetrates the PhC in the  $\Gamma$ -M direction in addition to the holes in the  $\Gamma$ -K direction. The same is true for the quadrupole-mode. The hexapole-mode is symmetric and does therefore not depend on the pattern of the infiltration, although its shift does depend on the amount of liquid close to the defect. The wavelengths of the Q-modes is close to the wavelength of the H-mode. When the Q-modes are split apart by selective infiltration or evaporation, the Q- and H-modes are difficult to distinguish. Therefore, to examine the effects of the selective infiltration, only the D-modes are considered.

### 5.2.3 Mode splitting by selective removal of liquid

The spectrum of the empty H1 cavity, together with a microscope image and a schematic representation of the H1 cavity, is shown in Figure 36. The schematic presents an interpretation of what can be observed in the microscope image.

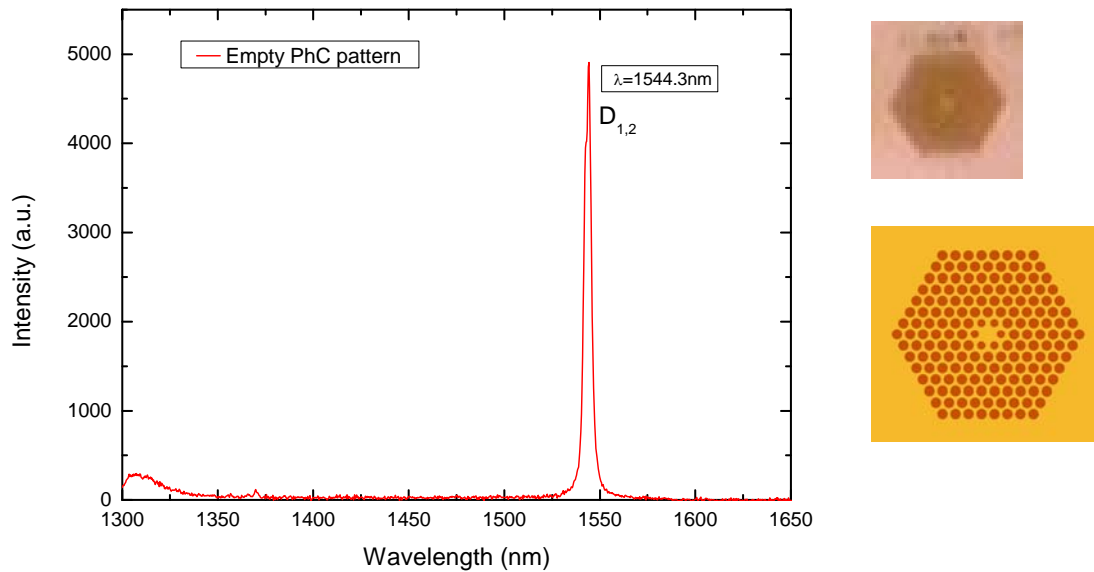


Figure 36: Spectrum of the empty PhC pattern H1 cavity.

The dipole-mode is still degenerate and the intensity of the Q- and H-modes is in the same order as the background of the spectrum. The position of the dipole-mode is indicated by a dashed blue line in the following spectra. The schematic representation, used to clarify what can be seen in the microscope image, has fewer rows of holes than the real structure. Only a part of the PhC pattern is shown because changes in refractive index of the holes close to the defect are most important.

The tapered fiber tip is dipped in a large DPO droplet next to the structure on the sample. The fiber tip is then landed on the PhC pattern surface at the position of the defect and a droplet is formed underneath the tip. After lifting the fiber the droplet remains on top of the defect. The PhC holes underneath the droplet are infiltrated with DPO. The spectrum of the cavity, with the droplet still on top of the defect is shown in Figure 37.

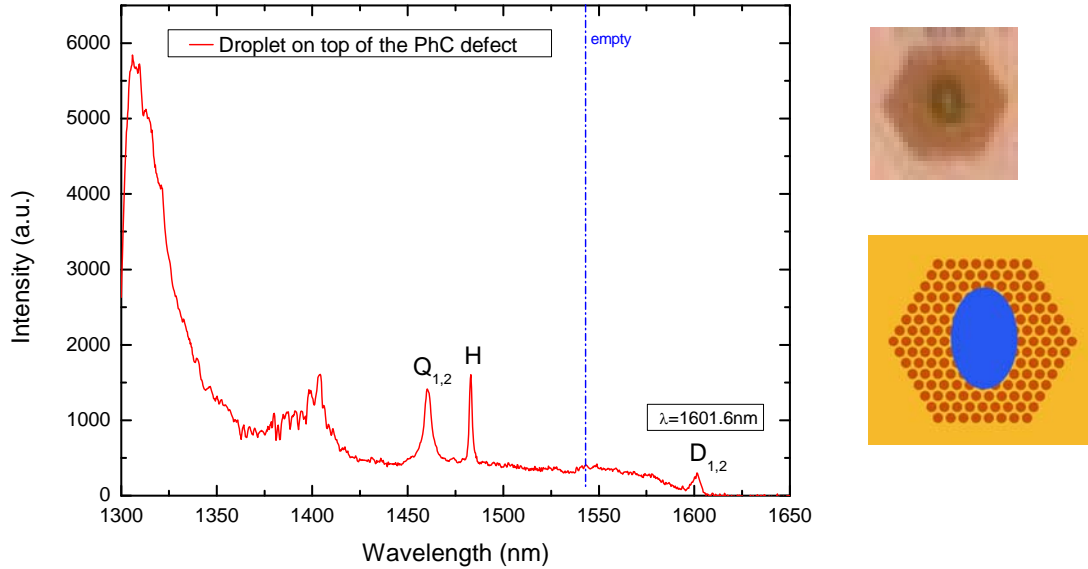


Figure 37: Spectrum of the H1 cavity, with a droplet on top of the defect. The PhC holes around the defect are infiltrated and the undercut is empty. The dashed blue line is a reference to the D-mode of the empty PhC pattern, shown in Figure 36.

The dipole-modes are shifted by 57 nm, but are not split due to the droplet or the infiltration. This is expected for a symmetric change of the refractive index surrounding the defect.

The droplet could not be lifted off the PhC pattern by the tapered fiber. The droplet was therefore moved off the sample from the bottom, leaving a path of infiltrated PhC holes. The holes surrounding the defect were also still infiltrated. The spectrum, together with a microscope image of the infiltration, is shown in Figure 38.

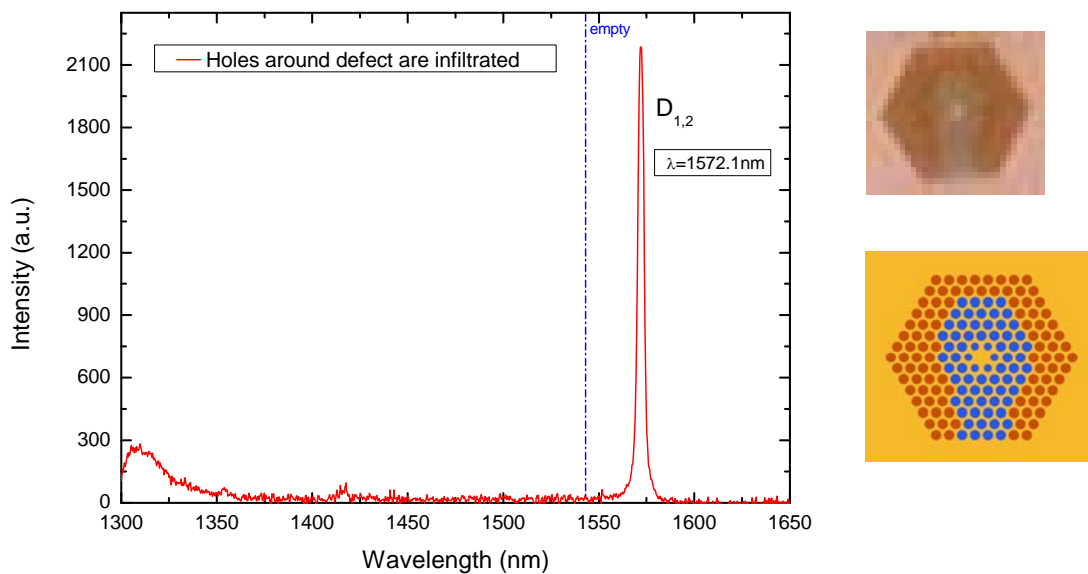


Figure 38: Spectrum of the H1 cavity after removing the droplet. The PhC holes surrounding the defect and a path downwards are infiltrated with DPO. The droplet is removed from the PhC pattern. The dashed blue line is a reference to the D-modes of the empty PhC pattern, shown in Figure 36.



The dipole-modes show a blue-shift of 30 nm, but are still red-shifted by 28 nm from the dipole-mode of the empty PhC pattern presented in Figure 36. The position of the D-modes will be indicated as a dashed line in the following spectra, as a reference to the infiltrated state of the defect.

The laser spot is focussed on the holes to the right of the defect. Several times the PhC pattern was exposed for 60 s with laser power 0.102 mW. The oil was evaporated and the PhC pattern on the right side of the defect was freed of liquid, as can be seen in the microscope image in Figure 39. The spectrum of the infiltrated structure is shown in Figure 39. Note that the spectrum is zoomed-in on the dipole mode and shows a smaller range than the previous spectra.

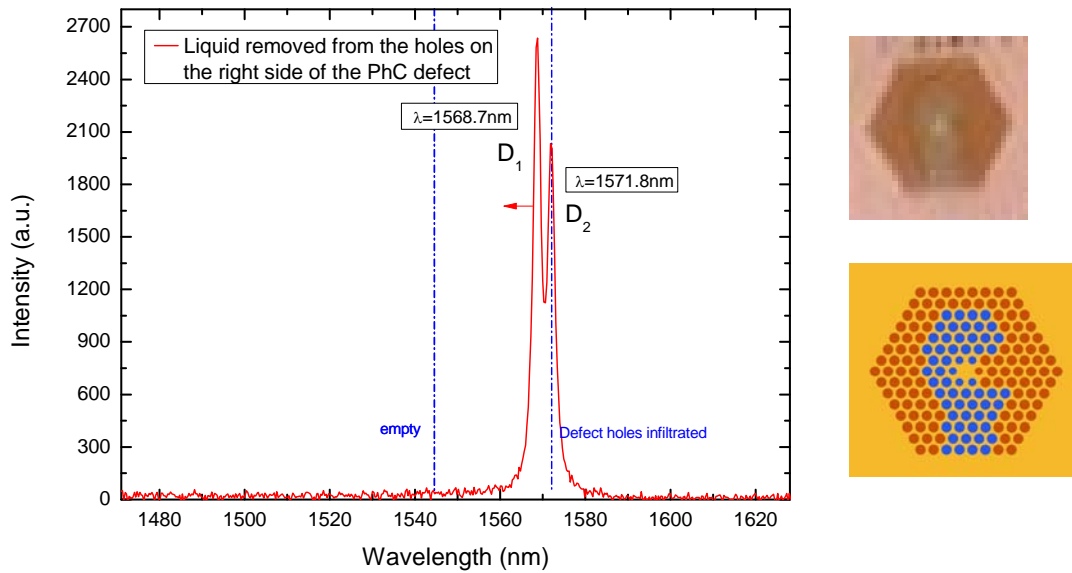


Figure 39: Spectrum of the H1 cavity after removing the oil from the holes on the right side of the defect. The left and right dashed blue lines are references of the D-modes of the empty and infiltrated PhC pattern respectively (Figure 36 and Figure 38).

The D-modes are now separated from each other. One of the modes is still in the infiltrated position, while the other blue-shifted by 3 nm. From the  $H_z$ -field profiles shown in Figure 35 it can be seen that decreasing the refractive index on the right side of the defect should have no result on the  $D_2$ -mode, while a significant portion of the  $H_z$ -field of the  $D_1$ -mode penetrates this area. We can therefore identify the blue-shifted peak as the  $D_1$ -mode and the un-shifted peak as the  $D_2$ -mode. This proves the possibility of selective tuning of the normally degenerate cavity modes.

To continue, the liquid in the holes to the left of the defect was removed by several exposures of 60 s with laser power 0.102 mW. The spectrum and the microscope image are shown in Figure 40.

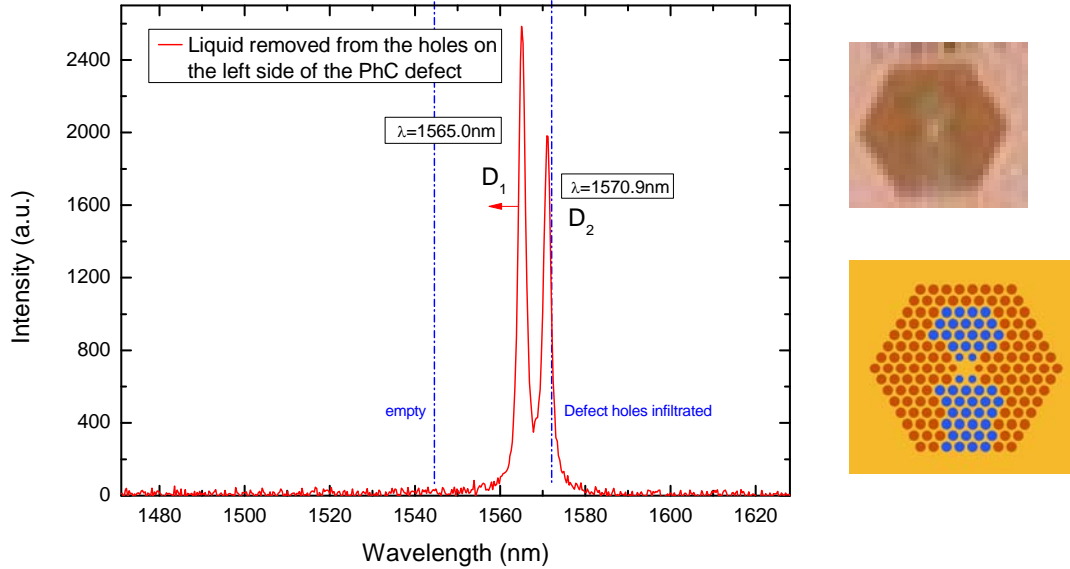


Figure 40: Spectrum of the H1 cavity after removing the oil from the holes on the left and the right side of the defect. The left and right dashed blue lines are references of the D-modes of the empty and infiltrated PhC pattern respectively (Figure 36 and Figure 38).

The splitting of the dipole-modes has increased. The  $D_2$ -mode is now also blue-shifted by 1 nm. From the mode profile of the  $D_2$ -mode shown in Figure 35 it can be seen that a small portion of the field penetrates the second and even third row of holes. The small blue-shift is probably the result of the change in refractive index of these holes. The blue-shift of the  $D_1$ -mode is now 7 nm, showing approximately the same shift for removing liquid from the holes on the right and the left side of the defect. The  $H_z$ -field profile of the mode shows that a significant part of the mode penetrates the PhC pattern on the top and the bottom of the defect. This explains why the  $D_1$ -mode is still red-shifted by 21 nm from the empty PhC pattern.

The next step was to remove the liquid from the holes above the defect. Again the liquid was evaporated by several exposures of 60 s with laser power 0.102 mW. During the last exposure the major part of the liquid was removed from the holes and the emission from the cavity was continuously collected. Due to the size of the laser spot and the higher intensity of the laser a low intensity spectrum, large enough to distinguish the dipole-modes in the spectrum, could still be collected. It should be taken into account that the modes experience a red-shift due to the increased temperature of the membrane. A part of the collection is shown in Figure 41. Already in the first spectrum part of the liquid was already evaporated, blue-shifting the modes to approximately the position shown in Figure 40.

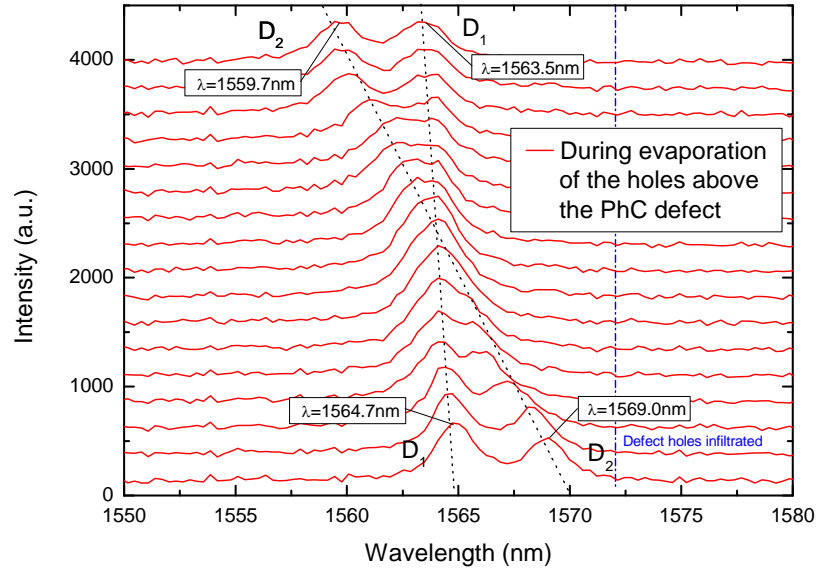


Figure 41: Spectrum of the H1 cavity while removing the liquid from the holes directly above the defect. The laserspot is not focussed on the defect and the modes are thermally shifted due to higher laser power. The spectra do not show the full 60 s of exposure but only the part where the dipole modes cross.

In the spectrum it can clearly be seen that the two dipole-modes cross each other. As can be seen in the  $H_z$ -field profiles in Figure 35, the penetration in the PhC of  $D_2$ -mode is strongly confined in the four holes directly above and below the defect. The  $D_1$ -mode is more spread out over the surrounding cavity holes. Also the mode penetrates deeper into the PhC, as can be seen from the  $H_z$ -field intensity in the second row of holes around the cavity. This results in a stronger effect of the vertical infiltration on the  $D_2$ -mode, than the horizontal infiltration on the  $D_1$ -mode. This is why the  $D_2$ -mode blue-shifts past the  $D_1$ -mode when the liquid in the holes above the defect is evaporated.

The stacked spectra in Figure 41 show only the part of the crossing and not the whole 60 s of laser induced evaporation. The dashed blue line is a reference to the dipole-modes of the infiltrated spectrum (Figure 38) taken at laser power 0.054 mW. The spectra are taken with laser power 0.102 mW and are thermally shifted. After the evaporation a spectrum is taken at laser power 0.054 mW and is shown, together with the microscope image, in Figure 42.

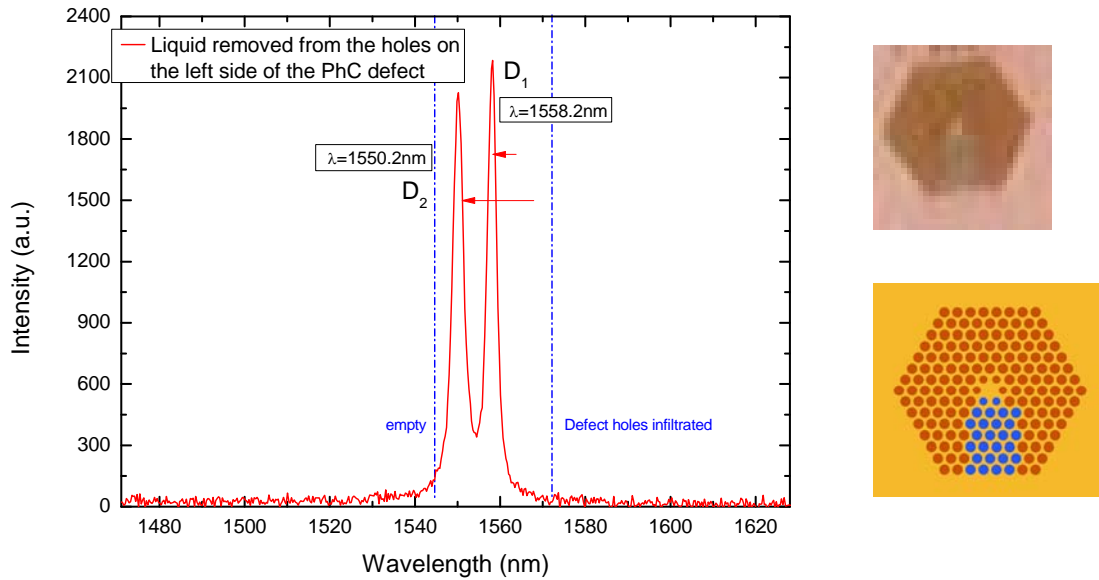
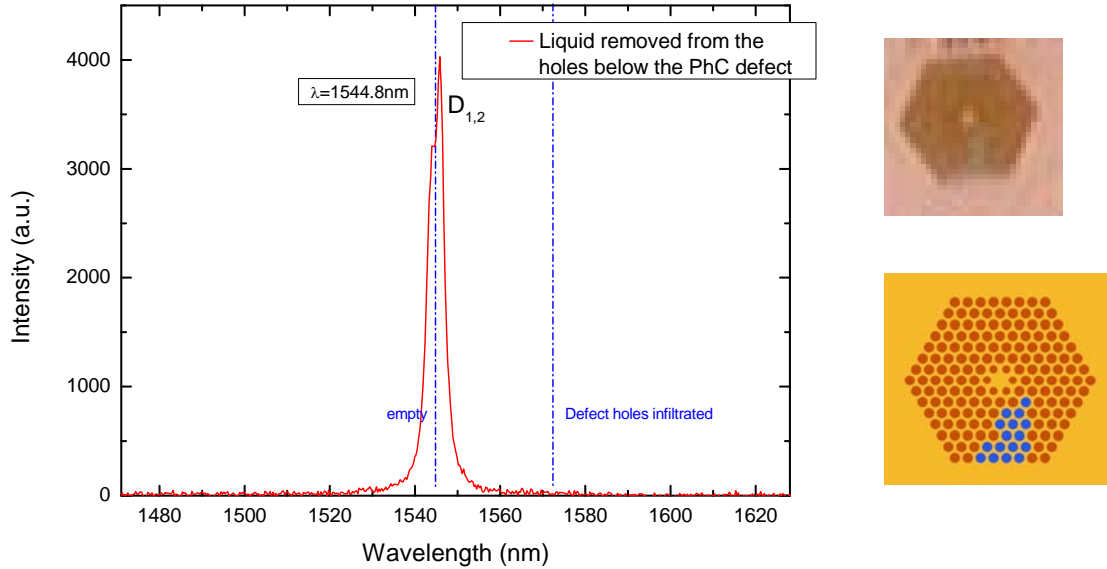


Figure 42: Spectrum of the H1 cavity after removing the oil from the holes on the left, right and top side of the defect. The left and right dashed blue lines are references of the D-modes of the empty and infiltrated PhC pattern respectively (Figure 36 and Figure 38).

The final spectrum shows a 7 nm blue-shift for the  $D_1$ -mode and a 21 nm blue-shift for the  $D_2$ -mode. The data in Figure 40 - Figure 42 show that selective infiltration enables identification of cavity modes, gives a fair indication of their spatial distribution and, by this, identifies their polarization. A future next step of the investigation would be to use the SNOM setup to measure the in plane electric fields of the modes as reported by Vignolini et al. [64] and confirm the interpretation of the infiltration results.

In the last step the liquid from the holes below the defect was evaporated. The spectrum and the microscope image are shown in Figure 43.



**Figure 43: Spectrum of the H1 cavity after evaporating the oil from all the holes surrounding the defect. The left and right dashed blue lines are references of the D-modes of the empty and infiltrated PhC pattern respectively (Figure 36 and Figure 38).**

From the contrast in the microscope image it can be seen that the holes surrounding the defect are now empty. The spectrum confirms this and shows hardly degenerate dipole-modes, back to the wavelength of the empty spectrum in Figure 36. The width of the spectrum indicates that there is still a small amount of splitting between the modes, but they cannot be distinguished with the optical resolution of the detection.

#### 5.2.4 Mode splitting by selective infiltration of liquid

The splitting of the dipole-modes by selective mode tuning is reproduced by local infiltration of the PhC pattern holes. This part of the experiment was performed on a slightly different H1 structure. The PhC defect is the same as the previous one, except for the shift of the defect holes. The holes directly surrounding the defect are shifted outwards by 30 nm instead of 15 nm. The spectrum of the un-infiltrated structure is shown in Figure 44.

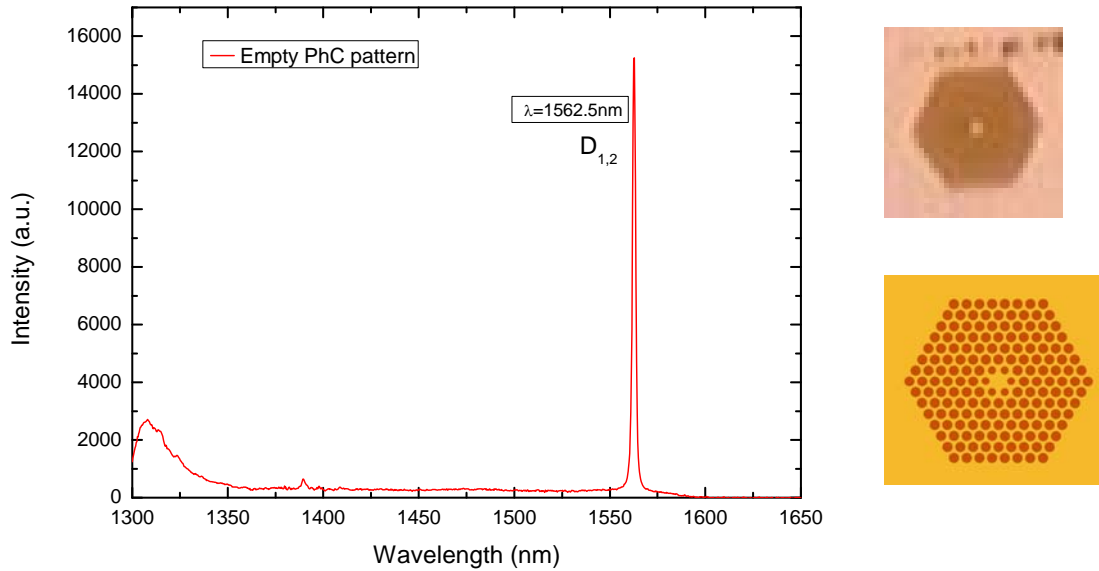


Figure 44: Spectrum of the empty PhC pattern H1 cavity.

The dipole-modes are still degenerate in this case. Again the intensity of the Q- and H- modes is too low to be distinguishable from the background. The position of the dipole-modes is indicated in the following spectra by a dashed blue line.

The tapered fiber tip was used to pull a droplet of DPO over the PhC pattern surface of the H1, infiltrated the holes in its path. It is possible to infiltrate PhC pattern without infiltrating the holes to the left and the right of the defect. In this case a slightly too large droplet was used and the liquid in the holes to the left of the defect was later evaporated using laser power.

First the PhC pattern is infiltrated in the  $\Gamma$ -M direction. The microscope image and spectrum are shown in Figure 45.

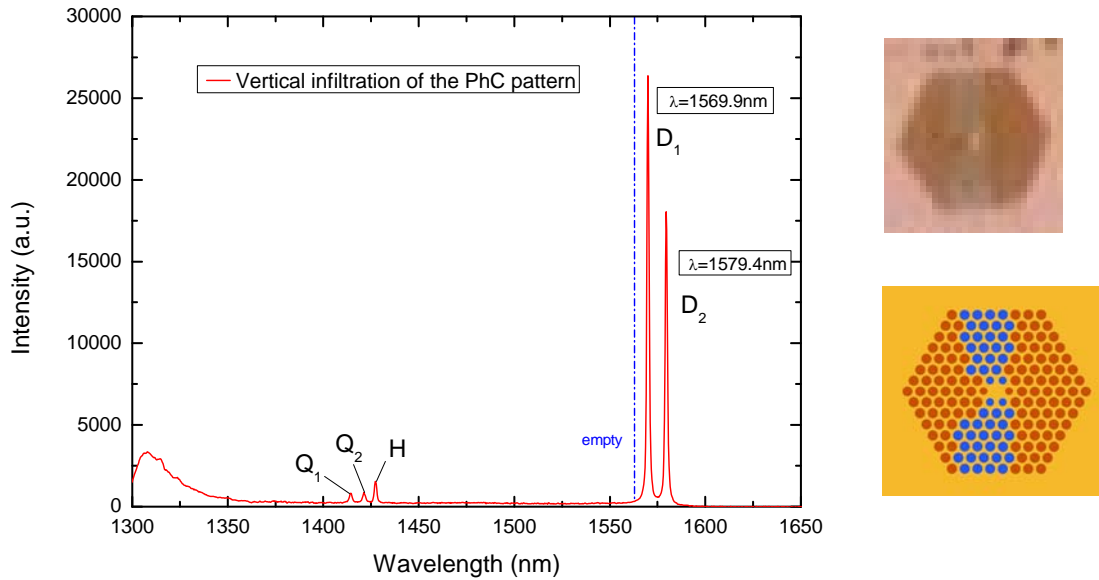


Figure 45: Spectrum of the H1 cavity after a line of infiltration in the  $\Gamma$ -M direction of the PhC pattern. The dashed blue line marks the position of the dipole-modes of the empty PhC pattern (Figure 44).

The dipole modes are both red-shifted. The  $D_2$ -mode is shifted by 17 nm and the  $D_1$ -mode is shifted by 7 nm. The modes are actually identified by their different shifts, combined with the calculations in Figure 35 and the experiments of the previous section. The infiltration pattern is similar to the pattern in Figure 40 of the previous section. The holes to the left and the right of the defect are still empty while the other holes surrounding the defect are infiltrated with DPO. As can be seen from the  $H_z$ -field profiles in Figure 35, the  $D_2$ -mode is mostly polarized in the  $\Gamma$ -M direction, while the  $D_1$ -mode is predominantly polarized in the  $\Gamma$ -K direction. Therefore the change in effective refractive index is larger for the  $D_2$ -mode than for the  $D_1$ -mode and as a result more red-shifted.

The liquid was removed from the holes using laser induced evaporation. This was again done in several steps and confirmed the observations of the previous section. After the evaporation of all the liquid from the PhC holes, the experiment was repeated for an infiltration in the  $\Gamma$ -K direction. The spectrum and the microscope image are shown in Figure 46.

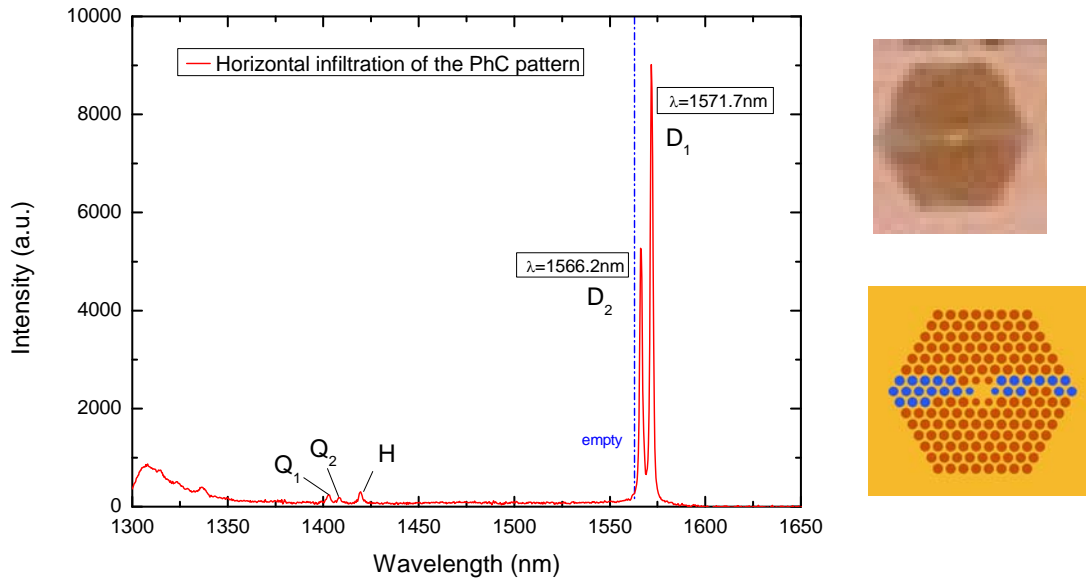


Figure 46: Spectrum of the H1 cavity after a line of infiltration in the  $\Gamma$ -K direction of the PhC pattern. The dashed blue line marks the position of the dipole-modes of the empty PhC pattern (Figure 44).

This time one D-mode is red-shifted by 1nm and the other by 6 nm. The modes are identified by  $D_2$ - and  $D_1$ -mode respectively. The penetration of the  $D_2$ -mode into the PhC in the  $\Gamma$ -K direction is small, resulting in the small shift shown in the spectrum. The mayor part of the  $D_1$ -mode field is positioned  $\Gamma$ -K direction, resulting in a larger shift than the  $D_2$ -mode. Still the  $D_1$ -mode has a considerable amount of the field in the  $\Gamma$ -M direction, which was already determined in the spectrum in Figure 45. This explains why the shift in the spectrum in Figure 46 is small compared to the shifts from the vertical infiltration.

### 5.2.5 Mode splitting in a L3 cavity

The group of Kallasi et al. [34] reported mode-specific tuning by local changes in refractive index. They used a PhC pattern with a line defect of three holes in the  $\Gamma$ -K direction. This type of structure is called a L3 cavity. They fully infiltrated the PhC pattern and the undercut with a liquid monomer. They subsequently used UV-laser light to locally polymerize the liquid monomer. The residual, un-polymerized, monomer was removed from the PhC pattern using organic solvents. They examined the selective infiltration by only shifting the modes polarized in the direction of the infiltration.

In this chapter this work was repeated by using selective DPO infiltration. An L3 cavity with a lattice constant of 511 nm and an  $r/a$  of 0.3 was used. The PhC holes on the left and the right of the L3 cavity were reduced in size by 51nm but were not shifted outwards.

#### L3 mode identification

The spectrum of the empty L3 cavity is shown in Figure 47. The electric-field profiles of the modes that are shown in the spectrum were calculated using MEEP and are also shown in Figure 47. The identification of the modes in the spectrum is based on the work of Kallasi et al. [34].



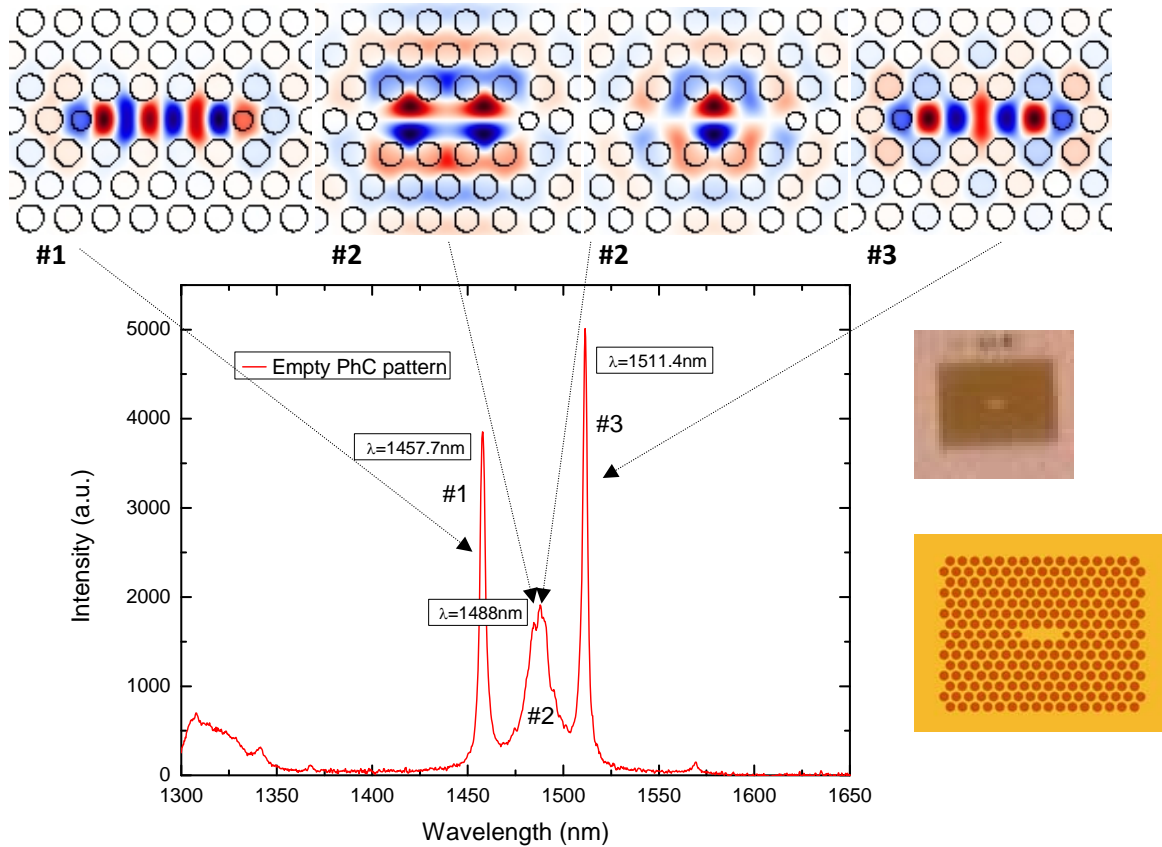
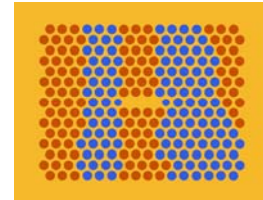
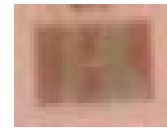
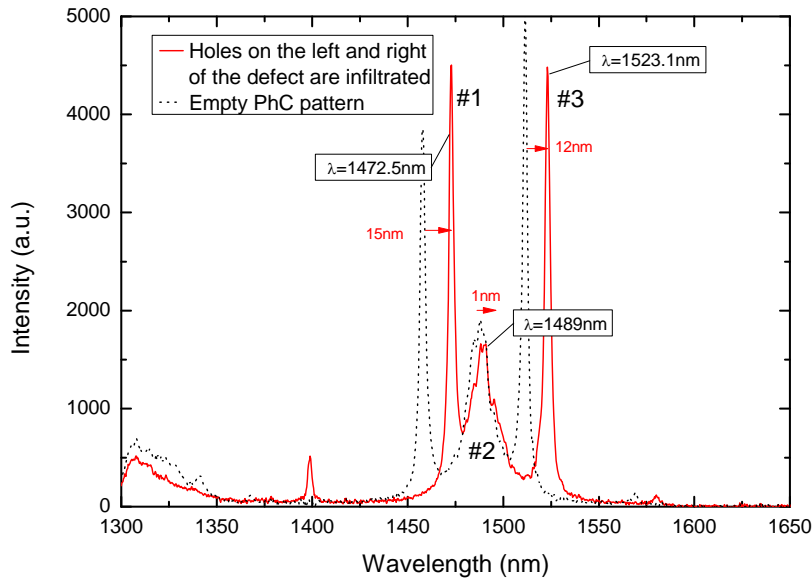


Figure 47: Bottom: Spectrum of the un-infiltrated L3 structure and a microscope image of the structure. Top: calculated  $H_z$ -field profiles of the modes shown in the spectrum. The calculations were performed by Joost Voorbraak [42] using Meep.

The #1- and the #3-mode are confined to the  $\Gamma$ -K direction. The penetration of the modes is small in the  $\Gamma$ -M direction, although slightly larger for the #3-mode than for the #1-mode. Both modes have a considerable portion of their  $H_z$ -field in the holes on the left and right of the defect. The #2-modes are polarized in the  $\Gamma$ -M direction. These modes penetrate the PhC pattern mostly in the  $\Gamma$ -M direction. Similar to the  $D_2$ - and  $Q_2$ -mode, they show no field penetration in the holes to the left and the right of the L3 defect.

### Results

The PhC pattern was infiltrated by two vertical lines of DPO, to the left and the right of the defect. The holes right next to the defect, to the left and the right were infiltrated with liquid. The holes directly above and below the defect were still empty. The spectrum and the microscope image are presented in Figure 48.



**Figure 48: Spectrum of the vertically infiltrated L3 cavity. The holes to the left and the right of the defect are infiltrated with liquid. The dotted black line shows the spectrum of the empty L3 cavity (Figure 47).**

The #2-modes are red-shifted for  $\sim 1$  nm, which was expected for these modes that have almost no mode penetration in the  $\Gamma$ -K direction. The #1 and #3 are red-shifted by 15 nm and 12 nm respectively. Their mode profile penetrates the PhC holes in the  $\Gamma$ -K direction and should experience a strong change in refractive index. Also the larger shift of the #1-mode than the #3-mode could be predicted from the  $H_z$ -field calculations. The #3-mode also slightly penetrates the PhC pattern in the un-infiltrated  $\Gamma$ -M direction and thus experiences a smaller effective change in refractive index than the #1-mode that almost only penetrates the  $\Gamma$ -K direction.

The liquid was removed from the PhC pattern using laser induced evaporation. The sample was rotated on the sample stage and the tapered fiber was again used to infiltrate the PhC pattern. The spectrum and the microscope image are shown in Figure 49.

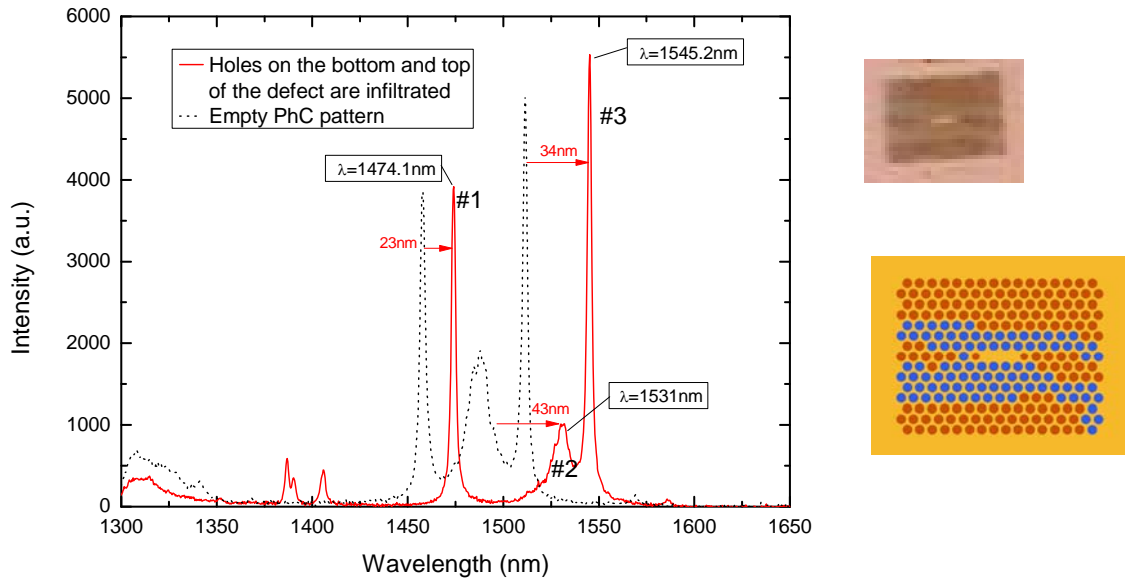


Figure 49: Spectrum of the horizontally infiltrated L3 cavity. The holes above and below the defect are infiltrated with liquid. The dotted black line shows the spectrum of the empty L3 cavity (Figure 47).

This time the #2-modes are shifted for 43 nm. Their weak confinement to the cavity and strong mode penetration in the  $\Gamma$ -M direction results in a large red-shift. From the microscope image it can be seen that a part of the holes on the right side of the defect are infiltrated with liquid. This could explain why the #1- and #3-mode are shifted. It cannot explain why their shift is larger in this case than in the infiltration in the  $\Gamma$ -M direction. Even though these modes are confined to the  $\Gamma$ -K direction, they still respond to the overall change in effective refractive index of the L3 cavity. The larger shift of #3-mode than the #1-mode can be explained by the slightly larger PhC pattern penetration of the #3-mode into the  $\Gamma$ -M direction.

## 5.3 Breaking degeneracy by micro-droplet positioning

### 5.3.1 Description of the experiment

In this chapter the asymmetric change in refractive index change around the H1 cavity was investigated using droplets. As described in the previous chapter, the different modes in the H1 cavity can be selectively tuned by changing the refractive index of only a part of the holes surrounding the defect. In this chapter the same effect is reproduced by positioning a droplet of PDO on top of the fully infiltrated PhC pattern, right next to the defect. With fully infiltrated is meant that we repeatedly strike the tapered fiber tip with a large droplet of DPO over the PhC pattern, so that the PhC holes and the undercut are filled with oil. The change in effective refractive index in the PhC membrane due to a change in refractive index of the background caused by the droplet, is the same as in the droplet DHS experiments. There the possibility of inducing a cavity with a droplet on top of the PhC waveguide was presented.

In this experiment the same H1 cavity as before was used. The PhC pattern has a lattice constant of 480 nm and the  $r/a$  is 0.3. The six holes surrounding the defect are reduced in size by 38 nm and radially shifted outwards by 15 nm for increased Q-factor of the cavity modes. The liquid used for infiltration and for the droplets was the same Santovac 5, a diffusion pump oil with refractive index 1.63.

The sample was positioned on the infiltration stage. After the full infiltration of the structure, the tapered fiber was used to put droplets on top of the PhC pattern. The fiber was inserted into a large droplet of DPO. When the fiber was taken out of the droplet there was always a small amount of liquid on the fiber. The fiber tip was then positioned over the defect of the PhC pattern and moved downwards. When it touched the PhC surface, a droplet would form at the tip of the fiber. When the fiber was removed, a small droplet would remain. The droplets could be reduced in size by first making a droplet on the sample surface next to the cavity. When a droplet was formed on the surface, there was a still smaller amount of liquid on the fiber tip that could be used again for another droplet. This could be repeated several times, every time reducing the size of the droplet that is left on the sample surface.

The experiments were performed by exciting the quantum dots inside the PhC membrane and measuring the far-field PL with the microscope objective. The spectra together with the microscope images were used to investigate the droplet structures.

### 5.3.2 Results

The structure is fully infiltrated as described before. The spectrum and microscope image is shown in Figure 50.

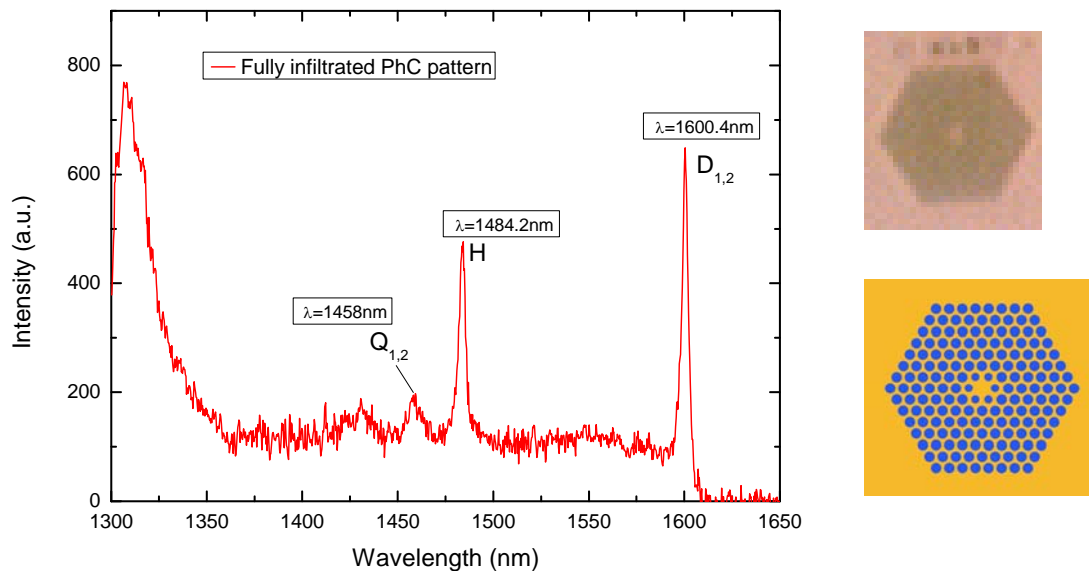
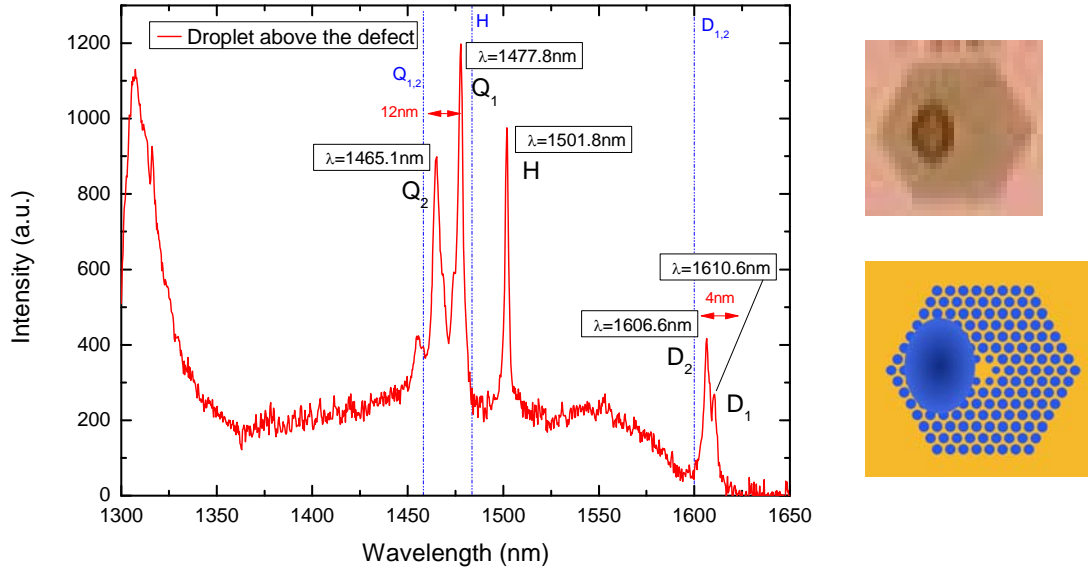


Figure 50: Spectrum of the fully infiltrated H1 cavity.

The D- and Q-modes are degenerate and all the modes are red-shifted from the empty structure. The dipole-modes are shifted by 56 nm. The other modes could not be distinguished in the empty spectrum.

A droplet was positioned on top of the PhC pattern, directly to the right of the defect. The spectrum and microscope image are shown in Figure 51.



**Figure 51: Spectrum of the fully infiltrated H1 cavity, with a droplet on top of the PhC pattern, to the left of the defect. The dashed blue lines indicate the position of the H1 modes in the fully infiltrated situation (Figure 50).**

The droplet covered the hole directly to the left of the cavity. This results in a strong red-shift of the  $D_1$ - and  $Q_1$ -mode as was expected from the mode profiles shown in Figure 35. The droplet probably also covers part of the upper- and lower-left holes directly surrounding the defect. This results in the small red-shift of the  $D_2$ - and  $Q_2$ -mode. The Q-modes are split by 12 nm and the D-modes by 4 nm. The change in refractive index influences the Q-modes more than the D-modes, which might be explained by stronger in-plane confinement of the D-modes.

The droplet was removed from the PhC pattern surface. A new droplet was made and positioned on top of the PhC pattern directly above the defect. The spectrum and the microscope image are shown in Figure 52.

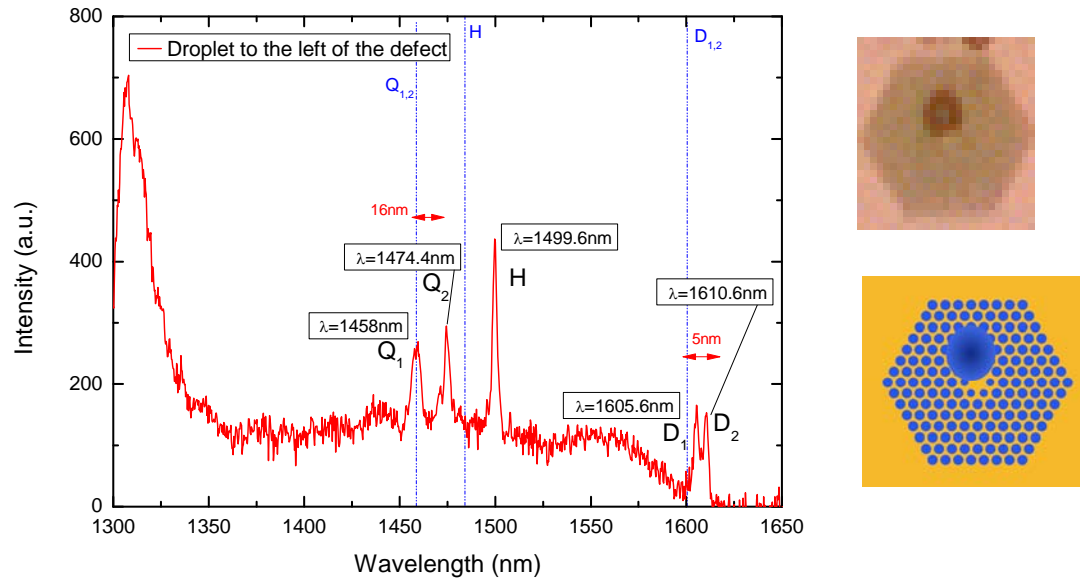


Figure 52: Spectrum of the fully infiltrated H1 cavity, with a droplet on top of the PhC pattern, above the defect. The dashed blue lines indicate the position of the H1 modes in the fully infiltrated situation (Figure 50).

This time the holes directly above the defect are covered by the droplet and results in splitting of the Q- and D-modes again. The  $Q_2$ - and  $D_2$ -modes have the stronger shift this time as would be expected from the mode profiles. Again the splitting of the D-modes of 5 nm is smaller than the splitting of the Q-modes. This indicates the difference in confinement to the slab as mentioned before.

### 5.3.3 Conclusion

The selective tuning of the dipole-modes is presented by selective evaporation of the liquid in the holes. The holes around the defect were infiltrated by positioning a droplet on top of the PhC pattern. After removal of the droplet, the holes surrounding the defect were still infiltrated with oil. The liquid was locally removed from the holes by laser induced evaporation. The two orientations of the dipole-modes are identified by the different patterns of infiltration combined with the calculated mode profiles. The crossing of the modes was presented and indicates the level of control than can be realized in selectively tuning the normally degenerate modes. Several other experiments were performed on the selective evaporation and proved the reproducibility of the selective tuning of the modes.

The selective tuning of the dipole-modes was repeated using selective infiltration of the PhC pattern. By infiltration of a narrow path in  $\Gamma$ -M and the  $\Gamma$ -K direction of the PhC membrane, the difference in tuning of the dipole-modes was investigated. It was confirmed that confinement of the  $D_2$ -mode to the  $\Gamma$ -M direction was stronger than the confinement of the  $D_1$ -mode to the  $\Gamma$ -K direction. This resulted in minor shifts for the  $D_1$ -mode in both the situations. The  $D_2$ -mode on the other hands experiences a negligible red-shift for infiltration in the  $\Gamma$ -K direction and a strong red-shift for infiltration in the  $\Gamma$ -M direction.

The group of Kallassi et al. [34] presented a way to selectively split the modes in a L3 cavity by local infiltration of UV-curable polymers. Their experiments were reproduced by selective liquid infiltration using the tapered fiber. Selective mode tuning was presented for the L3 cavity and this time in a reconfigurable way. The infiltration can be adjusted by laser induced evaporation. The structure can easily be brought back to the original state by evaporating all the liquid. The type of infiltration Kallassi et al. used could in principle be reconfigured, but requires cleaning with organic solvents and starting the infiltration and exposure from the start.

The shifting of the holes by local index changes was repeated by using droplets on top of the PhC pattern. The mode in the H1 cavity could be manipulated by changing the refractive index of the background, similar to the effect used for the droplet DHS cavities. It was shown that both the quadrupole- and the dipole modes can be split. The splitting is proven to be polarization selective. By changing the position of the droplet on top of the PhC pattern either the  $D,Q_2$ - or the  $D,Q_1$ -mode could be shifted to higher wavelengths. The droplet can be moved to any position on the PhC pattern with great ease, making it a very versatile way of tuning the modes.

## 6. Optical fluid-manipulation

### 6.1 Introduction

In the previous experiments a mechanical way of local liquid infiltration is discussed, which is not suitable for chip integration. Local liquid infiltration of PhCs has been achieved in several other ways. The refractive index of the holes can be changed in a non-reconfigurable post-processing way. An example is using UV-curable polymers [34], where a monomer is infiltrated in the holes and locally polymerized by focused UV laser power, to later remove the unexposed monomer.

The group of Intonti et al. [65] reports on the controlled micro-infiltration of water in single holes in PhC membranes. More importantly they show the controlled evaporation of the water with a continuous spectral shift as result. They show that infiltration is stable over a time of five days, which differs from the findings in our experiments. Still it means that a microfluidic channel system will be required to supply the structures with liquid.

The group of Erickson et al. [66] demonstrated such a nanofluidic delivery structure with microfluidic control engines. With a soft-lithography layer and a control layer they manage to selectively infiltrate one row of holes in a PhC, creating a waveguide. By rapidly varying the refractive index of the liquid they can tune the modes in the waveguide.

The group of Faraon et al. [67] proposed the tuning of the modes in a structure by depositing a chalcogenide glass layer on top of the fabricated devices using a thermal evaporation method. By optical excitation the chemical configuration of the glass can be changed. This way its refractive index can be controlled by the duration of the exposure. The chemical configuration can be restored by heating the sample, which makes it a reconfigurable process. The locality of the tuning is limited by the size of the laser beam focus and is shown to be in the order of a few square microns.

The selective removal of liquid has already been described in previous chapters. Although this is a local reconfiguration of the infiltration in the structures, the cavity needs to be re-infiltrated to use it again. Here we investigate the possibility of using laser power to manipulate the liquid in the PhC structures and make it truly reconfigurable without the use of mechanical methods.

The method used in this investigation is based on the experimental results of Liu et al. [68]. They describe a method to use a laser to move liquid around on a sample surface. The process is depicted in Figure 53.



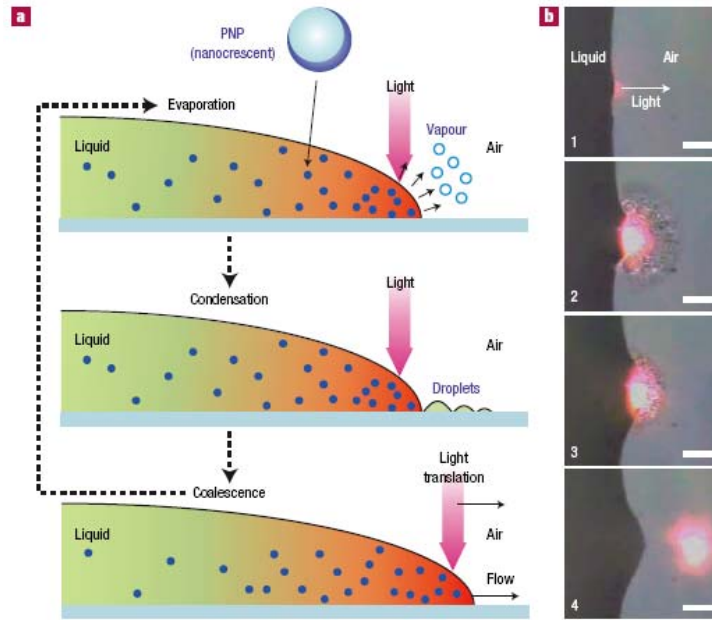


**Figure 53:** Image taken from Liu et al. [68]. (a) Schematic overview of the process described in [68]. In the first step a light beam is focused on photothermal nanoparticles in the liquid. As a result the liquid is evaporated by the heat generated in the particles. In the second step the vapour condenses and forms droplets on the sample surface. In the third step the droplets coalesce to form bigger droplets and eventually merge with the original liquid extending its contact line. The light is transposed in the direction of the liquid extension and the process is repeated. (b) Video prints of the process described in (a).

In the experiment they use a liquid with suspended photothermal nanoparticles (in their case gold nanocrescent particles) positioned on a hydrophobic surface. Due to contact-line pinning and the ‘coffee-ring’ effect, the concentration of particles is highest on the liquid-air interface. The particles in the liquid are illuminated with a focused light beam and the heat generated in the particles is transferred to the liquid on a nanosecond timescale, producing a vapour. The vapour condenses almost immediately after the evaporation due to the colder air in the surrounding. Droplets are formed on the surface close to the liquid-air interface, where they coalesce to form bigger droplets and eventually merge with the original liquid body extending its contact line.

## 6.2 Description of the experiment

In this experiment the same type of H1 PhC pattern as in the previous chapter is used. The PhC is fabricated with a lattice constant of 480 nm and  $r/a$  of 0.3. The holes surrounding the cavity are reduced in size by 15 nm and radially shifted outwards by 30 nm to improve the quality factor of the cavity. On the same sample a range of H1 patterns was fabricated, where the lattice constant is varied from 480 nm to 530 nm while maintaining a  $r/a$  of 0.3. The increase in lattice constant results in a red-shift of the modes due to the increased cavity length, as has been described before. This specific PhC pattern is chosen for having its dipole mode still in the range of the monochromator when being fully infiltrated with diffusion pump oil (DPO). The spectrum of the empty and fully infiltrated cavity is shown for reference in Figure 54.

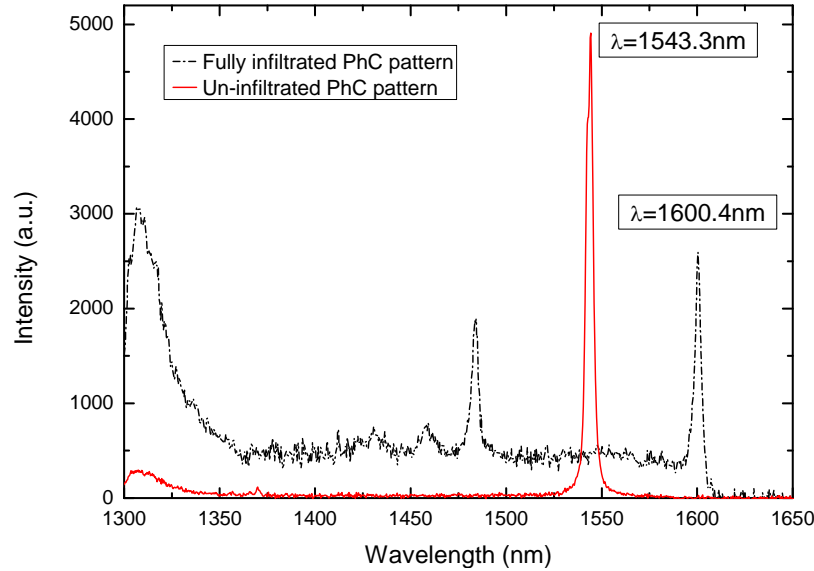


Figure 54: Spectral response of the H1 pattern in the empty (solid red line) and the fully infiltrated case (dotted black line). The position of the dipoles resonance is also shown in the following graphs as a reference.

Identification of the modes in of the spectrum of the H1 cavity was presented in Figure 34, using the calculated  $H_z$ -field profiles shown in Figure 35. The hexapole-mode that can be seen in the infiltrated spectrum (dashed black line) cannot be distinguished from the background in the empty spectrum (solid red line).

The sample is positioned on the infiltration stage described before and is infiltrated with DPO using the tapered fiber. Both the undercut and the holes of the pattern are infiltrated, which can be seen from the contrast under the microscope and is confirmed from the spectral shift. The spectrum of the defect is measured using PL-spectroscopy collecting the far-field response with the microscope. The laser beam used to excite the quantum dots in the sample is also used to locally heat the sample as has also been done in previous experiments. The microscope images and spectral responses of the defect are used to investigate the manipulation of the DPO by using laser power.

Due to the design of the structure used in these experiments the temperature in the cavity can become rather high. The thermal conductivity of InP is 68 W/mK [69] while that of bulk InGaAsP is only 4 W/mK [70] and of air 0.025 W/mK [71]. The air-filling factor of the InGaAsP membrane is 0.3 and the membrane is suspended in air, which means that also the area above and below the membrane consists of air. The holes are filled using a DPO, called Santovac 5, with a thermal conductivity of 0.13 W/mK, which is significantly lower than that of the surrounding InGaAsP. Only where the membrane is attached to the sample there is contact with the InP. It is therefore assumed that the total thermal conductivity of the structure is low enough to be able to heat the cavity and locally enhance evaporation of the DPO from the holes. In the article of Dundar et al. [72] a temperature of 200°C is reported when exciting a InGaAsP membrane with 0.5 mW laser power. This is in the range of the operation temperature of a diffusion pump using santovac, which confirms the possibility of evaporating the DPO from the holes of the PhC pattern. A formal calculation and simulations has to be done to confirm this assumption but is outside the scope of this research.

## 6.3 Results

### 6.3.1 Laser power required for evaporation

First the laser is focussed on the cavity and the laser power on the PhC surface is increased from 0.1 to 0.5 mW in steps of 0.1 mW. The calibration of the laser power was taken from [72]. For each step the laser is focused on the cavity with higher laser power for 60 s. After the exposure the laser power was reduced (to 0.05 mW) to measure the spectral response of the cavity and to capture the image from the optical microscope. An image of the fully infiltrated cavity can be seen in Figure 55 (a). The exposure power as a function of the time is also shown in Figure 55, which gives a guideline to the experiment.

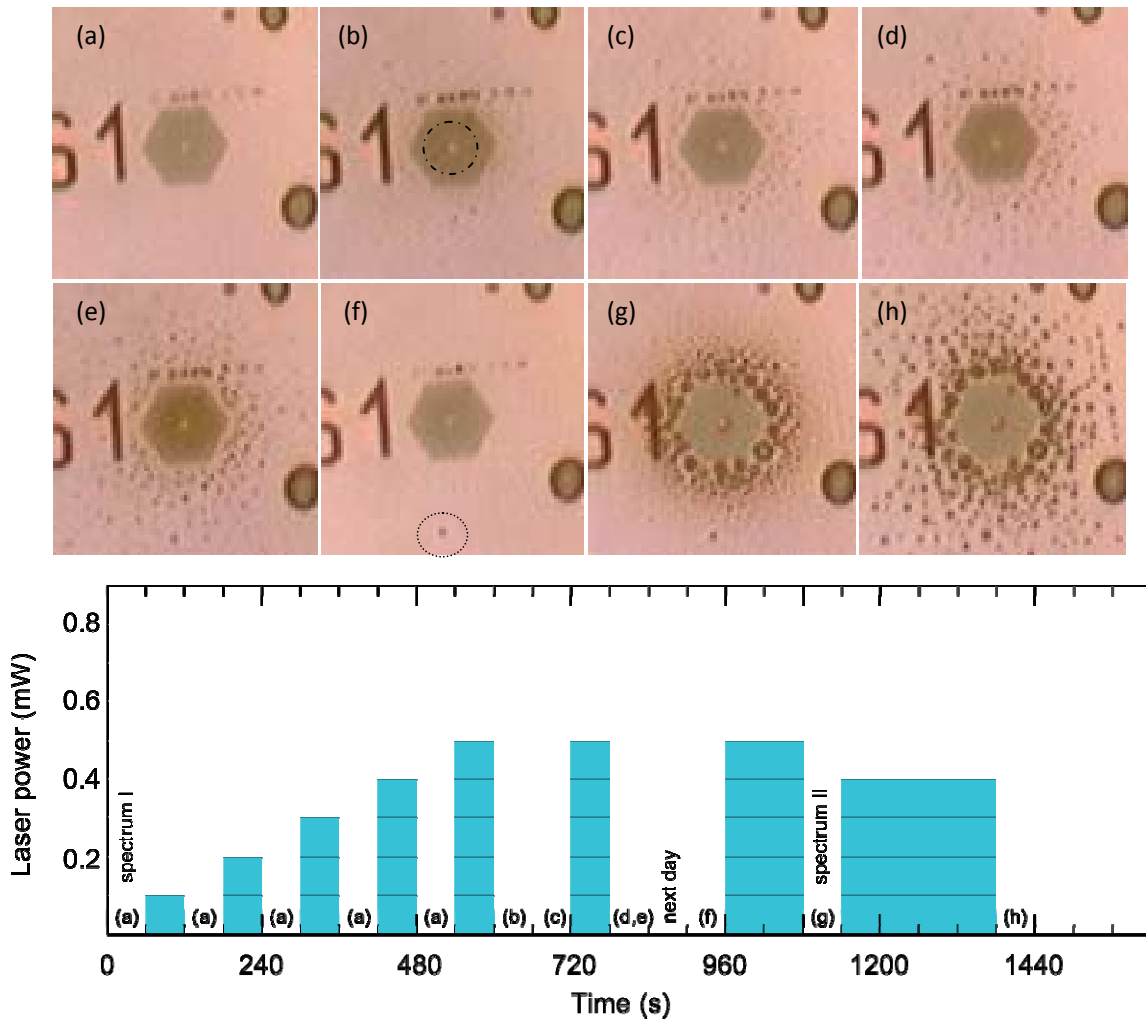


Figure 55: Top: set I of the microscope images of the investigated H1 structure in several stages of the experiments. Bottom: timeline of the laser power exposure and reference to microscope images and spectra. The time between the exposures is arbitrary. Spectrum I refers to Figure 54 and spectrum II refers to Figure 58.

Up until the laser power of 0.4 mW there is no change in either the microscope image (Figure 55 (a)) as the spectrum (dashed black line in Figure 54). Only after 60 s of 0.5 mW laser power, small splashes of DPO can be seen around the cavity as can be seen in Figure 55 (b). An estimate of the temperature of the PhC at laser spot as function of the laser power can be extrapolated from the information from [72] (200°C at 0.5 mW) and the temperature of 25°C at zero laser power. From

this the temperature at the laser spot with 0.4 mW laser power can be estimated to be 165°C. From the graph in Figure 56 we can see that the vapour pressure of the santovac DPO is an exponential function of temperature. The difference in laser power from 0.4 to 0.5 mW results in a factor 10 difference in vapour pressure. This shows that the abrupt change in evaporation rate is reasonable.

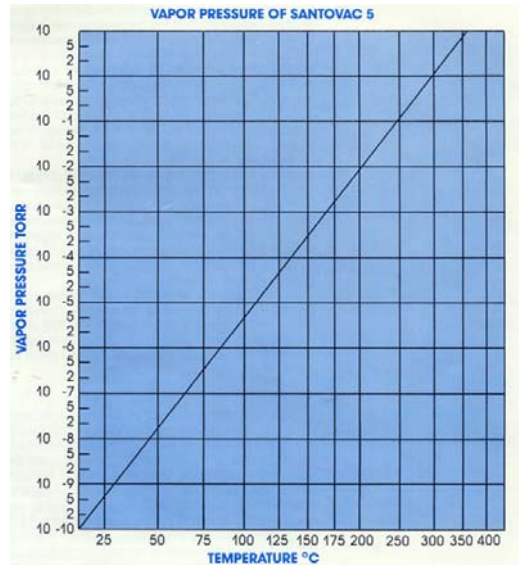


Figure 56: Vapor pressure as a function of the temperature for santovac 5, the diffusion pump oil used for infiltration.

After a short time of waiting, the droplets coalesce and become bigger as can be seen in (c). It is difficult to see from the microscope images (b,c), but directly from the microscope a contrast difference between the area around the defect and the border of the PhC pattern can be observed (indicated by a dashed circle in Figure 55 (b)). In the darker area the DPO in the undercut is not touching the membrane anymore, as is illustrated in a schematic cross-section shown in Figure 57.

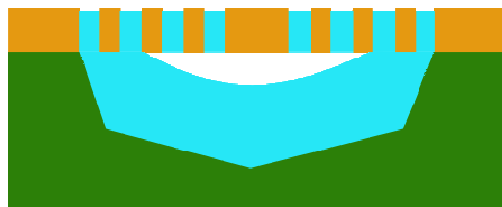


Figure 57: Schematic of a cross-section of a DPO infiltrated H1 pattern. The illustration explains the contrast difference seen in Figure 55 (b-f).

Repeating the 60 s exposure of 0.5 mW laser power on the defect results in more splashes that also coalesce and become bigger after a short time as can be seen in Figure 55 (d-e). The experiment was continued the next day, after which the droplets disappeared as can be seen in Figure 55 (f). The sample was covered during the night and it is unclear if the droplets evaporated or again formed bigger droplets and returned to the PhC structure. In the image in Figure 55 (f) a small droplet is marked that has not disappeared since the day before and has a comparable size to some of the droplets that used to be there, closer to the PhC. This disagrees with the hypothesis of the evaporation of the liquid overnight.

The heating with 0.5 mW laser power is repeated but now with an exposure time of 120 s. A much larger amount of DPO is evaporated from the PhC and is condensed on the sample surface around the PhC pattern as can be seen in Figure 55 (g). An area around the defect is now cleared from liquid as can be seen from the contrast in the image and is confirmed by a clear 48 nm blue-shift in the spectral response shown in Figure 58. The spectral position of the dipole resonance in the empty and fully infiltrated case from the graph in Figure 54 are shown as dashed blue lines in the graph in Figure 58 and all following graphs in this chapter. The spectrum almost shifts to the empty case, which confirms that the most of the holes directly surrounding the defect are empty. This also indicates the importance of the first row of holes surrounding the defect and shows the strong confinement of the dipole.

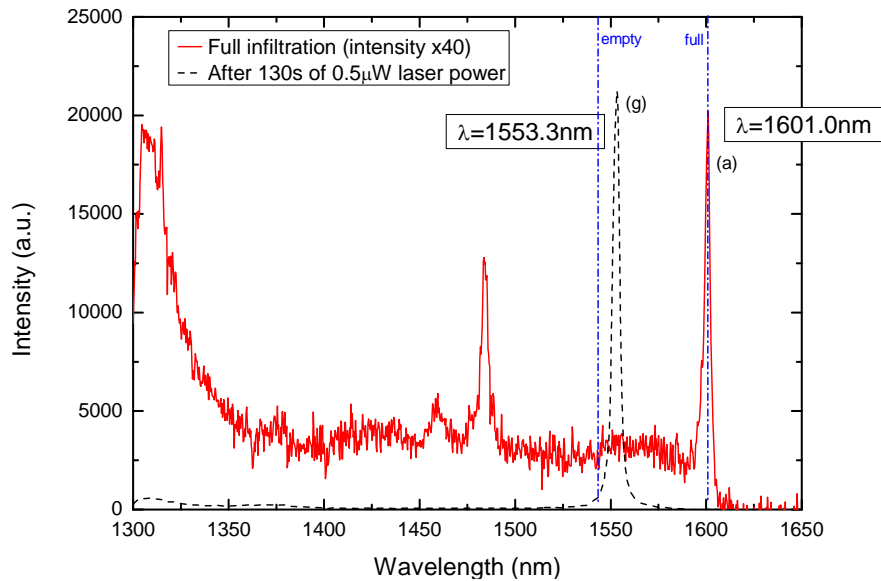


Figure 58: The spectral response of the H1 structure before and after 120 s of 0.5 mW laser power on the cavity. The intensity of the spectrum before exposure is multiplied by 40 to be able to compare the spectral position. The dashed blue lines show the position of the dipole resonance in empty and the fully infiltrated case.

The exposure with 0.4 mW laser power was repeated for 240 s to confirm the requirement of 0.5 mW for the DPO. The microscope image is shown in Figure 55 (h). The droplets further away from the PhC seem to have grown in size, but also increased in separation from each other which is probably due to the coalescence of the droplets. The droplets right next to the PhC have not visibly changed in size. The empty area directly next to the defect is unchanged and also the spectral response does not show a change. This proves that 0.5 mW is the minimal required laser power to provoke the evaporation of the DPO.

The laser power is again increased to 0.5 mW and focussed on the cavity for 240 s to try and free all the holes around the cavity from liquid. The result is shown in Figure 59 (a). Again a timeline of the laser exposures, PL-measurements and microscope images is added as a guide to the experiment.

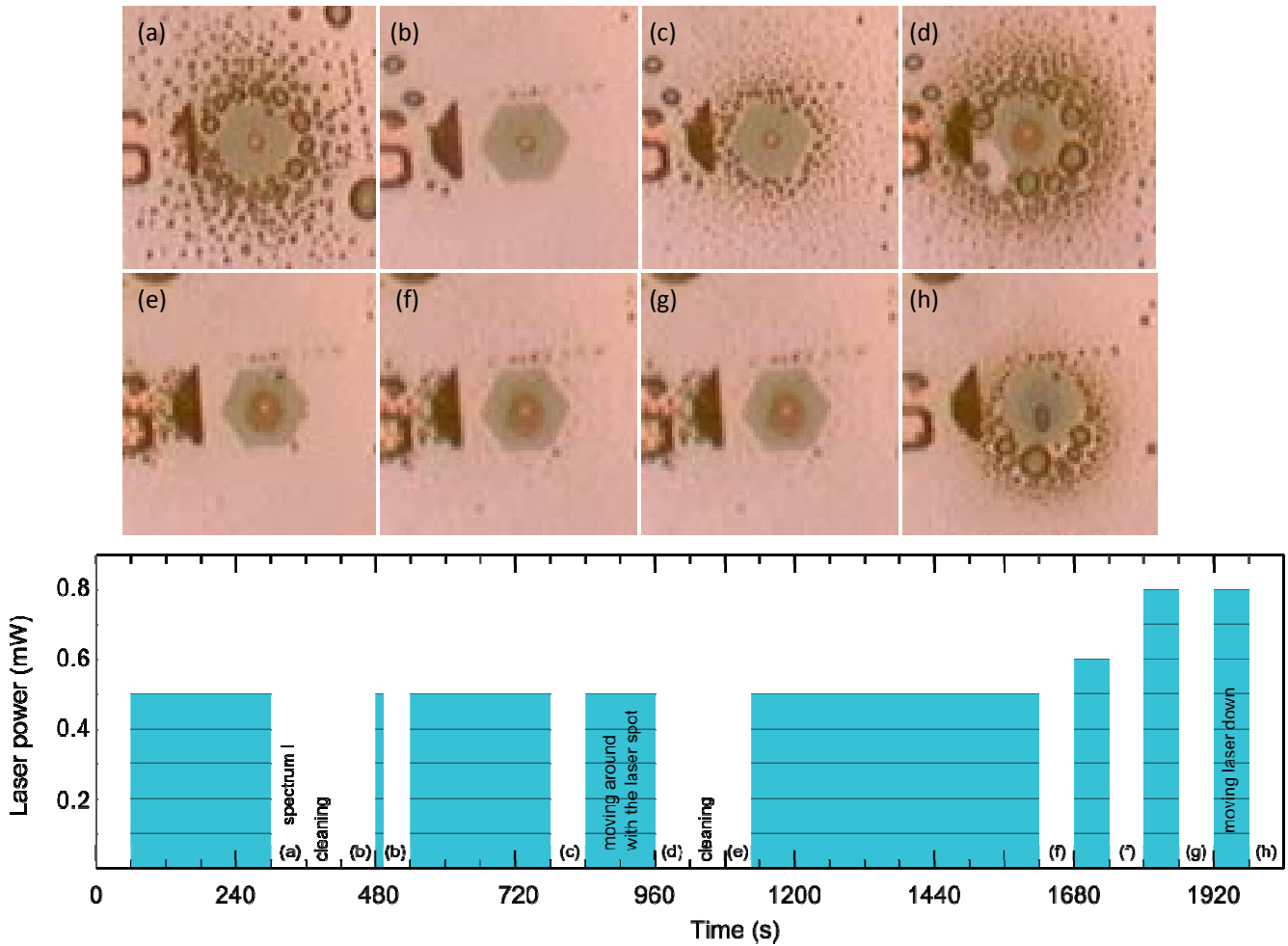


Figure 59: Top: microscope images of the investigated H1 structure in several stages of the experiments. Bottom: timeline of the laser power exposure and reference to microscope images and spectra. The time between the exposures is arbitrary. Spectrum I refers to the graph in Figure 60.

From the contrast in the microscope image we can now see that all the holes immediately around the defect are now empty and the droplets around the PhC have increased in size. This result confirms that 0.4 mW is not enough to evaporate the oil from the holes. The spectrum in Figure 60 shows an 8 nm blue-shift, which is the result of the slightly increased empty area around the defect. To be able to use the microscope images to investigate the evaporation process, the sample surface is cleaned by moving the liquid with the infiltration fiber. The result is shown in Figure 59 (b). While cleaning, the fiber broke off part of the '1' that has been etched next to the H1 pattern.

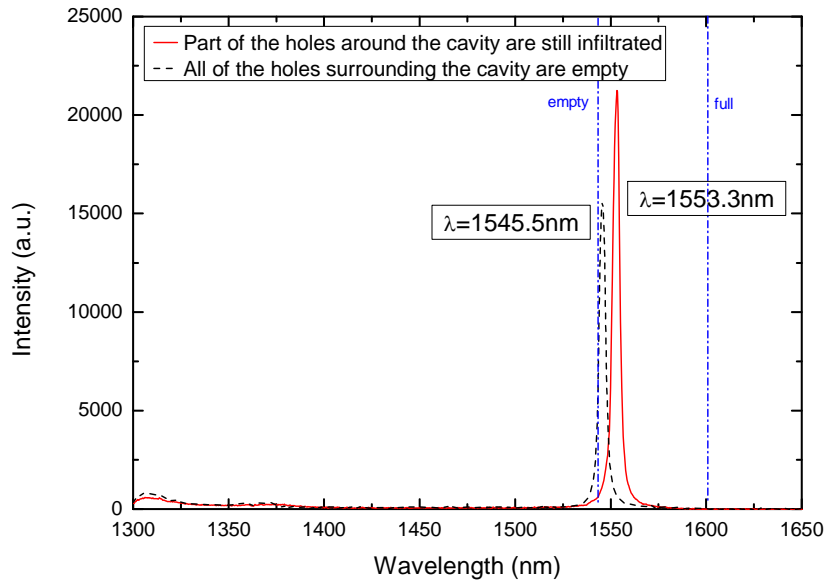


Figure 60: The spectral response of the H1 structure. The red solid line corresponds to the situation in Figure 55 (h). The black dashed line corresponds to the situation in Figure 59 (a). The holes around the cavity are freed from liquid by 240 s of 0.5 mW. The dashed blue lines show the position of the dipole resonance in the empty and fully infiltrated case.

### 6.3.2 Exposure time required for evaporation

To investigate the dependence on exposure time the laser is focussed on the defect for 10 s with 0.5 mW. The microscope image does not show a change of the infiltration (still the same as Figure 59 (b)) and also no splashes around the structure. The PL of the cavity does not show a spectral shift. The status of the infiltration was in this case different from the previous cases (until Figure 55 (g)), in that the holes directly surrounding the defect are now not infiltrated anymore (depicted in the illustration in Figure 61).

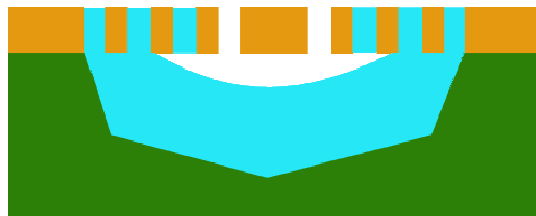


Figure 61: Schematic of a cross-section of a DPO infiltrated H1 pattern. The holes immediately around the defect are now empty.

The 10 s exposure can therefore not be compared with the results of the previous longer (240 s) exposure time (Figure 55 (a)). To investigate the exposure time, the 240 s at 0.5 mW experiment is repeated. The resulting microscope image is shown in Figure 59 (c). This time splashes of liquid can be seen on the sample surface and the size of the area of empty holes around the defect has increased slightly. This means that the amount of evaporated liquid depends on time, which is consistent with the model of evaporation and re-condensation. The spectrum of the cavity is unchanged which proves again the importance of the first few rows of holes around the defect.

To further empty the pattern from liquid, the laser is focussed on the sample with 0.5 mW laser power. The laser spot is then moved over the PhC pattern for small distances around the defect. The result is shown in the microscope image in Figure 59 (d), and shows again a large amount of oil

condensed on the sample around the structure. A larger area around the cavity is now free from liquid. It is expected that the temperature of the membrane decreases with increasing distance from the laser focus and thus that also the evaporation rate depends on the distance from the laser spot. To confirm this, the sample surface around the cavity is cleared from liquid with the fiber tip (Figure 59 (e)) and the experiment with the light focussed on the centre of the defect with laser power 0.5 mW is repeated with a duration of 460 s. The result is shown in a microscope image in Figure 59 (f) and shows that there is no evaporation of the oil. The temperature of the PhC membrane at the location where there is still liquid inside the holes is too low to evaporate the oil. The experiment is repeated for 60 s with laser power 0.6 mW and 0.8 mW, but in both cases does not result in evaporation as can be seen in Figure 59 (g).

### 6.3.3 Optical re-infiltration of the PhC membrane

To see if the evaporation and condensation of the oil can be used to re-infiltrate the holes around the defect, the laser (still with 0.8 mW laser power) is focussed on the centre of the cavity and then moved downwards until the spot is on the sample surface below the PhC pattern. The microscope image, shown in Figure 59 (h), shows an asymmetrical droplet distribution on the sample surface, where the area below the PhC pattern shows a larger amount of liquid than the area above the PhC pattern. More importantly, it can be seen from the contrast, that the holes around the defect are again filled with liquid. This shows the first successful re-infiltration of holes using only laser power.

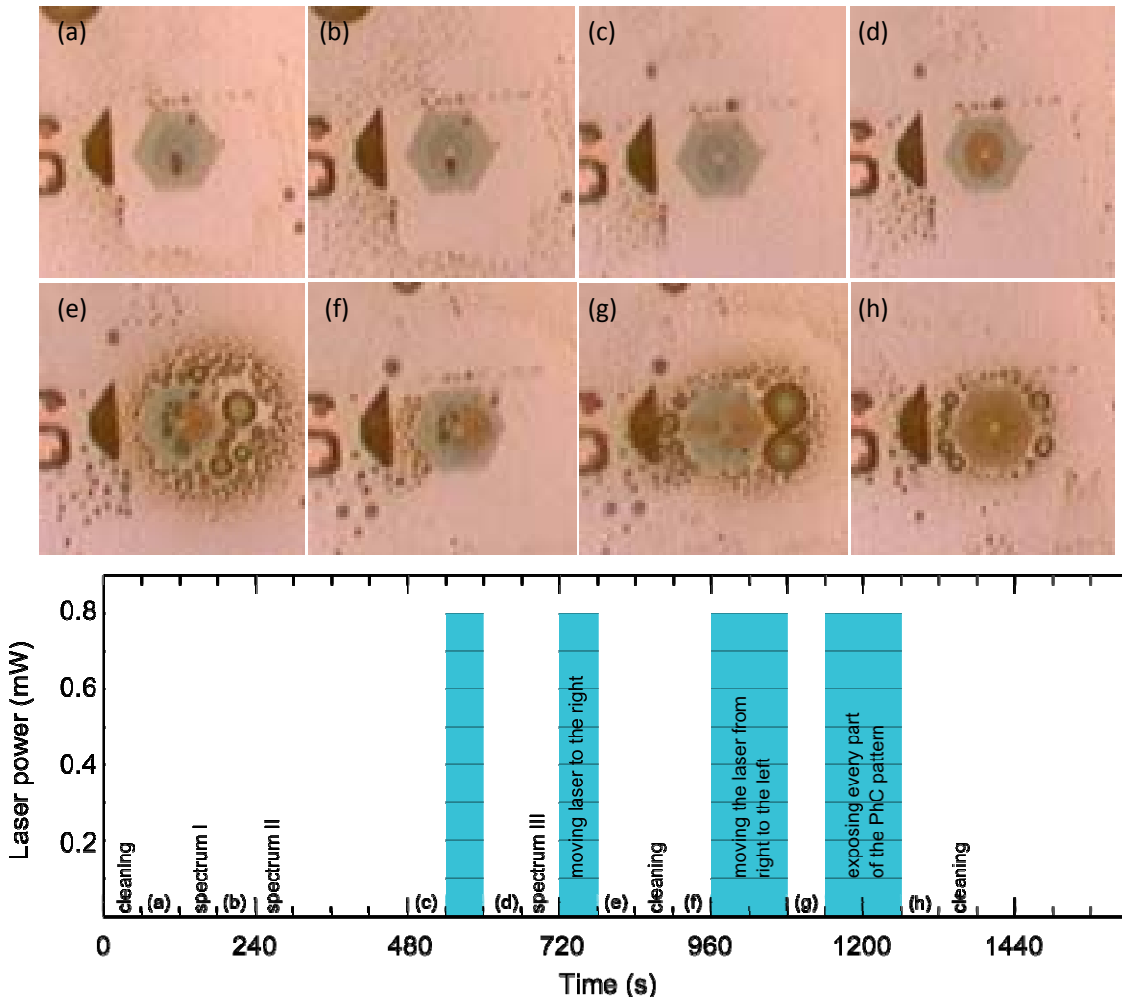




Figure 62: Top: microscope images of the investigated H1 structure in several stages of the experiments. Bottom: timeline of the laser power exposure and reference to microscope images and spectra. The time between the exposures is arbitrary. Spectrum I refers to the graph in Figure 63, spectrum II to the inset in Figure 63 and spectrum III to the graph in Figure 64.

There also seems to be liquid on top of the PhC pattern. After cleaning the surrounding sample surface, there is still a droplet on top of the membrane touching the cavity, see Figure 62 (a). The spectral response is shown in Figure 63, and shows a clear red-shift of the dipole, which confirms the re-infiltration of the holes around the cavity. The oil that evaporated from the holes during the transposing of the laser focus has condensed and is spread over a circular area, the same as before. Part of the liquid can be seen on the sample surface, below the PhC pattern, and part has returned to the holes of the pattern and even on top of the holes. The wavelength of the dipole resonance is in between the empty and the fully infiltrated case, which suggests that the holes are only partially infiltrated. This could have been observed from the slightly higher contrast of the area around the defect, as can be seen in Figure 62 (a). In the inset in Figure 63 a zoomed in graph of the same dipole resonance is shown. The splitting of the peak is a result of the broken symmetry due to the droplet on top of the structure, in contact with the defect. This was already observed in the previous chapters.

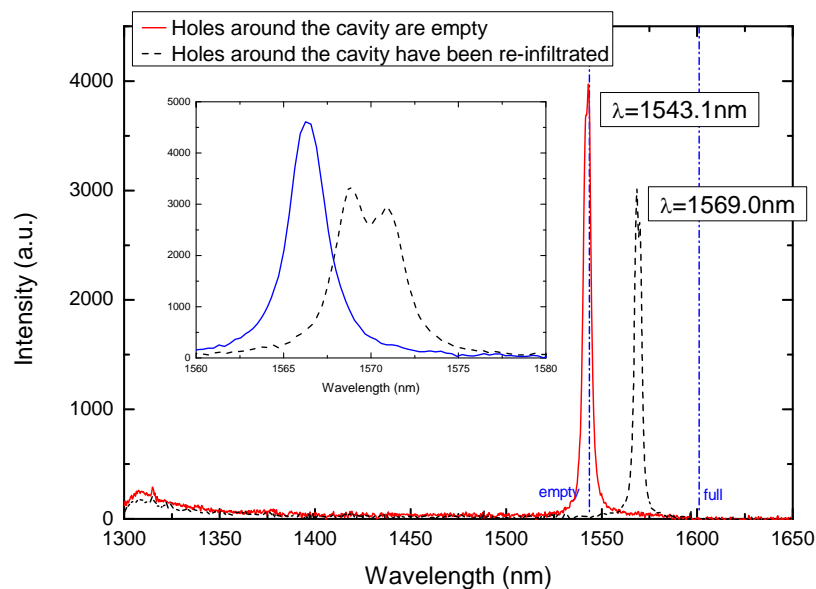


Figure 63: The spectral response of the cavity. The solid red line shows the spectrum before re-infiltration of the holes surrounding the cavity. The dashed black line shows the red-shifted spectrum of the cavity after the re-infiltration of these holes. In the inset the dashed black line is the same as in the bigger graph, but expanded for clarification and shows splitting of the dipole resonance due to the droplet on top of the PhC pattern. The solid blue line shows the spectrum, taken from the cavity two minutes later, when the droplet is not 'touching' the defect anymore.

After two minutes the droplet is slightly decreased in size and is now not in contact with the defect anymore as can be seen in Figure 62 (b). The solid blue line in the inset in Figure 63 shows the spectrum after the droplet has broken the contact with the defect and the dipole mode is degenerate again. This shows again how sensitive the cavity is to slight changes in refractive index on top of the membrane.

After another four minutes the droplet has disappeared totally, as can be seen in Figure 62 (c), but without a change in the spectral response. The small separation seen in Figure 62 (b) was already

enough for not influencing the modes of the cavity. This shows again how strongly the mode is localised near the defect.

To repeat the optical replacement of liquid, the holes surrounding the defect are again emptied with a 60 s exposure of 0.8 mW laser power focussed on the cavity. The microscope image is shown in Figure 62 (d) and shows a slightly larger empty area than before. More surprising is the fact that there is no liquid on the sample surface this time. As noticed before, the holes around the defect are only infiltrated by a small amount and apparently this liquid has, via the evaporation and condensation, re-infiltrated the outer area of the PhC pattern. The dipole is again blue-shifted as shown in the graph in Figure 64.

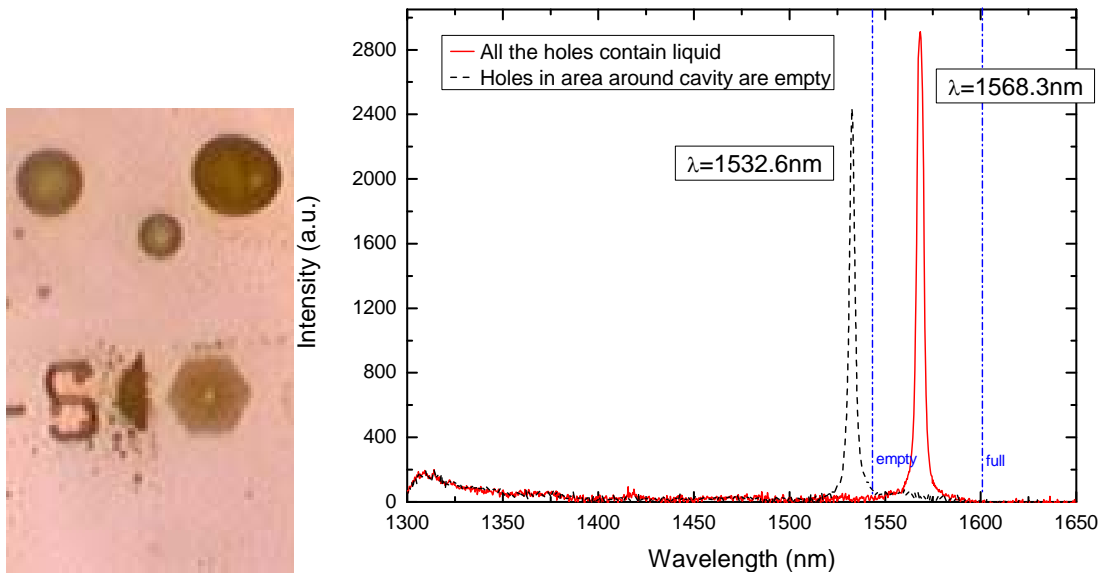


Figure 64: On the left: a microscope image of the H1 structure, where the three droplets above the structure show the volume of DPO taken from the cavity. On the right: the spectral response of the H1 structure. The solid red line shows the spectrum after the re-infiltration of the cavity, same as the solid blue line in the inset in Figure 63. The dashed black line is the spectrum after removing the liquid from the holes around the cavity.

The dipole resonance has blue-shifted past the wavelength of the empty reference spectrum. This could be the result of local oxidation produced by the high laser power, as reported by Lee et al. [73]. They describe a blue-shift of the modes in a L3-cavity after laser irradiation. Due to the local heating in air atmosphere, an oxide layer with a smaller refractive index than the InGaAsP can grow on top of the PhC pattern, shifting the modes to lower wavelengths. At the same time InGaAsP is consumed to form the oxidation layer, reducing the slab thickness and increasing the hole radii.

Now the laser is focussed on the cavity with 0.8 mW laser power and slowly moved to the right, until it is on the sample surface. The result is shown in Figure 62 (e). Again a large amount of liquid is condensed on the sample surface on the right side of the structure. The liquid has also re-infiltrated the holes to the left side of the defect, similar to the effect seen before. This time the liquid is not touching the defect and the spectrum is unchanged (dashed black line in Figure 64). Still we confirmed again that we can not only remove liquid from the cavity but also move it back into the holes by using the laser.

The sample surface is again cleaned from liquid using the infiltration fiber (Figure 62 (f)) and the laser is now focussed on the sample surface to the right of the pattern. With laser power 0.8 mW the spot is slowly moved all the way over the sample surface to the left of the pattern, moving over the PhC and the defect. The result is shown in Figure 62 (g). It looks like there is more oil condensed on the right side of the PhC pattern than on the left, which is the opposite of what happened before. But it should be taken into account that there is a gap left of the structure, the remains of the '1' that is also deeply etched during fabrication, which is probably infiltrated with the oil that condensed on this site of the PhC.

After cleaning the sample surface with the fiber, the PhC is cleaned by moving the spot with 0.8 mW laser power over every part of the membrane. The result is shown in Figure 62 (h) and shows a smaller amount of liquid that was left in the structure than would be expected.

The last amount of oil is also removed with a fiber and the total amount of liquid that is removed from the cavity in this part of the experiments is shown in the microscope image in Figure 64 on the left, above the PhC structure. The spectrum of the cavity at the end of the experiment is shown in Figure 65 (g). The holes in the area around the defect where already empty in the case of Figure 62 (g) and the 1.5 nm blue-shift can again be attributed to oxidation as a result of the high laser power.

### 6.3.4 Summary and overview of the experiment

The spectra of the important stages of the investigation are shown in Figure 65, together with their corresponding microscope images.

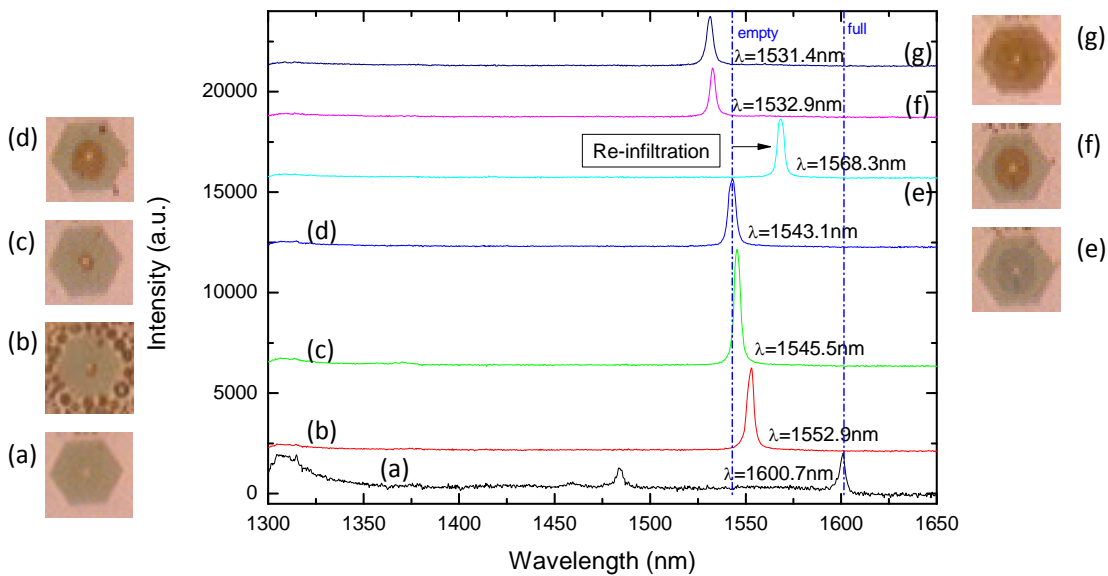


Figure 65: Spectral response of the H1 cavity of several steps of the experiments, together with the corresponding microscope image.

The step from (a) to (b) shows the largest blue-shift, indicating the importance of the infiltration of the holes surrounding the cavity. The small blue-shift from (b) to (c) shows the possibility of very small modification in spectral response by carefully manipulating the infiltration around the cavity. The difference in wavelength between (c) and (d) is small considering the relatively large change in infiltration. The step from (d) to (e) shows the successful re-infiltration of all the holes in the

structure. The contrast difference in (e), which has the same outline as can be seen in (f), indicates that the holes are not fully infiltrated. This can also be seen in the spectrum, where the dipole shows a relatively large red-shift, but only halfway to the fully infiltrated case (a). After re-infiltration the holes surrounding the defect (f) and later the whole PhC pattern (g) are cleared from liquid. In the spectra (f) and (g) the dipole resonance is blue-shifted beyond the empty reference wavelength, which can be contributed to the formation of a oxidation layer on top of the PhC pattern at high laser power.

## 6.4 Conclusion

In the first part of the investigation it is confirmed that focussed laser power can be used to evaporate the DPO from the membrane. The thermal conductivity of the structure is low, due to the disorder in the InGaAsP material, the isolation of air above and below the membrane, and the fact that the slab is perforated. The evaporated oil condenses and forms droplets on top of the sample surface where they either coalesce and form larger droplets, or are absorbed by the holes in the membrane.

By positioning the laser, the holes around the defect can be cleared from liquid and blue-shift the dipole by almost 50 nm. More importantly, by moving the laser spot away from the cavity, the liquid evaporated in a part of the membrane away from the defect, infiltrates the holes in its surroundings and was used to re-infiltrate the holes directly around the defect. This shows that it is possible to both red- and blue-shift the modes in a cavity, by selective removal and re-infiltration using exclusively optical means of manipulation.

## 7. Summary

The goal of the project was to explore the possibilities of integrating fluids in photonic crystals. The presented experiments were based on the selective tuning or inducing of PhC cavity modes by local liquid infiltration of the PhC holes. Also the possibilities to gain control over the transport of liquid by using light were investigated.

Part of the holes of a PhC waveguide was infiltrated with oil using a tapered optical fiber, to induce a DHS cavity. The infiltration of the holes results in an increased refractive index and locally decreases the frequency of the modes in the PBG. The shift of the resonances results in a mode-gap with high quality factor modes. The width of the cavity is determined by the amount of infiltrated columns of holes and can be adjusted by locally evaporating the liquid from the holes. Experimental results of a liquid DHS cavity induced by a single line of infiltration were presented. The near-field emission of the cavity was collected using SNOM and showed the high-Q Fabry-Perot resonances of the DHS. Due to fabrication problems of the undercut of the membrane structure, it was not possible to control the pattern of infiltration. PhC patterns were designed to solve these fabrication problems, but due to delay in processing capabilities in the cleanroom, they were not fabricated in time for this project. Calculations on liquid induced DHS cavities were presented and they predicted huge improvements in Q-factor for narrower waveguides.

The same type of DHS cavity was induced by positioning an oil droplet on top of the PhC pattern, to again locally increase the refractive index of the waveguide pattern. The droplets were varied in diameter, which was used to tune both the free spectral range of the Fabry-Perot resonances and to shift the spectral position of the cut-off modes. Not only the size, but also the position of the cavity in the waveguide could easily be changed by moving the droplet over the PhC pattern using a tapered optical fiber. By positioning the tapered fiber inside a droplet on top of the PhC structure, a mobile DHS cavity was presented. The cavity was moved into the focussed laser spot to collect the emission of the cavity and it was shown that the optical properties could be changed by slight translations of the fiber tip.

The selective tuning of the normally degenerate dipole modes in a point defect was presented by both selective infiltration and selective removal of the liquid in the PhC holes. The different polarizations of the modes were identified by carefully chosen infiltration patterns, combined with the calculated mode profiles. The crossing of the normally degenerate modes was presented and indicates both the range and selectivity of this reconfigurable tuning method.

The selective tuning of both the quadrupole and dipole modes was examined by using droplets positioned on top of the PhC pattern. The mobility of the droplet makes this a very versatile method of polarization selective tuning.

Besides the local evaporation already used in the previous experiments, it was shown that the condensation of the liquid could be used to re-infiltrate the PhC holes. The modes in a single defect cavity were first shifted to lower wavelengths by selective evaporation of the liquid in the holes surrounding the defect. The holes were then optically re-infiltrated, which was confirmed by the shift of the cavity modes to higher wavelengths.

## Acknowledgments

First of all I want to thank Rob for guiding and encouraging me throughout the whole project. His enthusiasm and love for physics kept me motivated and helped me to be creative during experiments. I want to thank Mehmet for sharing his knowledge and experience, for fabricating my samples and for teaching me how to operate the different setups used in the experiments. I also want to thank him for introducing me to the genuine Turkish cuisine and all the other fun times we had together. I want to thank my NI d1.05 roomies, Mehmet, Bowen, Timothy and Joost, for the interesting discussion (on and off topic), the encouragements, but most off all for the fun during the work. Your presence was missed in the days of writing my report and I wish you all the best for the future. There are many other people who helped me in some way or another during my project and even though I cannot thank you all by name, I want you to know that your support is greatly appreciated.

I want to thank all the people of PSN for being such a nice and friendly group, where I could always find nice relaxation during coffee-breaks. I can only hope to find a working environment where I can feel at home as much as I did in your group.

I would like to thank my parents, my brother and my friends for encouraging me, believing in me and for showing interest in my project. I especially want to thank my girlfriend Mirjam for always motivating and encouraging me when I needed it the most. She took care of me in the stressful period of writing my thesis and kindly accepted my increased absentmindedness. It would have been a lot harder doing it without her.

## Bibliography

- [1] C. X. Liu, J. Park, and J. W. Choi, "A planar lens based on the electrowetting of two immiscible liquids," *J. Micromech. Microeng.*, vol. 18, no. 3, p. 035023, 2008.
- [2] S. Grilli et al., "Liquid micro-lens array activated by selective electrowetting on lithium niobate substrates," *Optics Express*, vol. 16, pp. 8084-8093, 2008.
- [3] D. B. Wofe, et al., "Dynamic control of liquid-core / liquid-cladding optical waveguides," *Proc. Natl. Acad. Sci U.S.A.*, vol. 101, pp. 12434-12438, 2004.
- [4] S. K. Y. Tang, C. A. Stan, and G. M. Whitesides, "Dynamically reconfigurable liquid-core liquid-cladding lens in a microfluidic channel," *Lab Chip*, vol. 8, pp. 395-401, 2008.
- [5] D. B. Wolfe et al., "Diffusion-controlled optical elements for optofluidics," vol. 87, no. 18, pp. 181105.1-3, 2005.
- [6] D. Psaltis, S. R. Quake, and C. Yang, "Developing optofluidic technology through the fusion of microfluidics and optics," *Nature*, vol. 442, pp. 381-386, 2006.
- [7] X. Fan and I. M. White, "Optofluidic microsystems for chemical and biological analysis," *Nat. Photon.*, vol. 5, pp. 591-597, 2011.
- [8] H. Schmidt and A. R. Hawkins, "The photonic integration of non-solid media using optofluidics," *Nat. Photon.*, vol. 5, pp. 598-604, 2011.
- [9] C. Monat, P. Domachuk, and B. J. Eggleton, "Integrated optofluidics: A new river of light," *Nat. Photon.*, pp. 106-114, 2007.
- [10] A. Ashkin, "Acceleration and trapping of particles by radiation pressure," *Phys. Rev. Lett.*, vol. 24, pp. 156-159, 1970.
- [11] M. M. Wang et al., "Microfluidic sorting of mammalian cells by optical force switching," *Nature Biotechnology*, vol. 23, no. 1, pp. 83-87, 2005.
- [12] P. J. Reece, V. Garces-Chavez, and K. Dholakia, "Near-field optical micromanipulation with cavity enhanced evanescent waves," *Appl. Phys. Lett.*, vol. 88, no. 12, pp. 221116.1-3, 2006.
- [13] S. E. Chung et al., "Optofluidic maskless lithography system for real-time synthesis of photopolymerized microstructures in microfluidic channels," *Appl. Phys. Lett.*, vol. 91, no. 4, pp. 041106.1-3, 2007.
- [14] Y. Fainman, L. P. Lee, D. Psaltis, and C. Yang, *Optofluidics*.: McGraw-Hill, 2010.
- [15] P. Prasad, *Nanophotonics*. Hoboken: John Wiley and Sons, 2004.
- [16] J. D. Joannopoulos, R. D. Meade, and J. N. Winn, *Photonic Crystals: Molding the flow of light*.

Princeton, NJ: Princeton University Press, 1995.

- [17] E. Yablonovitch, "Inhibited spontaneous emission in solid-state physics and electronics," *Phys. Rev. Lett.*, vol. 58, p. 2059, 1987.
- [18] S. John, "Strong localization of photons in certain disordered dielectric superlattice," *Phys. Rev. Lett.*, vol. 58, p. 2486, 1987.
- [19] E. Yablonovitch, T. J. Gmitter, and K. M. Leung, "Photonic band structure: the face centered-cubic case employing nonspherical atoms," *Phys. Rev. Lett.*, vol. 67, p. 2295, 1991.
- [20] T. F. Krauss, R. M. De La Rue, and S. Brand, "Two-dimensional photonic band gap structures operating at near-infrared wavelengths," *Nature*, vol. 383, p. 669, 1996.
- [21] J. Vuckovic, M. Loncar, H. Mabuchi, and A. Scherer, "Optimization of the Q-factor in photonic crystal microcavities," *IEEE J. Quantum Electron.*, vol. 38, pp. 850-856, 2002.
- [22] T. Baba, N. Fukaya, and J. Yonekura, "Observation of light propagation in photonic crystal optical waveguides with bends," *Electron. Lett.*, vol. 35, p. 654, 1999.
- [23] Y. Akahane, T. Asano, B. S. Song, and S. Noda, "Investigation of high-Q channel drop filters using donor-type defects in two-dimensional photonic crystal slabs," *Appl. Phys. Lett.*, vol. 83, pp. 1512-1514, 2003.
- [24] T. Tanabe, M. Notomi, S. Mitsugi, A. Shinya, and E. Kuramochi, "All-optical switches on a silicon chip realized using photonic crystal nanocavities," *Appl. Phys. Lett.*, vol. 87, pp. 1511121-1511123, 2005.
- [25] O. Painter et al., "Two-dimensional photonic band-gap defect mode laser," *Science*, vol. 284, pp. 1819-1821, 1999.
- [26] H. G. Park et al., "Electrically driven single-cell photonic crystal laser," *Science*, vol. 305, pp. 1444-1447, 2004.
- [27] Z. Y. Li and L. L. Lih, "Evaluation of lensing in photonic crystal slab exhibiting negative refraction," *Phys. Rev. B*, vol. 68, p. 245110, 2003.
- [28] A. Berrier et al., "Negative refraction at infrared wavelengths in a two-dimensional photonic crystal," *Phys. Rev. Lett.*, vol. 93, p. 733902, 2004.
- [29] D. O'Brien et al., "Tunable optical delay using photonic crystal heterostructure nanocavities," *Phys. Rev. B*, vol. 76, pp. 1151101-1151104, 2007.
- [30] P. Halevi and F. Ramos-Mendieta, "Tunable Photonic Crystals with Semiconducting Constituents," *Phys. Rev. Lett.*, vol. 85, no. 9, pp. 1875-1878, 2000.



- [31] C. Schuller, F. Klopff, J. P. Reithmaier, M. Kamp, and A. Forchel, "Tunable photonic crystal fabricated in III-V semiconductor slab waveguides using infiltrated liquid crystals," *Appl. Phys. Lett.*, vol. 82, pp. 2767-2769, 2003.
- [32] S. F. Mingaleev, M. Schillinger, D. Hermann, and K. Busch, "Tunable photonic crystal circuits: concepts and designs based on designs based on single-pore infiltration," *Opt. Lett.*, vol. 29, pp. 2858-2860, 2004.
- [33] F. Intonti et al., "Rewritable photonic circuits," *Appl. Phys. Lett.*, vol. 89, p. 211117, 2006.
- [34] P.E. Kallassi et al., "Local infiltration of planar photonic crystals with UV-curable polymers," *J. Opt. Soc. Am. B*, vol. 25, pp. 1562-1567, 2008.
- [35] C.L.C. Smith et al., "Microfluidic photonic crystal double heterostructures," *Appl. Phys. Lett.*, vol. 91, p. 121103, 2007.
- [36] C. L. C. Smith et al., "Reconfigurable microfluidic photonic crystal slab cavities," *Opt. Exp.*, vol. 16, no. 20, pp. 15887-15896, 2008.
- [37] H. H. J. E. Kicken et al., "Wavelength tuning of planar photonic crystals by local processing of individual holes," *Opt. Express*, vol. 17, no. 24, pp. 22005-22011, 2009.
- [38] J. D. Jackson, *Classical Electrodynamics*.: Wiley, 1998.
- [39] M. A. Dunder, *Optofluidic and photothermal control of InGaAsP photonic crystal nanocavities*. Eindhoven: Technische Universiteit Eindhoven, 2011.
- [40] P. M. Petroff, *Single quantum dots: fundamentals, applications, and new concepts*. Berlin: Springer, 2003.
- [41] R. Notzel et al., "Self assembled InAs/InP quantum dots for telecom applications in the 1.55  $\mu$ m wavelength range: Wavelength tuning, stacking, polarization control, and lasing," *Appl. Phys. Lett.*, vol. 45, pp. 6544-6549.
- [42] J. A. M. Voorbraak, "Spectroscopy of Photonic Crystal Coupled-resonators using simultaneously Near-field and Far-field probes," 2011.
- [43] K. S. Yee, "Numerical solution of initial boundary value problems involving maxwell's equations in isotropic media," *IEEE. Trans. Antennas. Propogat.*, vol. 14, p. 302, 1966.
- [44] A. F. Oskooi et al., "Meep: A flexible free-software package for electromagnetic simulations by the FDTD method," *Comput. Phys. Commun.*, vol. 181, p. 687, 2010.
- [45] T. Siahhan, "Photonic Crystal Cavity Microparticles for Sensing," 2011.
- [46] B Song, T Asano, Y Akahane, Y Tanaka, and S Noda, "Transmission and reflection characteristics

- of in-plane hetero-photonic crystals," *Appl. Phys. Lett.*, vol. 85, no. 20, p. 4591, 2004.
- [47] B Song, S Noda, T Asano, and Y Akahane, "Ultra-high-Q photonic double-heterostructure nanocavity," *Nature materials*, vol. 4, pp. 207 - 210, 2005.
- [48] E Kuramochi, M Notomi, S Mitsugi, A Shinya, and T Tanabe, "Ultrahigh-Q photonic crystal nanocavities realized by the local width modulation of a line defect," *Appl. Phys. Lett.*, vol. 88, p. 041112, 2006.
- [49] T Asano, B Song, and S Noda, "Analysis of the experimental Q factors ( $\sim 1$  million) of photonic crystal nanocavities," *Optics Express*, vol. 14, no. 5, pp. 1996-2002, 2006.
- [50] S. Tomljenovic-Hanic, M. J. Steel, C. M. de Sterke, and D. J. Moss, "High-Q cavities in photosensitive photonic crystals," *Opt. Lett.*, vol. 32, no. 5, pp. 542-544, 2007.
- [51] A. Mock, L. Lu, E. H. Hwang, J. O'Brien, and P. D. Dapkus, "Modal Analysis of Photonic Crystal Double-Heterostructure Laser Cavities," *IEEE*, vol. 15, no. 3, pp. 892 - 900, 2009.
- [52] S. Tomljenovic, de, M.C. Sterke, and M.J. Steel, "Design of high-Q cavities in photonic crystal slab heterostructures by air-hole infiltration," *Opt. Expr.*, vol. 14, no. 25, pp. 12451-12456, 2006.
- [53] A. C. Bedoya et al., "Liquid crystal dynamics in a photonic crystal cavity created by selective microfluidic infiltration," *Opt. Exp.*, vol. 18, no. 26, pp. 27280-27290, 2010.
- [54] S. Tomljenovic-Hanic et al., "High-Q cavities in multilayer photonic crystal slabs," *Opt. Exp.*, vol. 15, no. 25, pp. 17248-17253, 2007.
- [55] Corning optical fiber. [Online]. [http://www.corning.com/opticalfiber/products/SMF-28e+ fiber.aspx](http://www.corning.com/opticalfiber/products/SMF-28e+fiber.aspx)
- [56] M. Larque, T. Karle, I. Robert-Philip, and A. Beveratos, "Optimizing H1 cavities for the generation of entangled photon pairs," *New J. Phys.*, vol. 11, p. 033022, 2009.
- [57] A. Faraon et al., "Local quantum dot tuning on photonic crystal chips," *Appl. Phys. Lett.*, vol. 90, p. 213110, 2007.
- [58] I. Marki, M. Salt, and H. P. Herzig, "Tuning the resonance of a photonic crystal microcavity with an AFM probe," *Opt. Express*, vol. 14, no. 7, pp. 2969-2978, 2006.
- [59] G. Le Gac et al., "Tuning of an active photonic crystal cavity by an hybrid silica/silicon near-field probe," *Opt. Express*, vol. 17, no. 24, pp. 21672-21679, 2009.
- [60] B. Wang et al., "Controlling mode degeneracy in a photonic crystal nanocavity with infiltrated liquid crystal," *Opt. Lett.*, vol. 35, no. 15, pp. 2603-2605, 2010.
- [61] M. A. Dundar et al., "Birefringence-induced mode-dependent tuning of liquid crystal infiltrated

- InGaAsP photonic crystal nanocavities," *Appl. Phys. Lett.*, vol. 95, p. 181111, 2009.
- [62] K. Hennessy, C. Hogerle, E. Hu, A. Badolato, and A. Imamoglu, "Tuning photonic nanocavities by atomic force microscope nano-oxidation," *Appl. Phys. Lett.*, vol. 89, p. 041118, 2006.
- [63] M. Shirane et al., "Mode identification of high-quality-factor single-defect nanocavities in quantum dot-embedded photonic crystals," *J. Appl. Phys.*, vol. 101, p. 073107, 2007.
- [64] S. Vignolini et al., "Polarization-sensitive near-field investigation of photonic crystal microcavities," *Appl. Phys. Lett.*, vol. 94, p. 163102, April 2009.
- [65] F. Intonti et al., "Tuning of photonic crystal cavities by controlled removal of local infiltrated water," *Appl. Phys. Lett.*, vol. 95, p. 173112, 2009.
- [66] D. Erickson, T. Rockwood, T. Emery, A. Scherer, and D. Psaltis, "Nanofluidic tuning of photonic crystal circuits," *Opt. Lett.*, vol. 31, no. 1, pp. 59-61, 2006.
- [67] A. Faraon et al., "Local tuning of photonic crystal cavities using chalcogenide glasses," *Appl. Phys. Lett.*, vol. 92, p. 043123, 2008.
- [68] L.G. Liu, J. Kim, Y. Lu, and L.P. LEE, "Optofluidic control using photothermal nanoparticles," *nature materials*, vol. 5, pp. 27-32, 2005.
- [69] I. Kudman and E. F. Steigmeier, "Thermal conductivity and Seebeck effect of InP," *Phys. Rev.*, vol. 133, no. 6A, pp. 1665-1667, 1964.
- [70] A. Shakouri, C. LaBounty, J. Piprek, P. Abraham, and J. E. Bowers, "Thermionic emission cooling in single barrier heterostructures," *Appl. Phys. Lett.*, vol. 74, no. 1, p. 88, 1999.
- [71] Wikipedia. [Online]. [http://en.wikipedia.org/wiki/Thermal\\_conductivity](http://en.wikipedia.org/wiki/Thermal_conductivity)
- [72] M. A. Dundar et al., "Lithographic and optical tuning of InGaAsP membrane photonic crystal nanocavities with embedded InAs quantum dots," *Journal of Nanophotonics*, vol. 3, p. 031765, 2009.
- [73] H. S. Lee et al., "Local tuning of photonic crystal nanocavity modes by laser-assisted oxidation," *Appl. Phys. Lett.*, vol. 95, p. 191109, 2009.